SVEUČILIŠTE U SPLITU

FAKULTET GRAĐEVINARSTVA, ARHITEKTURE I GEODEZIJE

DIPLOMSKI RAD

Tonko Faldić

Split, 2017

SVEUČILIŠTE U SPLITU
FAKULTET GRAĐEVINARSTVA ARHITEKTURE I GEODEZIJE

Tonko Faldić

Analiza nosivosti čeličnog stupa izloženog lokaliziranom požaru

Diplomski rad

Split, 2017

Analiza nosivosti čeličnog stupa izloženog lokaliziranom požaru

Sažetak:

U ovom diplomskom radu prikazana je analiza nosivosti čeličnog stupa izloženog djelovanju lokaliziranog požara. Budući da EN 1991-1-2(2002) ne propisuje pojednostavljeni postupak proračuna provođenja topline za vertikalne elemente, izrađen je CFD model na temelju prethodno provedenih požarnih eksperimenata. Na temelju CFD modela izrađen je model provođenja topline za lokalizirani požar kao i za ISO krivulju temperature-vrijeme. Naposlijetku, nelinearnim statičkim proračunom prikazana je analiza nosivosti čeličnog stupa u uvjetima lokaliziranog požara kao i pod djelovanjem visokih temperatura u obliku standardne požarne krivulje. Usporedba između lokaliziranog požara i model standarnog požara pokazuje da lokalizirani požar, ovisno o veličini opterećenja, može dovesti do ranijeg otkazivanja stupa.

Ključne riječi: ***P***požarna analiza, CFD, lokalizirani požar, ISO požar, provođenje topline, analiza nosivosti, nelinearna analiza, imperfekcije, čelik

Structural analysis of the steel column exposed to a localised fire

Abstract:

This thesis presents structural analysis of the steel column exposed to a localised fire. Since EN 1991-1-2(2002) doesn't provide simplified method to calculate heat transfer to the vertical elements, the CFD model of a localised fire is made, based on previously conducted experiments. Furthermore, heat transfer was calculated based on CFD model so as for ISO temperature-time curve respectively. Finally, nonlinear structural analysis of the steel column has been carried out for the localised fire scenario, as well as for the ISO temperature time curve. The comparison between the localised fire and ISO fire exposure points put that localised fire, depending on the level of external load, can lead to earlier failure of the column.

Keywords: Fire modelling, CFD; localised fire, ISO fire, heat transfer, structural analysis, nonlinear analysis, imperfections, steel

I would like to thank to my mentor Neno Torić for his support and advices throughout development of this thesis as well as on an encouragement to live and study in Portugal.

Furthermore, I would like to express my gratitude to Professor Aldina Santiago for acceptance to be my mentor and providing me a chance to develop a part of this thesis on University of Coimbra. Her support during my stay in Portugal was greatly appreciated.

I would also like to express my sincere appreciation to Helder David Craveiro for helping me on this work. I greatly appreciate that I could learn from his experience, his help has a great value in the development of this thesis.

Last but not least, I am grateful to my friends and family for their support during my studies.

SVEUČILIŠTE U SPLITU

FAKULTET GRAĐEVINARSTVA, ARHITEKTURE I GEODEZIJE

STUDIJ:	**DIPLOMSKI SVEUČILIŠNI STUDIJ GRAĐEVINARSTVA**
KANDIDAT:	**Tonko Faldić**
BROJ INDEKSA:	**575**
KATEDRA:	**Katedra za metalne i drvene konstrukcije**
PREDMET:	**Metalne konstrukcije II**

ZADATAK ZA DIPLOMSKI RAD

Tema: Analiza nosivosti čeličnog stupa izloženog djelovanju lokaliziranog požara

Opis zadatka:

Zadatak diplomskog rada je analiza razvoja požarnih temperatura uz pomoć CFD modela na temelju požarnih eksperimenata prethodno provedenih na Sveučilištu u Coimbri. Požarni eksperimenti bazirani su na analizi djelovanja lokaliziranog požara na čelični stup.
Na temelju rezultata požarnih temperatura dobivenih CFD modelom potrebno je analizirati njihov utjecaj na nosivost čeličnog stupa uz primjenu modela provođenja topline te nelinearnog statičkog modela čeličnog stupa.
Potrebno je u analizi uzeti u obzir utjecaj geometrijskih imperfekcija stupa te izvršiti usporedbu s djelovanjem visokih temperatura u obliku standardne požarne krivulje.

U Splitu, 15.09.2017.

Voditelj Diplomskog rada:	Predsjednik Povjerenstva za završne i diplomske ispite:
Doc.dr.sc. Neno Torić	Doc.dr.sc. Veljko Srzić

Table of Contents:

List of figures:

List of Tables:

1 INTRODUCTION

1.1 Motivation

Fire engineering's roots date back to the Ancient Rome and it has continuously growing up to today. Significant examples of some major fire disasters recorded in history are the King Cross Fire in London Underground which occurred on 18 November 1987, and the collapse of World Trade Centre Towers in New York on 11 September 2001. The hazard that these fires represent is usually associated with the uncontrolled nature of the exothermic chemical reactions, especially between organic or combustible materials and air and their interaction with the structural components. These catastrophic events have been main motivation to organize the discipline, define practices and conduct researches to support innovations in order to prevent these accidents of happening again. All of these accidents encouraged scientists to develop and build codes and mechanisms in order to protect people and property from fire.

Table 1. Physical responses for human exposed to high temperature [24]

Temperature	Physical influence on human
127°C	Difficult breathing
140°C	5-min tolerance limit
149°C	Mouth breathing difficult, temperature limit for escape
160°C	Rapid, unbearable pain with dry skin
182°C	Irreversible injury in 30 seconds
203°C	Respiratory systems tolerance time less than 4 minutes (wet skin)

Fire engineering is an application of science and engineering principles to protect people, property and their environments from the harmful and destructive effects of fire and smoke. It embraces numerous complicated physical and chemical interactions, which include fluid dynamics, thermodynamics, combustion, radiation or even multi-phase effects.

During the early investigations of enclosure fire development, a great deal of attention has been focused on better understanding the fire behaviours using experimental techniques and theoretical approaches. Experiments provide useful observations and measurements of the flaming process, while theoretical models employ a mathematical description of the physical phenomena trough the input of experimental data. There are, however, limitations in fully applying experimental techniques and theoretical approaches to a range of fire problems. Conducting full-scale experiments can be expensive compared to the computational costs with the use of theoretical approaches. However, these models are dependent on the experimental data from which they are correlated. [1]

Table 2. Fatality rate as a function of radiation level and exposure time [24]

Exposure time (s)	**TNO probit model (Naked human skin) Fatality rate (%)**		
	10 kW/m^2	20 kW/m^2	30 kW/m^2
10	0	5	39
20	1	53	93
30	11	87	100
40	31	97	100
50	53	99	100
60	71	100	100

The European Union has spent several years developing unified rules for the design of structures. In 1975, the European Commission launched a program responsible to establish a set of European standards, later called Eurocodes. In the fire situation, the combinations of actions are different from those at ambient temperature. EN 1990 (2009) gives the combinations for accidental fire exposure. Fire actions are given in EN 1991-1-2 (2002) and the fire design of structures can be assessed using part 1-2 of the Eurocodes EC. [2]

This work is dealing with the most advanced design procedure – Performance Based Approach.

1.2 Thesis overview

Main part of this work was developed on University of Coimbra, Faculty of Sciences and Technology, Department of Civil Engineering. Furthermore, this work is continuation of a previous SUSCOS thesis (Thermal analysis of steel columns exposed to localised fires, Gonçalo Ferraz, Coimbra, 2014).

Main task of this work was to perform an analysis to investigate behaviour of a steel column exposed to a localised fire, using performance based approach and compare it with prescriptive rules given by Eurocode (thermal action defined by Standard temperature-time curve).

As it is known, the performance based approach involves the assessment of three basic components, namely the fire modelling, the thermal analysis and the structural response.

Fire modelling was performed using CFD analysis of development of fire temperatures based on real fire scenario from experiments conducted as a part of previously mentioned SUSCOS thesis. Experiments included investigation of temperature evolution along the steel column exposed to a localised pool fire. CFD analysis was performed using CFD model Fire Dynamics Simulator (FDS) where thermal action was defined by the combustion and complex pyrolysis model of a diesel pool fire. Real thermal action within fire compartment was simulated, furthermore, steel temperatures were obtained using 1D heat transfer calculation.

Thermal analysis was performed in order to resolve 3D heat transfer phenomena using Finite Element software Abaqus/CAE. Heat transfer from flame consist of three basic components namely convection, radiation and conduction. As an input to resolve heat transfer and calculate steel temperatures adiabatic surface temperatures obtained from fire model were used, as well as standard temperature-time fire curve proposed by EN1992-1-2.

Structural analysis presents last step of the performance based approach. Purpose of structural analysis was to investigate behaviour of the steel column exposed to a localised fire. Nonlinear analysis with geometric imperfections included was carried out using same Finite Element software Abaqus/CAE. Thermal load was based on temperatures calculated within thermal analysis and combined with several axial compression load cases. Finally, comparison is made for column subjected to a thermal load calculated using standard temperature-time curve.

1.3 Thesis organization

This thesis consists of four chapters, shortly described in following text.

Chapter 1 – Introduction

This chapter presents an overview of a fire engineering from its early beginnings until now. It provides the reader briefly description of this thesis, focusing on most important parts of it.

Chapter 2 – Literature review

Chapter 2 consists of seven sections which covers literature review related to this thesis. First Section describes thermal action analysis methods provided by Eurocode (EN1991-1-2 (2002)) [27]. Second Section consists of theory background of the pool fires. Third and fourth sections are dealing with the theory behind Computational Fluid Dynamics and its model Fire Dynamics Simulator. Basic model algorithms are described, as well as the area of usage, limitations etc. In fifth section theory behind heat transfer phenomena is described. Sixth section covers description of methods used within structural analysis. Geometrical material non-linear analysis with imperfection included, used in this thesis, is described as well. Last but not least, experimental background for this thesis is briefly described.

Chapter 3 – Performance based approach

This chapter deals with performance based approach on analysis of steel column exposed to a localised fire. It is divided in three sections covering CFD, Thermal and Structural analysis. Process of numerical modelling is described, furthermore, results are presented and discussed.

Chapter 4 – Conclusions

Final chapter consists of summary of this thesis, conclusions are drawn as well as suggestions for future work.

2 LITERATURE REVIEW

2.1 Thermal actions for temperature analysis according to EN1991-1-2:2002

2.1.1 Introduction

EN 1991-1-2 describes the thermal and mechanical actions for the structural design of buildings exposed to fire, including following aspects of safety requirements:

‘‘The construction works must be designed and build in such a way, that in event of an outbreak of fire:

- The load bearing resistance of the construction can be assumed for a specified period of time;
- The generation and spread of fire and smoke within the works are limited;
- The spread of fire to neighbouring construction works is limited;
- The occupants can leave the works or can be rescued by other means;
- The safety of rescue teams is taken into consideration’’.

A full analytical procedure for structural fire design would take into account the behaviour of the structural system at elevated temperatures, the potential heat exposure and the beneficial effects of active and passive fire protection systems, together with uncertainties associated with these features and the importance of the structure (consequences of failure).

Application of this part of Eurocode 1-2 is illustrated below. The prescriptive approach and the performance-based approach are identified. The prescriptive based approach uses nominal fires to generate thermal actions, while the performance-based approach, using fire safety engineering, refers to thermal actions based on physical and chemical parameters.

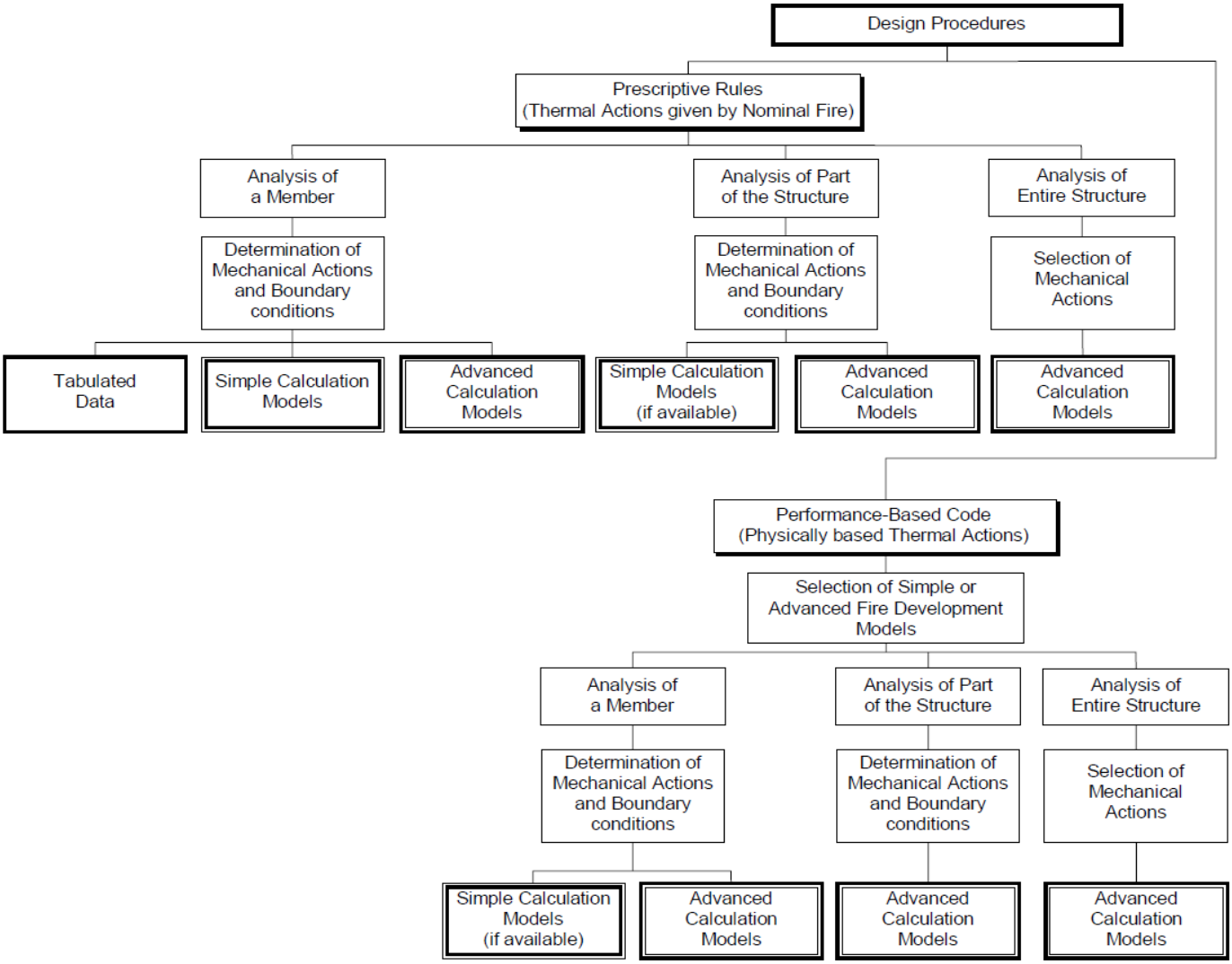

Figure 1: Design procedures according to EN 1991-1-2 (2002)

There is several different ways to define thermal action. EN 1991-1-2 (2002) prescribes two major groups of fire models: *nominal fire curves* and *natural fire models* which are described below.

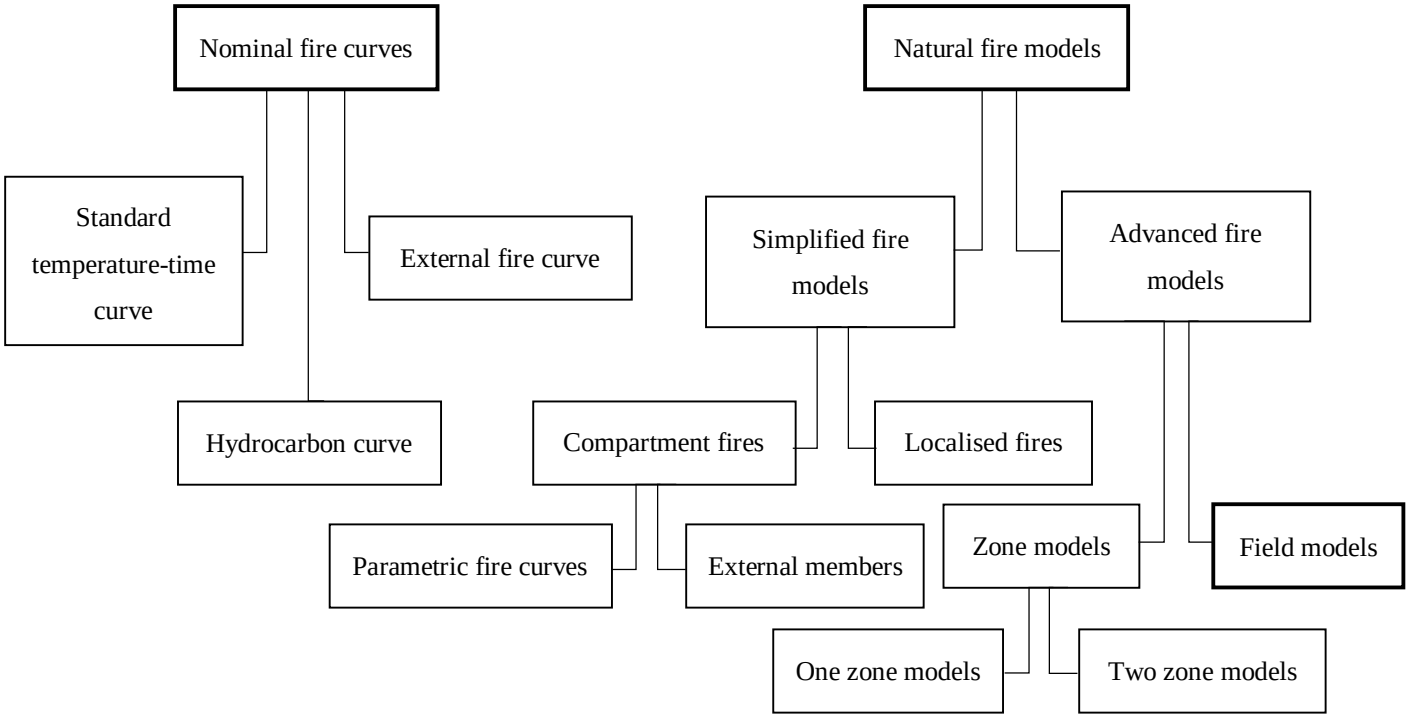

Figure 2: Schematic classification of fire models

The level of complexity increases from Simple nominal fire curves to the Field models, which is subject of this paper. Nominal fire curves and Simplified models represents a less complex and less time consuming methods, whereas, on the other hand Zone models and Field models represents Advanced fire modelling methods, which requires very detailed input and significant computational time. The most appropriate method has to be chosen depending on amount of resources, importance of observed structure, etc.

Following sections describes basics of standard procedures of thermal actions for temperature analysis.

2.1.2 Nominal temperature-time curves

Nominal temperature-time curves represents conventional curves which are adopted for classification or verification of fire resistance. They are representative fires that can be expressed by a simple formula and are used for purposes of classification of fire resistance, but without relationship to the observed subject (fire load, ventilation conditions etc.).

According to EN 1991-1-2 (2002) they can be classified as: *Standard temperature time-curve (ISO 834), External fire curve* and *Hydrocarbon curve.*

2.1.2.1 Standard temperature-time curve

The international standard fire curve ISO 834 representing a model of a fully developed fire in a compartment is often used to test the fire resisting properties of building components.

In EN 1991-1-2 (2002) the gas temperature is given by expression:

$$\theta_g = 20 + 345\log_{10}(8t+1) \qquad \text{(Eq. 1)}$$

Where:

θ_g - gas temperature in fire compartment (°C)

t - time (min)

Coefficient of heat transfer by convection should be taken as α_c=25 W/m^{2}K.

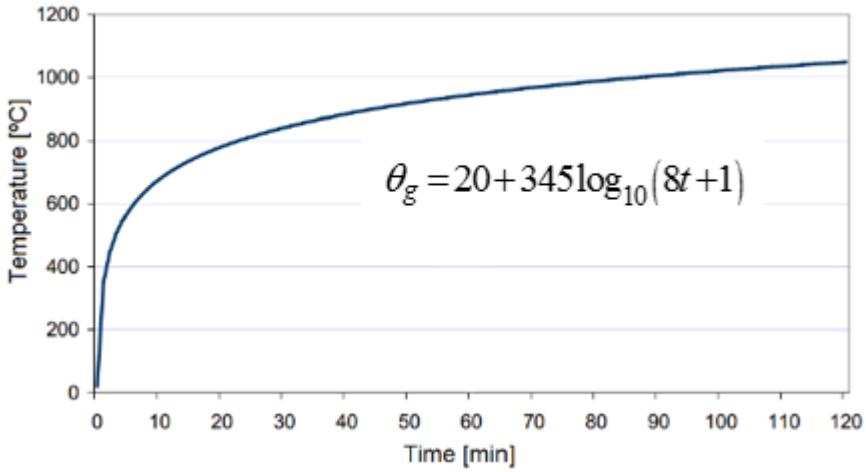

Figure 3: Standard time-temperature curve ISO 834

2.1.2.2 External fire curve

External fire curve represents a nominal temperature-time curve intended for the outside of separating external walls which can be exposed to fire from different parts of the façade, i.e. directly from the inside of the respective fire compartment or from a compartment situated below or adjacent to the respective external wall.

The external fire curve is given in EN 1991-1-2 (2002) by formula:

$$\theta_g = 660\left(1 - 0.687e^{0.32t}\, 0.313e^{-3.8t}\right) + 20 \qquad \text{(Eq. 2)}$$

Where:

θ_g - gas temperature near the member (°C)

t - time (min)

Coefficient of heat transfer by convection should be taken as α_c=25 W/m^{2}K.

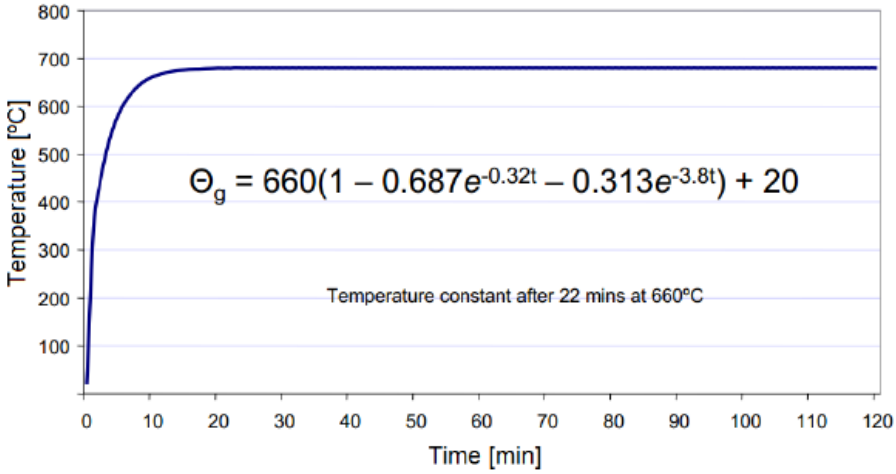

Figure 4: External fire curve

2.1.2.3 Hydrocarbon curve

The hydrocarbon fire curve is used for representing the effects of a hydrocarbon type fire. This curve is applicable where small petroleum fires might occur. This curve is more severe in comparison with previous two curves. It increases very quickly and reaches constant value of 1100°C after 30 min.

The hydrocarbon curve is given in EN 1991-1-1-2 (2002) by formula:

$$\theta_g = 1080\left(1 - 0.325e^{-0.167t} - 0.675e^{-2.5t}\right) + 20 \qquad \text{(Eq. 3)}$$

Where:

θ_g - gas temperature near the member (°C)

t - time (min)

Coefficient of heat transfer by convection should be taken as α_c=50 W/m^{2}K.

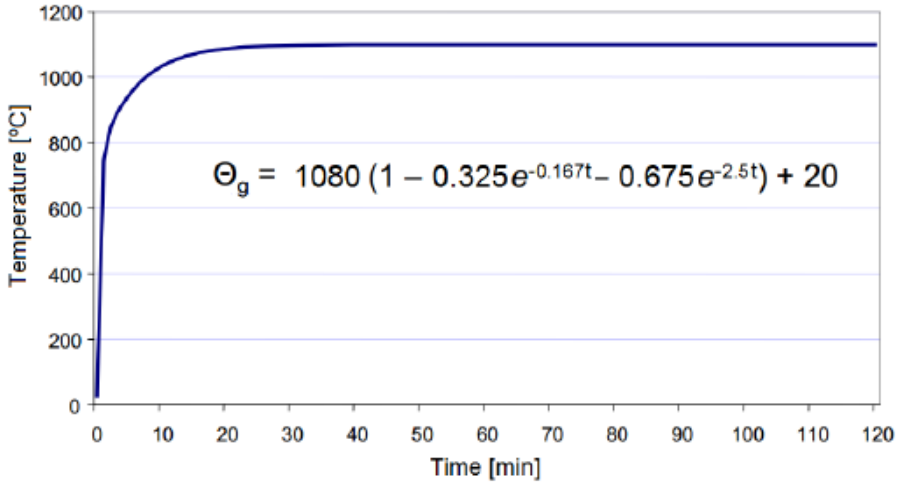

Figure 5: Hydrocarbon fire curve

2.1.3 Natural fire models

2.1.3.1 Simplified fire models

Simplified calculation method is based on specific physical parameters with a limited field of application. The temperature is determined from compartment fire models or from localised fire models, which depend, among other parameters, on the fire load and characteristics of the compartment in fire.

Simplified fire models are classified as a *compartment fires* and *localised fires.*

When using the simplified fire models, the coefficient of heat transfer by convection should be taken as α_c=35 W/m^{2}K.

2.1.3.1.1 Compartment fires

For compartment fires general assumption is that temperature is distributed as a uniform as a function of time. The gas temperature depends, among the other parameters, on the density of fire load and ventilation conditions. EN 1991-1-2 (2002) presents two methods for modelling these fires: *the parametric fire curves for inside compartments (Annex A)* and *the method for thermal action for external members (Annex B).*

Parametric fire curves define the evolution of gas temperature as a function of time, based on parameters that influence the development of the fire in a compartment. The parametric temperature-time described in Annex A of EN 1991-1-2 (2002) is valid for fire compartments up to 500m^2 of floor area, without openings in the roof and for maximum compartment height of 4 m and are based on the assumption that the fire load of compartment is completely burnt out.

Simplified calculation of ***thermal actions on external elements*** to the compartment fire is provided by Annex B of EN 1991-1-2 (2002). This method can be applied only for the fire loads higher than 200 MJ/m^2 and the size of compartment should not exceed 70 m in length, 18 m in width and 5 m in height. This method assumes a steady state situation of a fully developed compartment fire and does not consider the fire pre-flashover and cooling down phases.

Annex B of EN 1991-1-2 (2002) also considers the effects of the wind on the model. According to this Annex, the flames can leave the fire compartment through the windows either perpendicular to the façade or at a horizontal angle of 45° to the façade as shown in the following figure.

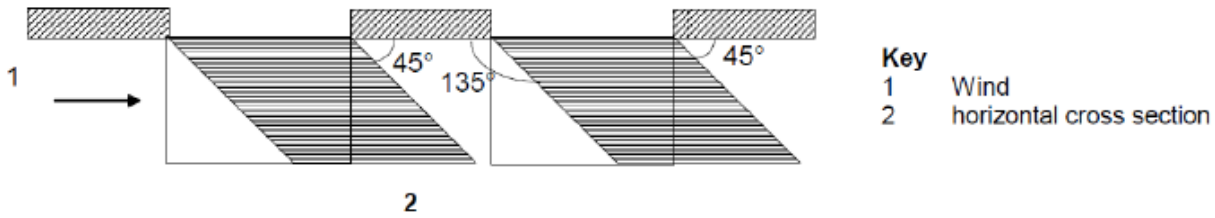

Figure 6: Deflection on flame by wind - EN 1991-1-2 (2002)

This method gives equations for the determination of the maximum temperatures of a compartment fire, the size and temperatures of the flame from openings and the radiation and convection parameters both with forced and no forced draught conditions.

2.1.3.1.2 Localised fires

Localised fire is considered as a fire involving only a limited area of the fire load in the compartment. Thermal actions of a localised fire should be taken into account only in

cases where flash-over is unlikely to occur. EN 1991-1-2 (2002) provides a simple approach for determining the thermal action of localised fires in Annex C. Depending on the height of the fire plume relative to the ceiling of the compartment, a localised fire can be defined as either a small fire or a large fire. For small fire, a design formula is given to calculate the temperature in the plume along the vertical flame axis. For a big fire, some simple steps have been developed to give the heat flux received by the fire exposed surfaces at the ceiling level.

The limitations of this approach include:

- The diameter of fire: D≤10 m;
- The heat release rate of the fire: Q≤50MW.

However, this approach can be applied to the cases of two localised fires:

- Smaller fires or Open air fires;
- Larger fires impacting ceiling.

Smaller fires

In a localised fire the highest temperature is at the vertical flame axis, decreasing toward the edge of the plume. The flame axis temperature changes with height. It is roughly constant in the continuous flame region and represents the mean flame temperature. The temperature decreases sharply above the flames as an increasing amount of ambient air is entrained into the plume [25]. EN 1991-1-2 (2002) provides a design formula to calculate the temperature in the plume of a small localised fire, based on the fire plume model developed by Hesketad [26] which can be applied to an open-air fires as well. The flame height L_f of the fire is given by:

$$L_f = -1.02D + 0.0148Q^{2/5} \qquad \text{(Eq. 4)}$$

Where:

D – diameter of the fire (m)

Q – heat release rate of the fire (W)

H – distance between the fire source and the ceiling (m)

In case the fire is not impacting ceiling of the compartment when $L_f<H$, or fire in open spaces, the temperature $\Theta_{(z)}$ in the plume along the symmetric vertical flame axis is given by:

$$\Theta_{(z)} = 20 + 0.35 Q_c^{2/3} (z - z_0)^{-5/3} \leq 900 \qquad \text{(Eq. 5)}$$

$$z_0 = -1.02D + 0.0524 Q^{2/5} \qquad \text{(Eq. 6)}$$

Where:

Q_c - the convective part of the heat release rate (W), with $Q_c = 0.8Q$ by default;

z – the height along the flame axis (m);

z_0 - the virtual origin of the axis (m).

The virtual origin z_0 depends on the diameter of the fire and the heat release rate. This empirical equation has been derived from experimental data. Value z_0 may be negative and locate beneath the fuel source, indicating that the area of the fuel source is large compared to the energy being released over that area. For fire sources where the fuel releases high energy over a small area, z_0 may be positive and located above the fuel source.

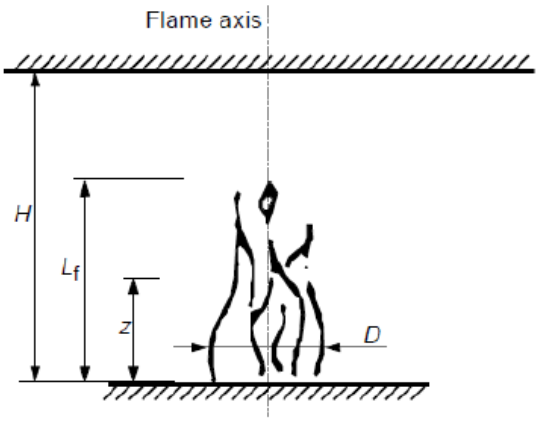

Figure 7: Schematic representation for small localised fires (27)

Larger fires impacting ceiling

When a localised fire become large enough with $L_f > H$, the fire flame will impact the ceiling of the compartment. The ceiling surface will cause the flame to turn and move horizontally beneath the ceiling. EN 1991-1-2 (2002) presents some design formulas, based on the fire plume model developed by Hasemi [28]. Following figure presents a schematic diagram of a localised fire impacting the ceiling with the ceiling jet flowing beneath an unconfined ceiling. As the ceiling jet moves radially outward, it loses heat to the cooler ambient air being entrained into the flow, as well as the heat transfer to the ceiling. Generally, the maximum temperature occurs relatively close to the ceiling [25].

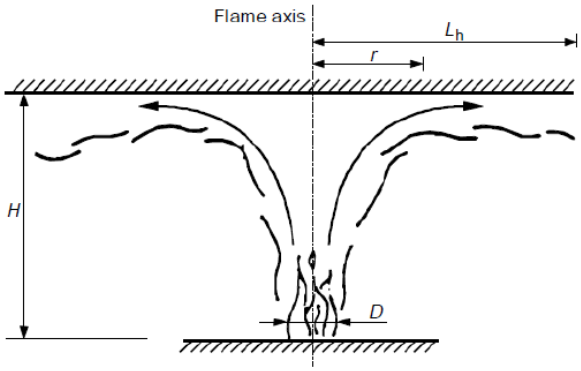

Figure 8: Representation of localised fire impacting ceiling (27)

EN 1991-1-2 (2002) only provides design formulas to determine the heat flux received by the surface area at the ceiling level, but not for calculating the ceiling jet temperatures. Considering a localised fire impacting ceiling of the compartment as shown in previous figure ($L_f > H$), the horizontal flame length (L_h) is given by:

$$L_h = (2.9H(Q^*_h)^{0.33}) - H \qquad \text{(Eq. 7)}$$

$$Q^*_h = \frac{Q}{1.11 \cdot 10^6 \cdot H^{2.5}} \qquad \text{(Eq. 8)}$$

Where:

L_h - horizontal flame length (m)

H - distance between the fire source and the ceiling (m)

Q^*_h - non-dimensional HRR

Q - HRR of the fire (W)

2.1.3.2 Advanced fire models

Advanced fire models take into account the gas properties, mass and energy exchange processes associated with real compartment fires, which means that they are able to predict compartment gas temperatures in a much more accurate way than simplified models. The advanced calculation models include iterative procedures that may require considerable computational effort. These models are suited well for the calculation of fire load density and HRR. If there is no detailed information available, the coefficient of heat transfer by convection should be taken as α_c=35 W/m^{2}K.

According to the EN 1992-1-2 (2002) Advanced fire models are classified as:

- Zone models: -one zone models
  -two zone models
- Field models: Computational Fluid Dynamics models (CFD)

2.1.3.2.1 Zone models

Zone models can be divided in one or two zones, with an assumption of the uniform temperature for each zone. Most of developed software's are based on the basis of differential equations expressing mass balance and energy balance equilibrium.

The ***one zone models*** should apply for post-flashover conditions where the whole compartment is defined as a one single zone with a uniform, time dependent distribution. Temperature, density, internal energy and gas pressure in the compartment are assumed to be homogeneous. In this models temperature is calculated by considering the resolution of equations of mass and energy conservation.

The ***two zone models*** represents a pre-flashover situation. According to Annex D of EN 1991-1-2 (2002), a two zone model is based on the assumption of accumulation of combustion products in a layer beneath the ceiling, with a horizontal interface. In these models, different zones should be defined: an upper layer (corresponding to the part where the smoke and toxic gases accumulate, where uniform characteristics of gas are assumed), a lower layer (where the temperature is lower), fire and its plume, external gas and the walls. Two zone models allow the calculation of exchanges of mass, energy and chemical substance between the different zones. In a given fire compartment with a uniformly

distributed fire load, a two zone fire model may develop into a one-zone fire in one of the following situations: if the gas temperature of the upper layer gets higher than 500°C, or if the upper layer is growing so to cover 80% of the compartment height.

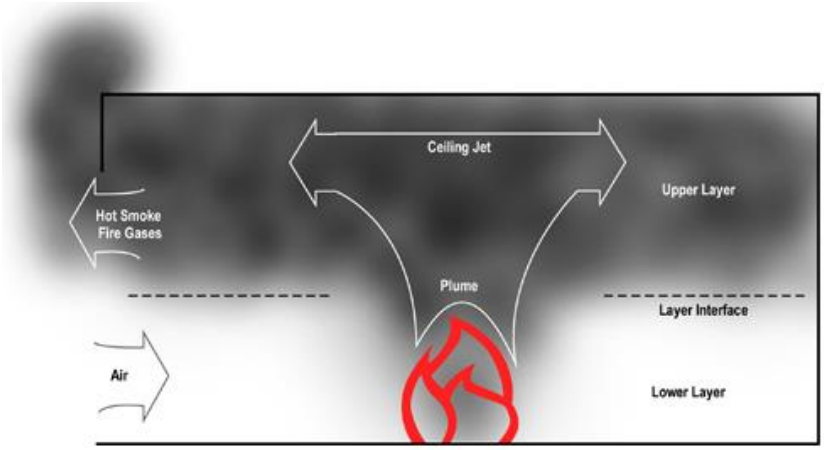

Figure 9: Schematic representation of two-zone model

2.1.3.2.2 Field models – Computational Fluid Dynamics models (CFD)

A CFD models may be used to solve numerically the partial differential equations giving, in all points of the compartment, the thermo-dynamic and aero-dynamic variables. It represents the most sophisticated modelling method and become increasingly popular in fire safety engineering. CFD models analyse systems involving fluid flow, heat transfer and associated phenomena by solving the fundamental equations of the fluid flow. These equations represent the mathematical statements of the conservation laws of physic:

- The mass of a fluid is conserved;
- The rate of change of momentum equals the sum of the forces on a fluid particle (Newton's second law);
- The rate of change of energy is equal to the sum of the rate of heat increase and the rate of work done on a fluid particle (first law of thermodynamics)

Since this work is focused on fire modelling using Field models, more detailed description on how CFD model works will be presented in following Chapters *2.3* and *2.4.*

2.2 Pool fires

2.2.1 Introduction

Pool fires represents one of the most common accidental events which can occur within an industrial installation, however, since it is generated by the ignition of the release of any flammable liquids, it can actually happen in a wide range of situations, like during the transportation of traditional liquid fuels from storage or production sites to the final destination as well as in everyday life conditions. The size of pool fires span several orders of magnitude, from matches (10^{-3} m) to fuel spills (10^{2} m). Unless a very large release has occurred, the consequences of such an event are usually limited to a relatively small area surrounding the location of the leak, compared with other more harmful accidents characterized by larger impact areas and more serious consequences such as domino effect.

Pool fires are a serious hazard to many industrial applications. The damages caused by a liquid fire are mainly connected with the heat radiated in the surrounding area, which depends on a number of parameters: the energy per unit time emitted by the flame, the distance from the fire, the characteristics of the target surface receiving the radiated heat, and a number of the other environmental conditions. Risk assessments in such applications require the availability of methodologies to predict with an acceptable degree of accuracy and fundamental outcomes.

Figure 10: Example of a pool fire [51]

Pool fires are buoyancy-drive diffusion flames fed by the vaporization of a horizontally aligned, condensed-phase fuel. Although the name implies that the fuel is a liquid, it may be a gas or a solid. The fuel bed may be of an arbitrary geometry, but for the simplicity, most studies consider a circular configuration characterized by a single geometrical scale – the pool diameter *(d)*. This was justified by Blinov and Kudiakov [3]; who demonstrated that burning rates of pool are a function of *d,* which determines the surface area of the fuel exposed to the oxygen. Although the fire hazard depends mostly on fuel properties and diameter of the pool, it also depends of quantity of the fuel and ambient conditions such as the absence or presence of an enclosure, a hot surface, wind currents or ventilation.

In theory, the heat received by a given target might be calculated by means of the classical Stefan-Boltzmann equation, but due to the wide range of variability of the involved parameters and to the uncertainty in their quantitive assessment, a number of theoretical and semi-empirical models have been proposed over the years and are still commonly adopted by safety engineers. Since they do not require the knowledge of many specific input parameters, another advantage of these correlations lies in the fact that they can be easily applied in a number of applications where a great amount of quick calculations have to be carried out, such as in Risk Analysis.

Nevertheless, because of lack of experimental data, uncertainties are still present about their practical applicability. In this view, and with reference to other dangerous phenomena like explosions, it has already been shown that an assessment of the reliability and of the range of applicability of these models of the higher importance (Bubbico and Mazzarota, 2013). [16]

Following sections are written mainly according to [17].

2.2.2 Heat Release Rate – HRR

The rate of which energy is released in a fire ($\dot{Q}_c$) is the most important single factor characterizing its behaviour. If the HRR is known, it can among other things be used to estimate the flame size and radiation to surroundings, and assess likely flame behaviour in practical situations. Energy released in a fire is the total amount of heat generated as a result of chemical reactions in the combustion.

$$E_{ch} = E_{convective} + E_{radiative} \qquad \text{(Eq. 9)}$$

The most accurate experimental method to determine rate of heat release is the method of oxygen consumption calorimeter (cone calorimeter), which is one of the most accurate and practical technique. A short introduction of this method based on [18] and [19] is further described.

The basis of this method is that most gases, liquids and solids release a constant amount of energy for each unit mass of oxygen consumed. After ignition, the combustion products are collected in a hood and removed trough exhaust duct in which the flow rate and compostion of the gases is measured to determine how much oxygen has been consumed. HRR is then calculated using the constant relationship between oxygen consumed and energy released.

There are limitations in fire sizes when using the cone calorimeter. As an alternative method, HRR is measured based on mass loss rate using simple scale (weight equipment). The time dependent mass loss rate measured from the fire experiment can then be used in the following equation to calculate the HRR [19].

$$\dot{Q}_c = \chi \cdot \Delta H_c \cdot \dot{m}'' \cdot A_f \quad \text{(kW)} \qquad \text{(Eq. 10)}$$

Where χ is a factor (<1) which is included to account for incomplete combustion ΔH_c is the heat of combustion of the colatiles (kJ/g), $\dot{m}''$ is the rate of burning or mass flux given as (g/m^{2}s) and A_f is the fuel surface area (m^2).

2.2.2.1 Heat of combustion and combustion efficiency

The heat of combustion (ΔH_c) value describes amount of energy released or consumed during complete combustion between fuel and oxygen. A reaction where energy is released (negative ΔH_c) is called exothermic.

Heat of combustion is normally determined using a ‘bomb’ calorimeter. In this method the volume is constant and a known mass of fuel is burnt completely in an atmosphere of pure oxygen. The change in enthalpy (ΔH_c) can also be calculated using the heat of formation (ΔH_f) values for all reactants and products in the chemical reaction. The heat of formation is defined as the enthalpy change when a compound is formed in its standard state from its constituent elements also in their standard states [19].

$$\Delta H_c = \frac{\Sigma \Delta H_{fproducts} - \Sigma \Delta H_{freactants}}{n_{fuel}} \quad \text{(kJ/mol)} \qquad \text{(Eq. 11)}$$

Since the enthalpy change is given for complete combustion it is necessary to correct it for incomplete combustion in a fire scenario. From [18] the combustion efficiency factor χ which account for incomplete combustion are defined as:

$$\chi_{ch} = \frac{\dot{Q}_{ch}"}{\dot{Q}_T"} = \frac{\dot{m}"\Delta H_{ch}}{\dot{m}"\Delta H_T} = \frac{\Delta H_{ch}}{\Delta H_T} = \frac{\Delta H_{convection} - \Delta H_{radiation}}{\Delta H_T} \qquad \text{(Eq. 12)}$$

Where $\dot{Q}_T"$ and ΔH_T are for complete combustion and $\dot{Q}_{ch}"$ and ΔH_{ch} are the chemical rates for the given fire. As described in [18] combustion efficiency generally depends on the fuel, ventilation conditions, soot production and flame site. The distribution of the chemical heat into convective and radiative components changes with fire size. Generally, larger fire size gives larger fraction of the chemical heat distributed into the radiative component. A clear sign of incomplete combustion is when the flame produces soot. Clean burning gaseous fuels such as methane has χ close to 1.

As described above the combustion efficiency (χ) is not only dependent of the fuel. For heptane liquid different combustion efficiency values are documented in literature, see table below. Experiments performed by Tewarson (2004) shows that for well ventilated pool fires within the range 0.1-2.0m, χ is weakly dependent of fire diameter. McCaffrey and Harkleroad (1989) studied heptane among other fuels in a O_2 depletion calorimetry. They found that the combustion efficiency varied with pool diameter. Work performed by Koseki and Mulholland (1991) showed that increased pan diameter lead to increased CO/CO_2 ratio. This increase in smoke and CO lead to decreased combustion efficiency.

Table 3. Combustion efficiency (χ) values for heptane and crude oil

χ	χ_{rad}	χ_{conv}	**Conditions**	**Reference**
0.69	0.316	0.374	Small diameter (cca 0.1m) External heat flux controlled	Table 5.12 (19)
0.924	0.305	0.619	Small diameter (cca 0.1m) Well ventilated External heat flux controlled	Table 3-4.14 (18)
0.94	-	-	Diameter of 0.5m	(20)
0.8	-	-	Diameter of 0.3m	
0.8±0.1	-	-	Diameter of 0.71-1.60m	(21)

2.2.2.2 Mass burning rate

This section is based on the book ‘‘An introduction to fire dynamics’’ by Drysdale (1999) [19].

The rate of supply of volatiles from a fuel surface is dependent of the rate of heat transfer from the flame to the fuel. In fire scenarios where radiation from surrounding equipment or smoke layer (outdoor) is neglected, the mass flux ($\dot{m}''$) is described by following equation:

$$\dot{m}'' = \frac{\dot{Q}''_F - \dot{Q}''_L}{L_v} \quad \text{(kg/s)} \qquad \text{(Eq. 13)}$$

Where $\dot{Q}''_F$ is the heat flux supplied by the flame (kW/m^2) and must in turn be related to the rate of energy released within the flame and the mechanism of heat transfer involved $\dot{Q}''_V$. $\dot{Q}''_L$ represent the losses expressed as a heat flux trough the fuel surface (kW/m^2) and L_v is the heat required to produce the volatiles (kJ/kg). This means that liquids have a lower L_v value than solids where chemical decomposition is involved.

In liquid pool fires the heat flux $\dot{Q}"_F$ from the flame to the liquid is expressed as the sum of the three terms, these are: *conduction, convection and radiation*. Conduction refers to heat transfer trough the rim of the container, expressed as:

$$\dot{q}"_{conduction} = k_1 \pi D(T_F - T_L) \quad \text{(W)} \qquad \text{(Eq. 14)}$$

Where T_F is flame temperature, T_L the liquid temperature, D is the diameter of the pool and k_1 is a constant which incorporate a number of heat transfer terms. Convection direct to the fuel surface is given by:

$$\dot{q}"_{convection} = k_2 \frac{\pi D^2}{4}(T_F - T_L) \quad \text{(W)} \qquad \text{(Eq. 15)}$$

Where k_2 is the convective heat transfer coefficient (h). The radiation to the surface can be expressed as:

$$\dot{q}"_{radiation} = k_3 \frac{\pi D^2}{4}(T^4{}_F - T^4{}_L)(1 - \exp(-k_4 D) \quad \text{(W)} \qquad \text{(Eq. 16)}$$

Where k_3 contains the Stefan-Boltzmann constant (σ) and the configuration factor (ϕ) for heat transfer from the flame to the surface, while $(1 - \exp(-k_4 D)$ is the emissivity of the flame. The factor k_4 must contain a factor of proportionality relating the mean beam length to the pool diameter, but also concentration and emission coefficients of the radiating species in the flame. The k_4 constant must also incorporate a factor for radiative blocking [19] when the vapours zone above the fuel becomes sufficiently thick to attenuate the flux falling on the surface.

Conductive heat transfer determines the mass burning rate when *D* is very small, but provided that the emissivity is of sufficient magnitude, radiation dominates for large pool diameters. The heat conduction trough the rim of the container is also a minimalistic contribution on a pool fire. This means that for most pool fires (no radiation from surroundings) it is only relevant to consider the radiation contribution from the flame back to the liquid and losses from the liquid surface.

2.2.2.3 Regression rate and flame behaviour

Blinov and Khudiakov (1957) studied the rates of burning for different pool sizes with different hydrocarbon liquids. They discovered that the rate of burning expressed as a

'regression rate' *R* (mm/min) was high for small-scale laboratory pools and exhibited a minimum around 0.1m diameter. From their results the regression rate dependents of pool sizes seems to be distinguished in three regimes. When the diameter is less than 0.03m, the flames are laminar and the regression rate, *R*, falls with increase in diameter. For larger diameters (D>1m) the flames are fully turbulent and *R* becomes independent of diameter. In the region with pool diameters from 0.03m to 1.0m transitional behaviour, between laminar and turbulent, is observed.

Following figure shows different fuels with different pool sizes regression rate.

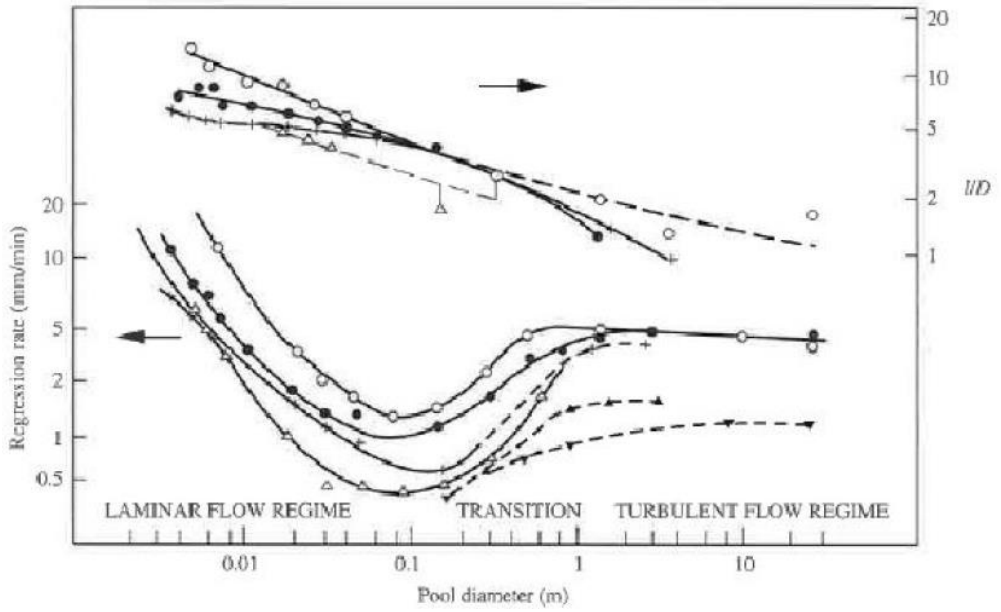

Figure 11: Regression rates and flame height results for liquid pool fires with diameters in the range 3.7 x 10-3m to 22m Gasoline (¤), tractor kerosene (•), diesel oil (+), petroleum oil (▲),mazut oil (▼), solar oil(Δ) ((Blinov and Khudiakov, 1957, 1961; Hottel, 1959) reported in Drysdale (1999))

2.2.3 Radiation

Liquids normally burn with luminous diffusion flames. The characteristic yellow luminosity is the net effect of emission from minute carbonaceous particle, known as *soot.* These particles (D=10-100nm) are formed within the flame, mainly on the fuel side of the reaction zone. If the particle does not burn as they pass through the oxidative region of the flame they will escape from the flame tip to form smoke. Generally the sootier the flame is the lower is the flames average temperature. This mainly because the soot particles in the

flame will attain high temperatures and act as minute black or grey bodies that radiate energy away from the flame.

As described in following equation the emissivity (ε) is an important parameter when describing in the radiation from a flame. Emissivity can be expressed with the following equation [19]:

$$\varepsilon = 1 - \exp(-KL) \qquad \text{(Eq. 17)}$$

Where L is the thickness of the flame or smoke layer and K is the effective emission coefficient which is dependent of the particle concentration of soot. To consider the radiation effect from a pool fire to a point in a distance *R (m)* from the fire following equation can be used:

$$\dot{q}''_R = \frac{\chi_{rad} \cdot \dot{m}'' \cdot \Delta H_c \cdot A_f \cdot \cos\theta}{4\pi R^2} \ (\mathrm{W/m^2}) \qquad \text{(Eq. 18)}$$

In the equation above it is assumed that the radiation originates from a point source on the flame axis at a height of *0.5l* above the pool surface. However, if the receiving point is at an angle θ, the heat flux $(\dot{q}''_R)$ will be reduced by a factor *cos* θ. If the amount of radiation from a fire is unknown it's sometimes assumed to be 0.30 [19].

2.2.4 Flame height

When working with fire safety design the flame height of a pool fire is an important factor that needs to be considered. Flame height may for instance affect fire heating of building structure, fire suppression systems, fire ventilation and escape possibilities. The height of the flame typically depends on the mass burning rate and the ventilation conditions. There are different methods defining the flame height criteria. Flame height is height at which flame is observed at least 50% of the time. Pool fire has highly intermittent pulsing structure, particular along its perimeter and near its top. This intermittence is driven largely by the turbulent mixing of air and subsequent combustion.

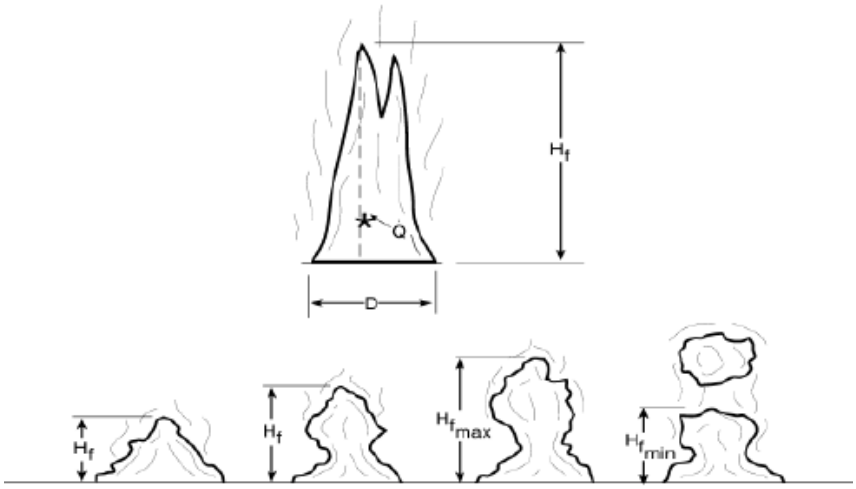

Figure 12: Flame structures (Naeem Iqbal, 2004)

From [18] two correlation defined by Heskestad and Thomas can be used to calculate the flame height of pool fires with no cross-wind:

$$H_f = 0.235\dot{Q}_c^{2/5} - 1.02D \quad \text{(m)} \qquad \text{(Eq. 19)}$$

$$H_f = 42D\left(\frac{\dot{m}''}{\rho_a\sqrt{gD}}\right)^{0.61} \quad \text{(m)} \qquad \text{(Eq. 20)}$$

Where D is the pool diameter, ρ_a is the ambient air density (kg/m^3) and $\dot{m}''$ is the rate of burning given as (g/m^{2}s). Equation 25 is valid only for normal atmospheric conditions.

2.2.5 Air entrainment and flame temperatures

The maximum possible theoretical temperature in fuel/oxidant combustion is called adiabatic flame temperature. This theoretical temperature is based on no heat losses to the surroundings. This means that all energy released by the chemical reaction is used to raise the temperature of the products (CO_2, H_2O and N_2 in fuel/air reaction). For instance, the adiabatic flame temperature for a heptane/air mixture is given as 1419°C (Table 1-5.6 in (18)). If the fuel is burnt in pure oxygen these temperatures are higher due to the heat of combustion is not used to raise the temperature of nitrogen.

Unlike a premixed flame where the mixing between fuel and air is quite homogeneous the flame zone of diffusion flames (pool fires) is highly heterogeneous as a result of the inadequate preparation of reactants before the combustion zone [23]. This results in generally variations in temperatures depending on the position in the flame. The main reason for this temperature difference is the narrow combustion zone have lower temperatures. Turbulent mixing of air in pool fires also leads to pulsing behaviour which in turns affects the temperature of the flame. This involves widely temperature fluctuations at a fixed position, particularly around the edges and near the top of the flame. This is why flame temperature is usually reported in terms of the average centreline temperature or average flame temperature [18].

In [18] some of the early work on temperatures in turbulent diffusion flames studied by McCaffrey is described. McCaffrey studied various characteristics of a fire plume from a gas burner (methane) in a pool fire mode (non-premixed). From his work three different regimes are described for such a fire plume:

- Continuous flame region which begins a slightly above the base of the fire. In this region the temperature is some below 900°C.
- Intermittent flame region above the continuous flame region. Temperature drops as a function of distance up the flume. A temperature around 320°C in the visible flame tip.
- Thermal plume region. No visible flames, temperature continuous to drop.

Very similar results were observed by French researchers at the University of Poitiers.

From the above documentation Naeem Iqbal (2004) [18] concluded that the flame tip temperature for turbulent diffusion flames could be expected to be around 320-400°C. For the small flames (D<1m), continuous flame region temperatures around 900°C should be expected, while in large pool fires, these values can rise to 1100 to 1200 °C.

2.3 Computational Fluid Dynamics (CFD)

Computational Fluid Dynamics (CFD) is a branch of study that continues to gain in popularity and importance in the modern practice of fluid dynamics. In essence, CFD is simply study of fluid systems that could be static or dynamically changing in time and space. The fluid dynamic component is performed trough numerical methods. It is most advanced and sophisticated fire modelling technique applied to assess fire behaviour. Use of CFD for fire modelling has increased significantly during the last few years, mainly due to the increased computational power and development of fire specific computer codes. CFD is use of applied mathematics, physics and computational software to visualize how a gas or liquid flows as well as how the gas or liquid affects on object as it flows past. Physical characteristics of a fluid in motion can be usually in partial differential form, governing a process of interest. In order to solve these mathematical equations, they are converted into discrete forms using advanced computer programming languages. CFD actually covers three major disciplines: fluids engineering, mathematics and computer science.

Most models are based on the Navier – Stokes equations. These equations describe how the velocity, pressure, temperature and density of a moving fluid are related. Also, highly complex combustion models with detailed solution of gas phase flows have been presented by the combustion research community for many years. CFD models provide complete temperature-time relationships. Temperature distribution is time and space dependent. Models require very detailed input in order to solve fundamental equations of the fluid flow.

In CFD we often talk about use of a pre-processor, solver and post-processor. The pre-processor is used to define observed problem and includes definition of geometry, mesh, material properties, boundary conditions, selection of calculation models to be used and what output is required etc. The solver uses the input data to find a solution to the problem. As the conservation equations are non-linear partial differential equations they have no simple analytical solutions. Instead, field model use different kinds of numerical techniques to find the solutions. Finally, obtained results are then examined and presented using some post-processor software. [4]

2.4 Fire Dynamics Simulator (FDS)

Fire Dynamics Simulator is a Computational Fluid Dynamics model (CFD) developed at the National Institute of Standards and Technology (NIST) and VTT Technical Research Centre of Finland. It has been under development for almost 25 years. In 2000 it was first released to the public and since then it has continued improvements. Applications in Fire Safety Engineering are various, from the fire investigations and research, design of smoke control systems to the assessment of evacuation. The contents of this chapter are mainly referenced from Webb [5], Floyd [6], SFPE handbook [7] FDS Technical reference Guide [8].

Furthermore, FDS is designed to model combustion and fire driven flows. The software numerically solves a form of the Navier – Stokes equations appropriate for low Mach formulation ($M_a < 0.3$) – low speed flows, thermal buoyancy driven flow, with a focus on smoke and heat transport from fires. Basic principle is that FDS calculations are performed within a domain that is made up of rectilinear volumes called meshes and each mesh is divided into rectangular cells. The equations and the numerical algorithm are presented in the following sections. Display of the results of a FDS simulation may be performed by a visualization program called Smokeview.

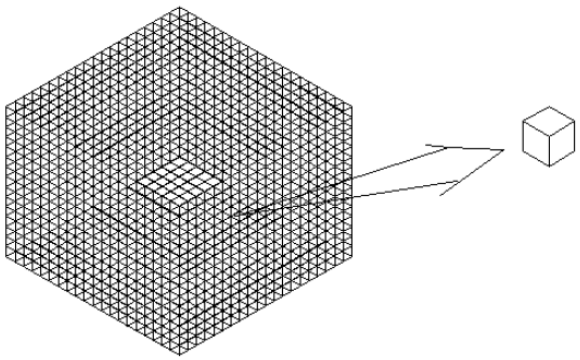

Figure 13: Schematic representation of computational domain

FDS can be used to model the following phenomena:

- Low speed transport of heat and combustion products from fire
- Radiative and convective heat transfer between the gas and solid surfaces
- Pyrolysis
- Flame spread and fire growth
- Sprinkler, heat detector and smoke detector activation
- Sprinkler spray and suppression by water

2.4.1 Treatment of turbulence

2.4.1.1 Overview of methods of treatment of turbulence

When talking about turbulence there is few methods to mention. Prior to the evolution of Large Eddy Simulation (LES), most CFD work was based on the concept provided by the Reynolds-averaged form of the Navies-Stokes equations (RANS). However, this technique has a fundamental limitation for fire. RANS models are a time-averaged approximation to the conservation equations of fluid dynamics. The averaging time is long enough to require the introduction of large eddy transport coefficients to describe the unresolved fluxes of mass, momentum and energy, what causes smoothing of the results. This property of RANS models is useful as it enables the ability to take large time steps.

The main assumption in the LES technique is that the eddies that account for most of the mixing are large enough to be calculated with reasonable accuracy from the equations of fluid dynamics, and that small-scale eddy motion can either be crudely accounted for or ignored. LES avoids time averaging of fluctuations of larger than grid scale so these are rigorously represented.

Direct Numerical Simulation (DNS) requires very fine mesh sizes (<1mm) to be able to use the diffusive parameters directly to model combustion, species behaviour, species viscosity and conductivity. The analogy of a very fine thermocouple with a near zero time constant is used, but with such fine grids domain size is restricted by computing power.

A useful analogy is presented by Cox and Kumar [7] of the fine wire thermocouple within a fire, with the results of temperature measure graphed in following Figure.

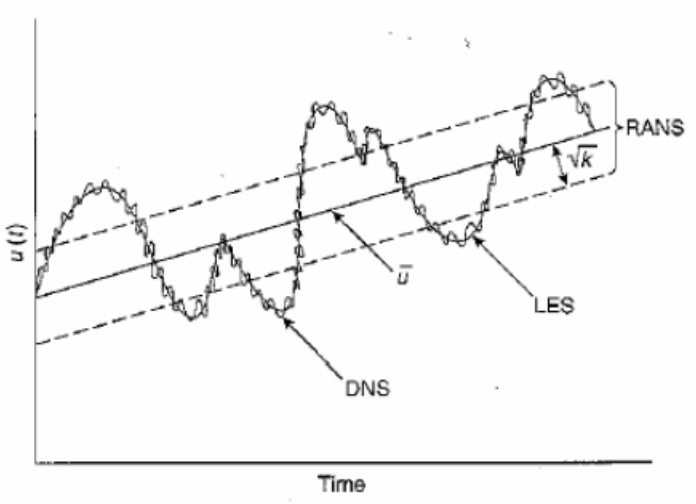

Figure 14: Schematic representation of different treatments for turbulence

The equations describing the transport of mass, momentum and energy by the fire induced flows must be simplified so that they can be efficiently solved for the parameters of interest. The calculation of relevant high speed and shock waves can also be ignored in fire simulation. The simplified equations, developed by Rehm and Baum [9], describe the low speed motion of a gas driven by chemical heat release and buoyancy forces. The low speed equations are solved numerically by dividing the physical space where the fire is to be simulated into a large number of rectangular cells. Within each cell the gas velocity, temperature, etc., are assumed to be uniform, changing only with time.

The accuracy with which fire dynamics can be simulated depends on the number of cells, limited by the computing power. Currently, the ratio of the largest to smallest eddy length scales that can be resolved is in order of 100. Combustion processes take place at length scales of 1mm or less, while the length scales associated with building fires are 10-100 meters. The range of length scales needs to be 10^4 to 10^5 to catch all fire processes.

2.4.1.2 Large Eddy Simulation (LES)

As mentioned before, in comparison with other CFD codes LES ignores aspects of flow that are not relevant to fire flows and increases the need for fine meshing and small time steps to add fidelity to the fire scale turbulence which gets smoothed in other codes.

The Smagorinsky treatment [12] of viscosity is to implement a model viscosity *(μ),* thermal conductivity *(κ),* and material diffusivity *(ϱD)* are related to viscosity. The model of

viscosity handily provides numerical stabilization as well as looking for all intents and purpose like the dissipation of kinetic energy.

Next sections consists of description of model algorithms.

2.4.2 Hydrodynamic model

FDS numerically solves a form of the Navier-Stokes equations for low speed, thermally-driven flow with an emphasis on smoke and heat transport from fires. The core algorithm is an explicit predictor-corrector scheme, second order accurate in space and time. Turbulence is treated by means of the Smagrinski form of LES. It is possible to perform DNS if underlying numerical grid is fine enough. LES is default mode of operation. In DNS the dissipative terms are computed directly. LES directly computes the large scale eddies and the sub-grid scale dissipative processes are modelled.

The conservation equations for mass, momentum and energy for a Newtonian fluid are presented below.

For the explanation of the terms, see the Nomenclature.

Conservation of Mass

$$\frac{\partial \rho}{\partial t} + \nabla \cdot \partial u = 0 \qquad \text{(Eq. 21)}$$

Conversation of Momentum (Newton's second Law)

$$\rho\left[\frac{\partial u}{\partial t} + (u \cdot \nabla) \cdot u\right] = -\nabla \cdot p + \nabla \cdot \tau + \rho \cdot g + f \qquad \text{(Eq. 22)}$$

Conversation of Energy (First Law of Thermodynamics)

$$\frac{\partial}{\partial t} \cdot (\rho \cdot h) + \nabla \cdot \rho \cdot h \cdot u = \frac{Dp}{Dt} + q''' - \nabla \cdot q + \Phi \qquad \text{(Eq. 23)}$$

Equation of state for a perfect Gas

$$p = \frac{\rho \cdot R \cdot T}{M} \qquad \text{(Eq. 24)}$$

Conversation of mass in terms of the mass fractions of individual gas

$$\frac{\partial}{\partial t}\cdot\left(\rho\cdot Y_i\right)+\nabla\cdot\rho\cdot Y_i\cdot u=\nabla\cdot\rho\cdot D_i\cdot\nabla\cdot Y_i+\dot{m}_i''' \qquad \text{(Eq. 25)}$$

2.4.2.1 Conservation of mass

The general conservation of mass equation states that the rate of mass storage within a given control volume, due to density changes, is balanced by the net rate of inflow of mass by convection. In the case of a steady flow situation, the conservation of mass equation states that what flows in must come out. Where the first term of Conservation of mass equation describes the density changes with time and the second term defines the mass convection (mass moving through a cell face). The vector *u* describes the velocity in *u, v* and *w* directions.

2.4.2.2 Conservation of species

In the presence of a vector *u*, the conservation of mass fraction Y of a chemical species *i* is given by Equation of State for a perfect Gas. Where the first term on the left side represents the accumulation of species due to change in density with time, the second term is the inflow and outflow of species from the control volume due to diffusion and production/consumption rate of particular species within the control volume caused by chemical reaction.

The mass conservation mass equation is often written in terms of the mass fractions of individual species as in Equation of Conservation of mass in terms of the mass fractions of individual gas.

2.4.2.3 Conservation of momentum

The equation for the conservation of momentum (Eq: Conversation of Energy) is derived by applying Newton's second law of motion, which states the rate of momentum of a fluid element is equal to the sum of the forces acting on it [10].

Left side of equation represents the increase of momentum and inertia forces, while right side comprises forces acting on it. These forces include pressure *p,* gravity *g,* an external force vector *f* (which represents the drag associated with sprinkler droplets that

penetrate the control volume) and a measure of the viscous stress tensor τ acting on the fluid within the control volume. Among these forces, gravity is the most important because it represents the influence of buoyancy on the flow.

2.4.2.4 Conservation of energy

The equation for Conservation of energy is the first law of thermodynamics which states that the increase in energy of the control volume is equal to the heat added minus the work done by expansion. Here the left side describes the net rate of energy accumulation, whereas the right side comprises of the various energy gain or loss terms that contribute to this energy accumulation. Notate use of material derivative, $D( )/Dt = \partial( )/\partial t\, u \cdot \nabla( )$. These include the pressure work term, energy driving the system, represented by HRR per unit volume q'''. $\nabla \cdot q$ represents the conductive term $\nabla . k \nabla T$ and radiative heat flux vector q_{rad}. The term Φ is known as dissipation function, the rate at which kinetic energy is transferred to thermal energy due to the viscosity of a fluid. The term is usually neglected because it is very small relative to the heat release rate of the fire.

The energy equation is never explicitly solved, but its source terms are included in the expression for the flow divergence.

2.4.2.5 Equation of state

The conservation of equations are supplemented by an equation of state relating the thermodynamic quantities [11]. In FDS, due to the low Mach number assumption the equation of state can be expressed in the form of:

$$p = \rho \cdot R \cdot T \cdot \sum_i (Y_i / M_i) \qquad \text{(Eq. 26)}$$

2.4.2.6 Summary

In this section we have discussed a fundamental feature of nature, namely the principle of conservation. In mathematical terms, this was described using partial differential equations. As these conservation equations involve fluid motion, they are sometimes refers to as transport equations. If these transport equations are compared to each other, it soon becomes evident that there are several similarities in the structure of the equations. They all contain one term for the time rate of change of the dependent variable, one term describing

property change due to macroscopic movement in space (or convection) and one term representing transport due to microscopic movement (or diffusion).

2.4.3 Low Mach number assumption

Unlike low speed solvers, CFD codes for high speed flows involve compressibility effects and shock waves. Low speed solvers, however, explicitly eliminate compressibility effects that give rise to acoustic waves. As written above, the Navier-Stokes equations describe the propagation of information at speeds comparable to that of the fluid flow (for fire, 10-20 m/s), but also at speeds comparable to that of sound waves (for still air, 300 m/s).

Decomposing the pressure into a ‘‘background’’ component, a hydrostatic component, and a flow induced perturbation:

$$p = p0 - \rho_\infty gz + \bar{p} \qquad \text{(Eq. 27)}$$

For most applications, p_0 is constant and the other two components are relatively small, leading to the approximation of the Equation of state.

The pressure p in the state and energy equations is replaced by the background pressure p_0.

2.4.4 Combustion model

A common source of confusion in FDS is the distinction between gas phase combustion and solid or liquid phase pyrolysis. The former refers to the reaction of fuel vapor and oxygen; the latter the generation of fuel vapor at a solid or liquid surface. Whereas there can be many types of combustibles in an FDS fire simulation, in the simple chemistry, mixing controlled combustion model there can be only one gaseous fuel. The reason is cost. It is expensive to solve transport equations for multiple gaseous fuels. Consequently, the burning rate of solids and liquids are automatically adjusted by FDS to account for the difference in the heats of combustion of the various combustibles. In effect, you specify a single gas phase reaction as a surrogate for all potential fuels.

In an LES calculation where the grid is not fine enough to resolve the diffusion of fuel and oxygen, a mixture fraction-based combustion model is used. The mixture fraction as the fraction of gas that originated as fuel. The model assumes that combustion is mixing-

controlled and that the reaction of fuel and oxygen is infinitely fast. The mass fractions of all of the major reactants and products can be derived from the mixture fraction by means of ‘‘state relations’’, empirical expressions arrived at by a combination of simplified analysis and measurement.

The state relation for the oxygen mass fraction provides the information needed to calculate the local oxygen mass consumption rate. Classical laminar diffusion flame theory and requirement that fuel and oxygen simultaneously vanish when reacting leads to a ‘‘flame sheet’’ model. The local heat release rate assumes that the heat release rate is directly proportional to the oxygen consumption rate (at the flame surface), independent of the fuel involved.

The mixture fraction is defined as:

$$Z = \frac{sY_F - (Y_0 - Y_0^\infty)}{sY_F^1 + Y_0^\infty} \quad ; \quad s = \frac{\nu_0 M_0}{\nu_F M_F} \qquad \text{(Eq. 28)}$$

Z varies from Z=1 in a region containing only fuel to Z=0 where the oxygen mass fraction is ambient value, Y_0^∞. An ideal reaction of hydrocarbon fuel is used to derive the state relations.

2.4.5 Radiation transport

For most FDS simulations, thermal radiation transport is computed by default and you need not set any parameters to make this happen. Radiative heat transfer is included in the model via the solution of the Radiation Transport Equation (RTE) for a non-scattering grey gas. Soot is the most important combustion product controlling the thermal radiation from the fire hot smoke, closely followed by CO_2 and water. In optically thin flames where amount of soot is small compared to the amount of CO_2 and water, the grey gas assumption may produce significant over-prediction of the emitted radiation.

In the calculations of limited spatial resolution, the source term in the RTE requires special treatment in the neighbourhood of the flame heat because the temperatures are averaged over a grid cell. The equation is solved using a technique similar to Finite Volume Methods (FVM) for convective transport.

2.4.6 Geometry

FDS approximates the governing equations on a rectilinear mesh. Input file requires use of the rectilinear geometry that are forced by the software to conform the underlying grid. Circular geometry can be approximated by using several small rectangular obstructions. That requires finer mesh which can significantly extend calculation time. Also, more than one rectangular mesh can be used in the calculation in order to optimize calculation time.

2.4.7 Boundary conditions

By default, the outer boundary condition of the computational domain as assumed to be a solid boundary that is maintained at ambient temperature, same as all obstructions added to a model. Material properties can be drawn from the database provided. Where necessary, information about burning behaviour of the material is also included. Heat and mass transfer to and from solid surfaces is usually handled with empirical correlations, although is possible to compute directly the heat and mass transfer when performing a DNS.

2.4.8 Limitations

Although FDS can address most fire scenarios, there are limitations in all of its various algorithms. Some of the more prominent limitations are listed below. This section is mainly based on FDS User Guide [8].

2.4.8.1 Low speed flow assumption

As written in Section 2.4.3 FDS deals only with low-speed Mach numbers less than about 0.3 flows with an emphasis on smoke and heat transport from fires So, FDS cannot be used for high-speed flows, shock waves such as engine combustion or jet fires where other CFD codes can be used.

The elimination of compressible flows and high speeds enables several assumptions and a simplification to the equation of state. This limits simulation so that is not appropriate for tightly sealed enclosures and fires at altitude, which means that reasonable openings must be provided in the model.

2.4.8.2 Rectilinear geometry

Description of FDS geometry can be found in Section 2.4.6. Main limitation when modelling curved and angled structures is that the grid in FDS must be rectilinear. There are

techniques in FDS in order to lessen the effect of ‘‘saw tooth’’ obstructions used to represent non rectangular objects, but these cannot be expected to produce good results if, for example, the intent of the calculation is to study boundary layer effects.

2.4.8.3 Fire growth and spread

Because the model was originally designed to analyse industrial scale fires, it can be used reliably when the Heat Release Rate (HRR) of the fire is specified and the transport of heat and exhaust products is the principal aim of the simulation. In these cases, the model predicts flow velocities and temperatures to an accuracy within 5% to 20% of experimental measurements, depending on the resolution of the numerical grid. The most accurate calculations using FDS do not introduce significantly greater errors in these quantities than the vast majority of fire experiments.

However, for fire scenarios where the HRR is predicted rather than specified, the uncertainty of the model might be higher, because of following reasons:

- Properties of real materials and real fuels are often unknown or difficult to obtain;
- The physical processes of combustion, radiation and solid phase heat transfer are more complicated than their mathematical representations in FDS;
- The results of calculations are sensitive to both the numerical and physical parameters. Current research is aimed at improving this situation, but it is safe to say that modelling fire growth and spread will always require a higher level of user skill and judgment than that required for modelling the transport of smoke and heat from specified fires.

2.4.8.4 Combustion

As written in Section 2.4.4 FDS uses a mixture fraction-based combustion model for most applications.

Assumptions from mentioned section are working well for large-scale, well ventilated fires. However, if a fire is in an under-ventilated compartment, or if a suppression agent like water mist or CO2 is introduced, fuel and oxygen are allowed to mix and not burn, according to a few empirically-based criteria.

The physical mechanisms underlying these phenomena are complex, and are tied closely to the flame temperature and local strain rate, neither of which are readily-available in a large scale fire simulation.

Sub grid-scale modelling of gas phase suppression and extinction is still an area of active research in the combustion community.

Until reliable models can be developed for building-scale fire simulations, simple empirical rules are used by FDS that prevent burning from taking place when the atmosphere immediately surrounding the fire cannot sustain the combustion.

2.4.8.5 Radiation

Radiation transport is described in Section 2.4.5.

There are few limitations of the model:

- The absorption coefficient for the smoke-laden gas is a complex function of its compostion and temperature. Because of the simplified combustion model, the chemical compostion of the smokey gases especially the soot content, can effect both the absorption and emission of thermal radiation
- The radiation transport is discretized via approximately 100 solid angles, although the user may choose to use more angles. For targets far away from a localised source of radiation, like a growing fire, the discretization can lead to a non-uniform distribution of the radiant energy. This error is called ‘‘ray effect’’ and can be seen in visualization of surface temperatures, where ‘‘hot spots’’ show the effect of the finite number of solid angles. The problem can be lessened by inclusion of more solid angles, but at a price of longer computing times. In most cases, the radiative flux to far-field targets is not as important as those in the near-field, where coverage by the default number of angles is much better.

2.4.9 Validation and verification

The terms validation and verification [13] are often used interchangeably to mean the process of checking the accuracy of a numerical model. For many, this entails comparing model predictions with experimental measurements. According to ‘‘Standard Guide for Evaluating the Predictive Capability of Deterministic Fire Models’’ validation is:

The process of determining the degree to which a calculation method is an accurate representation of the real world form from the perspective of the intended uses of the calculation method.

And verification is:

The process of determining that the implementation of a calculation method accurately represents the developer's conceptual description of the calculation method and the solution to the calculation method.

Simply put, verification is check of the math; while validation is check of the physics. If the model predictions closely match the results of experiments, using whatever metric is appropriate, it is assumed by most that the model suitably describes, via its mathematical equations, what is happening. It is also assumed that the solution of these equations must be correct. The reason that we do verification is that model and measurement rarely agree so well in all applications. Because there is inevitably errors in the numerical solution, physical sub-models or both. On the other side, model validation consists mainly of comparing predictions with measurements.

The efforts to validate FDS have come from comparisons with full scale tests for specific evaluation, previously released publications, with standard tests, documented fire experiences and with engineering correlations. Collectively, these attempts provide useful calibration of the model.

2.4.9.1 Pool fires

Xin [14] used FDS to model a 1 m diameter methane pool fire. The computational domain was 2 m x 4 m with a uniform grid size of 2.5 cm. The predicted results were compared to experimental data and found to quantitatively reproduce the velocity field. The same authors performed similar study of a 7.1 cm methane burner and helium plume.

The 7.1 cm diameter buoyant diffusion flame has been extensively studied both experimentally and computationally. Zhou and Gore reported radial profiles of mixture fraction and vertical velocity estimation of thermal expansion for natural gas buoyant diffusion flames stabilized on a 7.1 cm diameter diffuser burner. Xin et al. used a Lagrangian thermal element based combustion model to simulate this flame. The authors noted that the simulations were sensitive to the burnout time utilized by the combustion model. To gain further insight into the species distribution inside the fire, Xin et al. performed fire dynamics simulations using a mixture fraction based combustion model. [15]

FDS studies on modelling of heptane pool fires [40] showed dependence of the burning rate on the heptane pool fire diameter, so as grid sizes as well. The concluded prerequisite was at least 20 computation grid cells within the diameter of the pool.

The cell numbers needed to define a fire suggest roughly twice as fine a grid is required for reliable prediction of burning rates of liquid fuels to predict velocities and temperatures. The reason for this is the prediction of the heat feedback to the burning surface necessary to predict rather than to prescribe the burning rate.

2.4.10 Final remarks on CFD

Fire safety engineering is relatively new area of research and it has been grown rapidly last decades, parallel with development of computational power. Until then, is was very hard and expensive to predict behaviour of fire plume and its impact on the structure, or some specific part of it.

EN 1991-1-2 (2002) proposes several fire modelling methods, from the simplest ones to the most complex ones. Our choice on fire modelling methods depends a lot of complexity of the problem we're observing as well as on amount of the every kind of resources we have.

Now days, usage of Computational Fluid Dynamics models is more and more common. Relatively low computer hardware costs are now ensuring greater accessibility, and inevitable improvements in hardware capacities are also fostering the type of CFD model that can be employed.

With the increasing complexity of modern buildings, the need to adopt high precision and growing validation of the deterministic CFD based fire models is growing, especially for performance based analyses of assess numerous fire safety aspects related to intricate

structural designs. General purpose of CFD commercial software packages that can be used for fire modelling applications and specific field modelling computer codes that are intended only for modelling fires have the propensity of simulating complex scenarios. In addition to the basic transport equations for mass, momentum and energy, along with appropriate turbulent models that can be readily applied to resolve the turbulent fluid flow, physical characteristics such as combustion, non-luminous and luminous radiation, soot production and even solid pyrolysis are progressively considered as essential requirements to be included in many field modelling investigations of compartment fires.

Nevertheless, advancements to the models are still required, especially to better resolve complicated flaming conditions in practical fire scenarios. Current combustion models that have been applied to solve a whole range of fire problems, need to be further improved beyond the fast chemistry assumption. Development of combustion models able to accommodate a wide range of chemical and turbulent time scales, will certainly assist in the predictive capability of the field model in simulating the growth and spread of fires of not only in a well-ventilated environment but also in an under ventilated environment such as the depletion of oxygen supply in a room with the door shut. The latter aspect has serious implication toward the possible direct consequence of a back-draft incident, usually persisting only few seconds before exhausting its fuel supply. Most commonly applied soot models in field modelling can still be regarded as very empirical in nature. The spread of smoke in a confined got sooty gases during evacuation. Complex and detailed attempts, especially trough the population balance approach to characterize the soot process via detailed models that seek to solve the rate of equations for elementary reactions, leading to soot and to predict the evolution of the size distribution of the soot particles generated by chemical reaction and/or undergoing chemical and physical processes, could provide better prediction of the soot concentration levels and thus a more realistic representation of the smoke barrier within the confined area. The development of soot pyrolysis models to cater for a wider range of fuels is necessary to predict the fire spread in a more fundamental way in order to characterize actual flaming behaviours in real fires. [1]

2.5 Thermal analysis

2.5.1 Heat Transfer phenomena

The heat transfer from the flame and hot gases to a surface consist of three main components, absorbed radiation ($\dot{q}"_{abs}$), emitted radiation ($\dot{q}"_{emi}$) and connective heat transfer ($\dot{q}"_{con}$).

$$\dot{q}"_{tot} = \dot{q}"_{abs} - \dot{q}"_{emi} + \dot{q}"_{con} \qquad \text{(Eq. 29)}$$

Normally in fire sciences surface emissivity (absorbivity) is taken to be wavelength independent and the absorbed radiant heat flux is simply a portion of the incident radiant heat flux. This portion is determined by the surface emissivity, i.e. $\dot{q}_{abs}" = \varepsilon_s \dot{q}_{inc}"$. The incident radiation, $\dot{q}"_{inc}$, depends on flame temperature, the view angle between flames and surface (ϕ) and the flame emissivity.

The emitted radiation, $\dot{q}"_{emi}$, is determined by the surface temperature (T_s) and the surface emissivity (ε_s) only:

$$\dot{q}"_{emi} = \varepsilon_s \sigma T_s^4 \qquad \text{(Eq. 30)}$$

Convective heat transfer is generally assumed to be linear with respect to the difference between the surface and the gas temperatures (T_s *and* T_c). The proportionality constant is called the convective heat transfer coefficient (h_c):

$$\dot{q}"_{con} = h_c (T_g - T_c) \qquad \text{(Eq. 31)}$$

For adjacent fires the gas temperature is assumed to be equal to the temperature of the flames and the hot gases (T_{fl}). Thus, the total heat transfer to a surface exposed to a localised fire can therefore be expressed as:

$$\varepsilon_{fl} = 1 - e^{-KL} \qquad \text{(Eq. 32)}$$

Where K is the absorption coefficient and L the flame thickness. Unfortunately little data are available in the literature on K except for some common fuels [44].

In this work steel temperature is calculated using adiabatic surface temperatures from CFD model.

2.5.2 The Adiabatic Surface Temperature

Concept of *Adiabatic surface temperature (AST)* is introduced in practical means to express the thermal exposure of a surface, thus it can be used successfully when the exposure conditions are obtained from a fire model. *AST* is what would be measured by an ideal plate thermometer which is used in fire resistance testing *(ISO 834* and *EN 1363-1).*

Considering previous section, the total net heat flux can be expressed:

$$\dot{q}_{tot}'' = \varepsilon(\dot{q}_{inc}'' - \sigma T_s^4) + h(T_g - T_s) \qquad \text{(Eq. 33)}$$

Consider the surface of a perfect insulator exposed to the same heating conditions as the real surface. Its real temperature shall be referred to as the *AST*. The total to this ideal surface is by definition zero, so:

$$\varepsilon(\dot{q}_{inc}'' - \sigma T_s^4) + h(T_g - T_s) = 0 \qquad \text{(Eq. 34)}$$

Numerically, the *AST* provides a natural interface between fire and structural models. CFD models may only approximate a bounding solid as an infinitely thick slab for the purpose of estimating its surface temperature. In order to perform a more detailed heat transfer calculation within the solid, some sort of interface is required to transfer information at the gas-solid interface. The solution for that is to use adiabatic surface temperature T_{AST}, as an intermediary between fire and structural models, which can be described in the following way.

At every surface point at which the fire model (FM) computes an incident radiation heat flux ($\dot{q}_{inc,FM}''$) and a corresponding gas temperature adjacent to the surface ($T_{g,FM}$) it is easy to solve the following equation for T_{AST}, assuming that the emissivity and convective heat transfer coefficient are constant:

$$\varepsilon(\dot{q}_{inc,FM}\,''-\sigma \mathrm{T}_{AST}^4)+h(T_{g,FM}-T_{AST})=0 \qquad \text{(Eq. 35)}$$

For the structural model (SM) the heat flux is computed based on fire conditions computed by the fire model and the surface temperature computed by the structural model:

$$\dot{q}_{tot,SM}\,''=\varepsilon(\dot{q}_{inc,FM}\,''-\sigma \mathrm{T}_{s,SM}^4)+h(T_{g,FM}-T_{s,SM}) \qquad \text{(Eq. 36)}$$

Finally, the total net heat flux to the surface can be computed as:

$$\dot{q}_{tot,SM}\,''=\varepsilon\sigma(\mathrm{T}_{AST}^4-\mathrm{T}_{s,SM}^4)+h(T_{AST}-T_{s,SM}) \qquad \text{(Eq. 37)}$$

Note that the AST is interpreted by the structural model as an effective black body radiation temperature for the purpose of computing the incident radiation and as the same gas temperature for the purpose of computing the convective heat flux. It may also be considered as a single fictitious temperature being used commonly for calculating both convective and radiative heat transfer [45].

2.6 Structural analysis

2.6.1 Introduction

When performing structural analysis of a structure or a certain part of it, there is several general types of analysis. The most efficient analysis should be chosen in dependence of complexity of the observed problem, all in order to satisfy Ultimate Limit States and Serviceability Limit States proposed by Eurocodes. This section is written mostly according to [47] and [48].

Generally, methods of analysis can be classified as an *elastic* and *non-elastic analysis.*

Elastic Analysis can be:

-*LA: linear elastic analysis* – the linearity of the theory results from the assumptions of a linear elastic material law and the linear small deflection theory that the assumed geometry remains that of the undeformed structure. This analysis is easy to perform and superposition is valid, but it gives approximate solution and it is necessary to include imperfections and 2nd order effects in other ways (such as reduction coefficients for buckling).

-*LBA: linear bifurcation analysis* – material assumptions are same as in the *LA*. This analysis obtains the lowest eigenvalues at which shell may buckle into a different deformation mode, assuming no change of geometry, no change in the direction of action of the load, and no material degradation. Imperfections of all kinds are ignored.

-*GNA: geometrically non-linear analysis* – this analysis satisfies both equilibrium and compatibility of the deflections under conditions in which the change in the geometry of the structure caused by loading is included. Benefit of this analysis is possibility of direct solution of elastic buckling, but superposition cannot be used, it requires software usage.

GNIA: geometrically non-linear analysis with imperfections included – similar to *GNA*, it delivers elastic buckling loads of the imperfect structure. Used where the compression or shear dominate. Care must be taken to ensure that the local stresses do not exceed values at which material nonlinearity may affect the behaviour.

Furthermore, *Non-Elastic Analysis* can be:

MNA: Materially non-linear analysis – the result of *MNA analysis* gives the plastic limit load, which increases load capacity. It can be used only if: steel is sufficiently ductile ($f_u/f_y \geq 1.1$; $\delta \geq 15\%$; $\varepsilon_u \geq 15e_y$), for global analysis the cross sections are of class 1, in global analysis the stability of members at plastic hinges is assured, software for plastic global analysis is desirable.

GMNA: geometrically and materially non-linear analysis – the result of a *GMNA analysis* analogously to *MNA analysis* gives the geometrically nonlinear plastic limit load of the perfect structure and the plastic strain increment.

GMNIA: geometrically and materially non-linear analysis with imperfections included – this analysis is used in cases where compression or shear stresses are dominant in the shell. It delivers elastic-plastic buckling loads for the ‘’real’’ imperfect structure.

This work is deals with the *GMNA* and *GMNIA analysis* for the observed column under different thermal and axial load cases, in order to verify their influence on the column behaviour.

2.6.2 GMNIA analysis

Although number of researches were conducted last decades, still there’s a gap concerning imperfection sensitivity on steel structures, regarding even basic buckling cases. A *geometrically and materially non-linear analysis with imperfections included* is currently the most accurate method of a numerical buckling strength verification. This procedure is most realistic if the inevitable deviations of the structure from the ideal geometry and material are consistently modelled by the geometric imperfections. By this way equivalent geometric imperfections are fundamental at this kind of analysis. They have to cover the influence of all deviations from the nominal data of the resistance parameters. The suitability of suggested equivalent geometric imperfections must be examined first at the basic buckling cases, because experimentally determined comparison loads exist only for these instability cases. Equivalent geometric imperfections are subsequently called consistent equivalent geometric imperfections, if a GMNIA-calculation including these imperfections results in

the experimentally based buckling cases. The problem of consistent equivalent geometric imperfections includes the problems of their shape and size [49].

Following sections are written mainly according to [50].

2.6.2.1 Material non-linearity effect

The behaviour of carbon and low-alloy steel grades is usually represented by means of the ideal elastic-plastic stress-strain model.

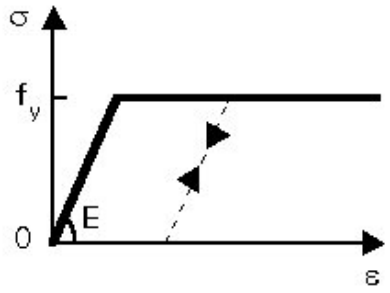

Figure 15: Ideal elastic-plastic stress-strain model

As long as the elastic critical buckling load N_{cr} is smaller than the squash load $N_{p1}=A \bullet f_y$, the member remains straight and undergoes elastic axial deformation. When collapse occurs by elastic critical bending at a load N = Ncr, the resulting lateral deflection induces bending moments, that increase the stress at the concave side of the member and decrease it at the convex side. Yielding occurs, in the central part of the member, in compression and more rarely in tension.

When, on the other hand, the squash load N_{p1} is reached prior to the elastic critical buckling load N_{cr}, the behaviour is similar to that of the rigid-plastic strut, but with additional elastic axial and bending deformations. The failure load, in this case, is the squash load, N_{p1}.

2.6.2.2 Strength curve for an ideal strut

Elastic column buckling analysis emphasizes the influence of the slenderness, $\lambda = l/i$, on the resistance; l is the strut buckling length, equal to the member length when the strut is pin-ended, and $i = \sqrt{I/A}$ is the radius of gyration for the plane of flexural buckling considered. Plotting the average compressive stress, σ_k, at failure against the slenderness, λ,

gives a clear understanding of the relationship between the two types of behaviour (see Figure 16 (a) below). Elastic critical buckling is represented by the hyperbola $\sigma = \sigma_{cr} = \pi^2 E/\lambda^2$; its range of application is limited by the plastic squashing line $\sigma = f_y$. The two lines intersect at the slenderness value λ_1, termed reference slenderness, such that $\pi^2 E/\lambda_1^2 = f_y$, which gives:

$$\lambda_1 = \pi^2 \sqrt{E / f_y} \qquad \text{(Eq. 38)}$$

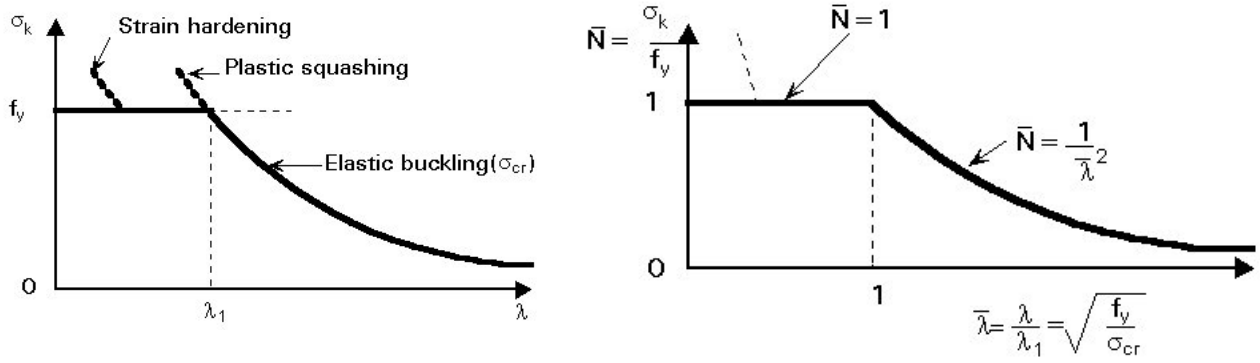

(a) In terms of σ_k and λ (b) Special non-dimensional form

Figure 16: Strength curves for initially straight pin-ended struts of ideal elastic-plastic material

Thus, collapse occurs by plastic squashing for $\lambda < \lambda_1$, and by elastic buckling when $\lambda > \lambda_1$. Usually the curve is drawn in a normalized form (Figure 3b), where $\bar{N} = \sigma_k / f_y$ is plotted against $\bar{\lambda} = \lambda / \lambda_1$, so that plastic squashing $(\bar{N} = 1)$ and elastic buckling $(\bar{N} = 1/\lambda^{-2})$ intersect at $\bar{\lambda} = 1$.

2.6.2.3 Effect of geometric imperfections

The previous sections considered highly idealized strut models which do not represent the real responses of compression members, because of the unavoidable imperfections resulting from any manufacturing process. The following sections consider the effect of these imperfections on real structural response.

Geometric imperfections correspond either to lack of straightness of the structural member (a), or to eccentricities of the applied load (b).

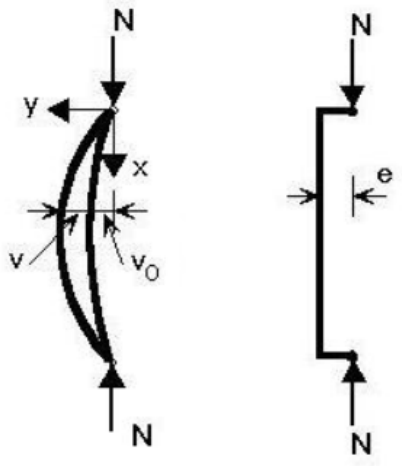

(a) (b)

Figure 17: Pin-ended strut geometrical imperfections

Initial curvature pin-ended strut causes a secondary bending moment as soon as any compression load is applied, which in turn leads to further bending deflection and a growth in the amplitude of the lever arm of the external end compression forces; this results in geometrically non-linear behaviour. A stable deflected shape is possible as long as the external moment, i.e. the product of the load and the lateral deflection, does not exceed the internal moment resistance of any section. Column buckling in the presence of an initial curvature is therefore by divergence of equilibrium, as opposed to the bifurcation type of instability typical of ideal compression members.

Any cross-section of the strut experiences combined bending and axial load, whatever the amount of loading. Because geometric linearity is no longer valid (equilibrium requires consideration of the deflected shape), the effects of bending and axial load cannot be simply superimposed in order to describe the actual response.

For some elementary loading and support conditions, a direct procedure can be used, based on integration of the appropriate equilibrium differential equation describing the deflected shape. The fundamental equilibrium equation for a strut having an initial elastic curvature $v_o(x)$ in the buckling plane, is as follows:

$$\frac{d^2v}{dx^2} + \frac{N(v_0 + v)}{EI_z} = 0 \qquad \text{(Eq. 39)}$$

Where v(x) is the additional buckling deflection associated with the axial load N. Because the first buckling mode of a pin-ended strut is a sine half-wave, the initial curvature is similarly chosen; it is then easy to show that the amplitude of the total deflection v_t at the critical section (at x = 0,5 L in this case) is as follows:

$$v_t = \frac{v_0}{1 - N / N_{cr}} \qquad \text{(Eq. 40)}$$

$$N_{cr} = \pi^2 EI_z / L^2 \qquad \text{(Eq. 41)}$$

Where Ncr is the critical column buckling load. The axial load, therefore, magnifies the initial out-of-straightness and the first-order bending moment Nvo by an amplification factor 1/(1 - N/Ncr):

$$M = N_{vt} = N_{v0} / (1 - N / N_{cr}) \qquad \text{(Eq. 42)}$$

Following figure plots the axial load N against the total lateral deflection vt in the buckling plane. Deflection seeks into infinity as the axial compression force N is approaching to the elastic critical force N_{cr}. As the axial load is increasing, plastic strain areas are appearing what results with the stiffness degradation of element.

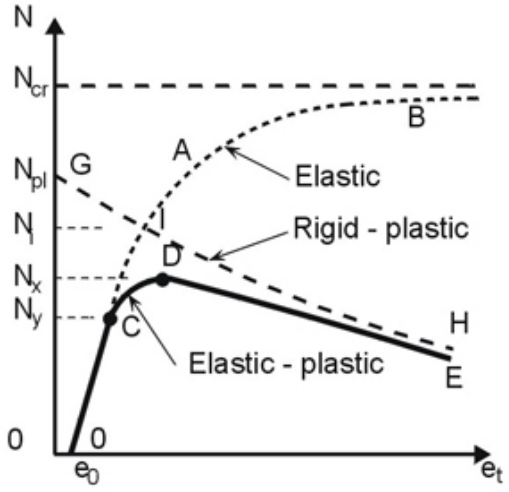

Figure 18: Response of a strut with an initial imperfection (assumption: $N_{pl} < N_{cr}$)

The distribution of bending moment along the member increases with the lateral deflection. Bending moment and stresses are the greatest at the critical sections; on the concave side of the strut, compressive stresses due to axial load and bending moment superimpose and the strut experiences the greatest stress. First yield will occur at this point as the axial load is steadily increased; the value of N corresponding to first yielding, termed N_y, constitutes the limit of validity C of the elastic response O'AB (Figure 18).

Any further increase of N above N_y results in a spreading of yielding, both along the strut and into the cross-section (Figure 19). This results in a further degradation of the strut stiffness, such that a maximum load N_K is attained, at which the strut fails (point D in Figure 18). The ultimate load carrying resistance is hence a function of two sources of flexural stiffness deterioration: the axial load (instability) and the spread of yielding (plasticity). The stress distributions across the strut cross-section at stages C and D are shown in Figure 20. Usually the concave side of the strut does not yield in tension at collapse.

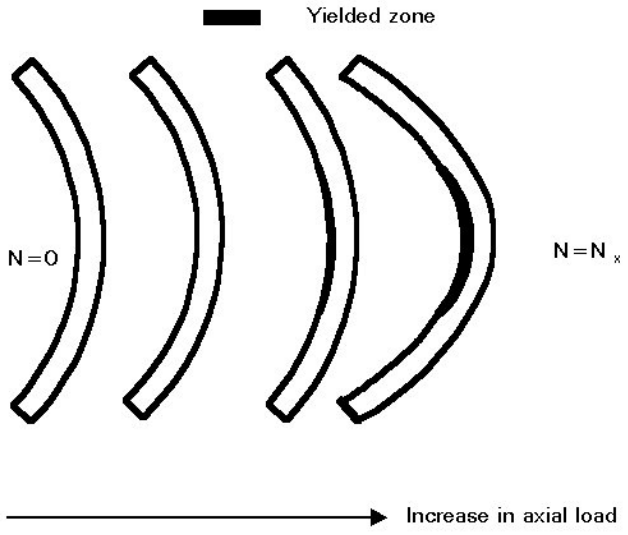

Figure 19: Spread of yielding as collapse approaches

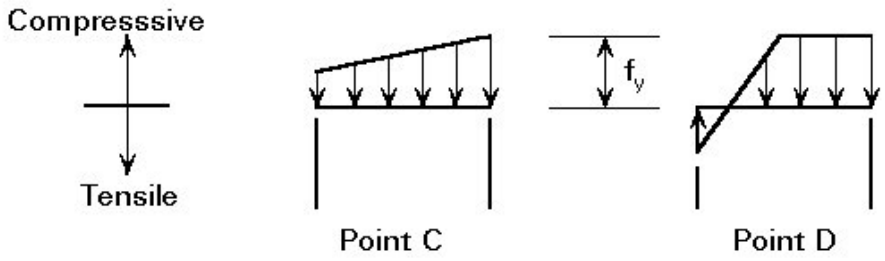

Figure 20: Stress distribution at the critical section of a strut with initial curvature

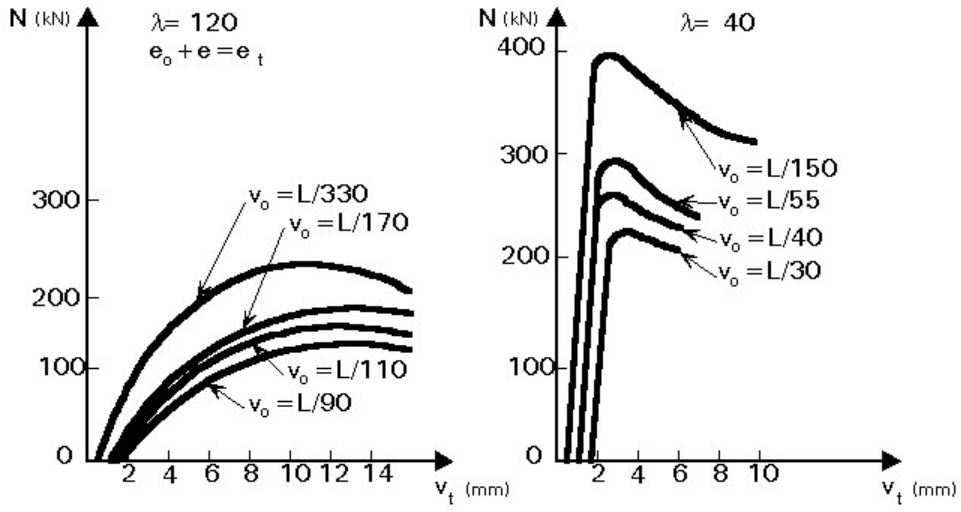

Figure 21: Elastic-plastic response example for different values of initial curvature

Provided the initial curvature is known beforehand, (if, for instance, it can be measured), it is possible to construct an ultimate resistance curve from the calculated collapse loads. Such a curve is of the form (a) shown in Figure 22. If the initial curvature is similar to the buckling mode, the resistance curve will start from $\sigma_K=f_y$ for vanishing slenderness and lie below that for initially straight struts, though approaching the latter, as slenderness increases. Indeed, for very stocky members, the influence of initial curvature is negligible and the plastic squash load is still the ultimate load. On the other hand, very slender struts exhibit an elastic critical load N_{cr} much lower that the squash load N_{pl}; in such cases, the point C of Figure 18 may be well up the elastic response curve, so that the collapse load is close to the elastic critical load. The influence of initial crookedness is especially marked for intermediate slenderness ratios; the greatest loss of resistance (strength) occurs in the vicinity of λ_1, where plastic squashing and elastic buckling are nearly coincident and therefore interact the most.

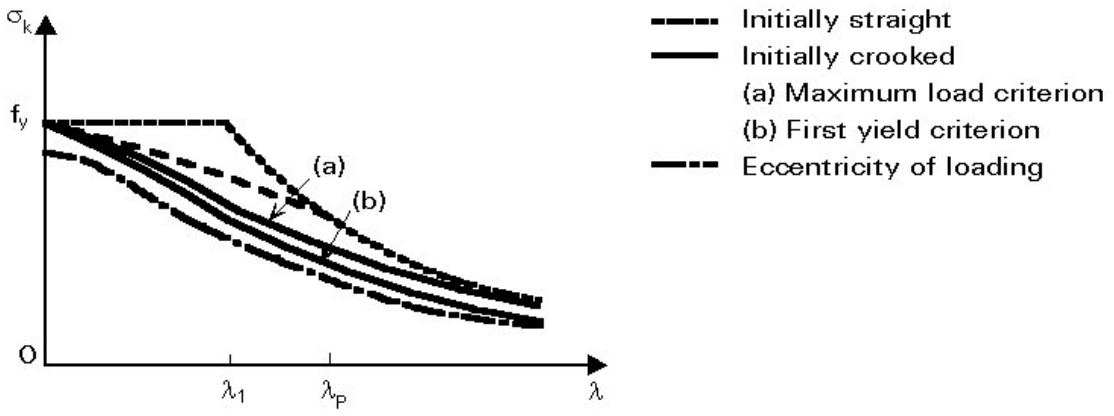

Figure 22: Strength curves

Eccentrity of loading - an end compressive load, N, applied with an eccentricity, v_o, to an initially straight pin-ended strut will induce a first-order bending moment in the strut which will begin to deflect laterally in a similar manner to the initially crooked strut analysed earlier.

The differential equilibrium equation in this case, is as follows:

$$\frac{d^2v}{dx^2} + \frac{N(v_0 + v)}{EI} = 0 \qquad \text{(Eq. 43)}$$

The amplification factors associated with the initial sine crookedness and the loading eccentricity are close to each other for the range of N/N_{cr} values encountered in practice. Therefore, the load-deflection response for an eccentrically compressed initially straight strut is similar to that plotted in Figure 18, except that the response curve starts at the origin of the axes.

Unlike the initial curvature, which is strongly dependent on the strut length, the loading eccentricity is more related to the section size. In addition, first-order bending is constant over the entire member length so that bending effects are likely to make the ultimate strength of very stocky members lower than the plastic squash load, giving, therefore, the form of strength curve (c) plotted in Figure 22.

2.7 Experimental work

As it was previously mentioned this work is continuation of a previous SUSCOS thesis carried out by Gonçalo Ferraz [2]. Experimental tests were performed with technical assistance provided by Laboratory of Testing Material and Structures of the University of Coimbra.

Full scale tests were performed in a large fire compartment, where a steel column was exposed to distinct localised fire scenarios. The compartment internal dimensions were 10 m x 9.75 m and the height of 3 m. During the fire experiments an unloaded steel column was subjected to the fire. Diameter of column was 245 mm, thickness 10 mm and height 2.90 m. Height was slightly lower than compartment height in order to avoid additional stresses caused by thermal elongation (EN 1993-1-2 (2005)). The interior of column was empty and the both ends of the column were sealed.

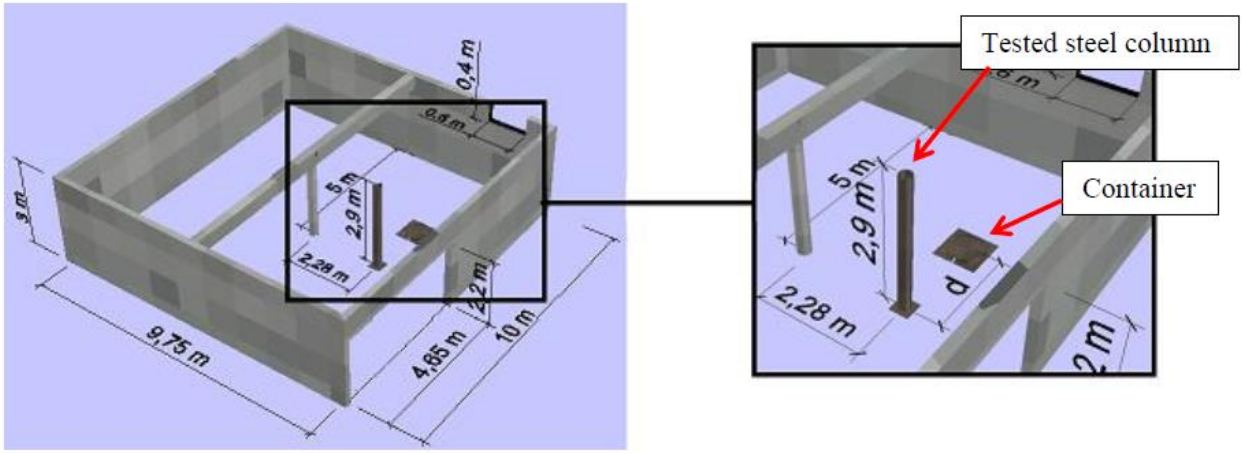

Figure 23: Original fire compartment configuration

Thermal action was applied trough pool fires filled with liquid fuel and placed in distinct positions inside the fire compartment.

Table 4. Experimental tests planning

Group	Test	Pool Diameter D [m]	Pool Distance d [m]	Openings [m]
1	1(*)	0.70	0.60	4.50 m x 2.55 m door
				0.60 m x 0.40 m window
	2	0.70	0.60	1.90 m x 2.55 m door
				0.60 m x 0.40 m window
				0.36 m x 0.30 m celling opening
	3	0.70	0.60	1.90 m x 2.55 m door
				0.60 m x 0.40 m window
				0.36 m x 0.60 m celling opening
	4	0.70	0.60	1.90 m x 2.55 m door opened 37°
				0.60 m x 0.40 m window
				1.10 m x 0.60 m celling opening
2	5	0.70	1.20	1.90 m x 2.55 m door
				0.60 m x 0.40 m window
				0.36 m x 0.60 m celling opening
	6	0.70	1.20	1.90 m x 2.55 m door opened 53 %
				0.60 m x 0.40 m window
				1.10 m x 0.60 m celling opening
3	7	1.10	0.80	1.90 m x 2.55 m door opened 53 %
				0.60 m x 0.40 m window
				1.10 m x 0.60 m celling opening
	8	1.10	1.20	1.90 m x 2.55 m door opened 53 %
				0.60 m x 0.40 m window
				1.10 m x 0.60 m celling opening
(*) In this test, it was used 15 l of fuel instead of 12 l (by measurement error). The effects of this exception are taken into account in the analysis of experimental results.				

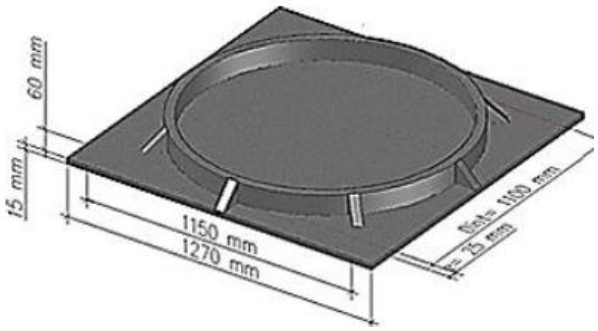

Figure 24: Steel container D=1.10m

Pool was filled with diesel fuel with measured density of 0.838 kg/l. No other properties of used fuel were available, what was one of the limitations of this work.

The temperatures were registered using wire thermocouples. 60 K-type thermocouples with two 0.5 mm diameter wires were used to monitor steel and gas temperatures in each test. Thermocouples measuring gas temperatures presented an exposed bare junction, while thermocouples measuring steel temperatures presented a grounded junction. In order to study the evolution of temperatures along the column height, measurements were made in 6 sections equally spaced by 0.47 m as represented in following Figure. In each section, four equally spaced thermocouples were welded to the column, monitoring steel temperature (TS_{ji}, where *j* is the section number and *i* is the cross section position number. In addition, gas temperatures were monitored by 4 thermocouples placed 5 cm away from the ones welded to the column (TG_{ji}). Furthermore, at the same levels temperature was measured along the vertical axis of fire plume (TF_j).

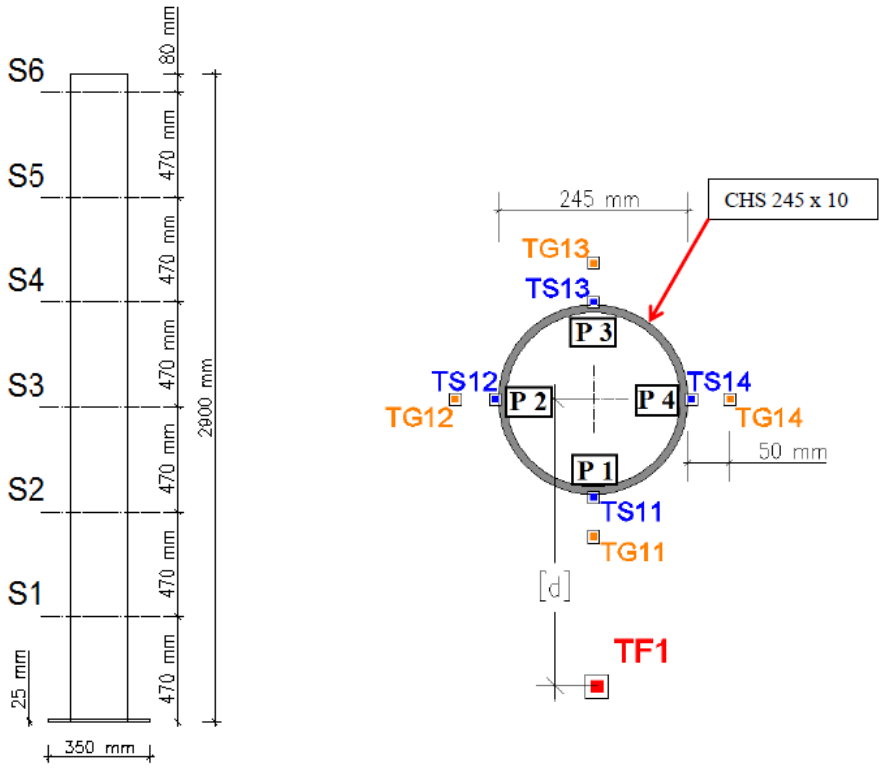

Figure 25: Experimental positioning of the thermocouples [2]

Detailed analysis of measured results and comparison with the numerical analysis will be presented in following sections.

3 PERFORMANCE BASED APPROACH

The most commonly used way of design is design following prescriptive rules, where thermal actions are given by nominal fire, whilst performance based code is built on physically based thermal actions. Although performance based design is more complex in its nature, it is becoming more and more common with the increasment of computational power, considering its capability of describing specific problems.

The performance based approach involves the assessment of three basic components, namely the fire modelling, the thermal analysis and the structural response, described in the following sections.

3.1 CFD Fire modelling

3.1.1 Introduction

Previously described experiment was modelled using PyroSim 2017 software – a graphical user interface for Fire Dynamics Simulator (FDS). Main goal of modelling was to calibrate temperatures in FDS model with those from previously conducted experiment. In order to achieve as realistic fire scenario as possible, a number of different cases were obtained. During process of calibration there were few main limitations:

- Limited FDS possibilities regarding the model geometry;
- Lack of experimental data regarding the fuel properties;
- Accidentally occurred wind effects during the experiments;
- Limited computational power, which influenced on mesh refinement and accuracy of the results - the more complex model is, the more computational time it requires.

However, process of calibration is done by trial and error methodology, but it can be roughly represented by the following steps:

- Calibration of the fuel properties in terms of fire duration and temperature values, using relatively small computational domain and coarse mesh;
- Test of the selected fuel properties on finer mesh model;
- Further model calibration on the complex geometry model – relatively coarse mesh;
- Calibration of the different ventilation conditions in order to find the one best matching with the experimental tests (using Smokeview);
- One more time, test of the selected fuel properties and ventilation conditions on the fine mesh model;
- Fine model calibration.

The computer simulations were carried out on two computers in dependence on model complexity:

Computer no1:

- Processor: Intel® Core™ i7 CPU 950 @ 3.07 GHz
- Total physical memory (RAM): 24.0 GB
- System type: 64bit OS, x64 – based processor
- System: Microsoft Windows 10 Professional

Computer no2:

- Processor: Intel® Core™ i5-4200H CPU@ 2.80GHz
- Total physical memory (RAM): 6.0 GB
- System type: 64bit OS
- System: Microsoft Windows 7 Professional

3.1.2 Geometry

3.1.2.1 Fire compartment geometry

During the process of calibration several different ventilation conditions were tested in order to find one with the smallest influence of the wind. Original fire compartment geometry is presented in the Section 2.5. In order to simplify model the mid-span beam and concrete column below it were neglected due to its no influence on the fire behaviour. As it was mentioned before, wind influence is important factor in fire plume behaviour, which directly reflects on recorded temperatures as in the full scale experiments, so as in the numerical model. It is worth to mention that in the experiments wind speed wasn't monitored.

However, some of the experiments showed small wind effect on the fire plume. Therefore, Test no. 7, from the group 3 (Table 4) is chosen as the most appropriate to calibrate. Geometry of the fire compartment in that case is slightly different from the original fire compartment geometry. Ventilation conditions:

- Door – 1.90 m x 2.55 m;
- Window – 0.60 m x 0.40 m;
- Ceiling opening – 1.10 m x 0.60 m.

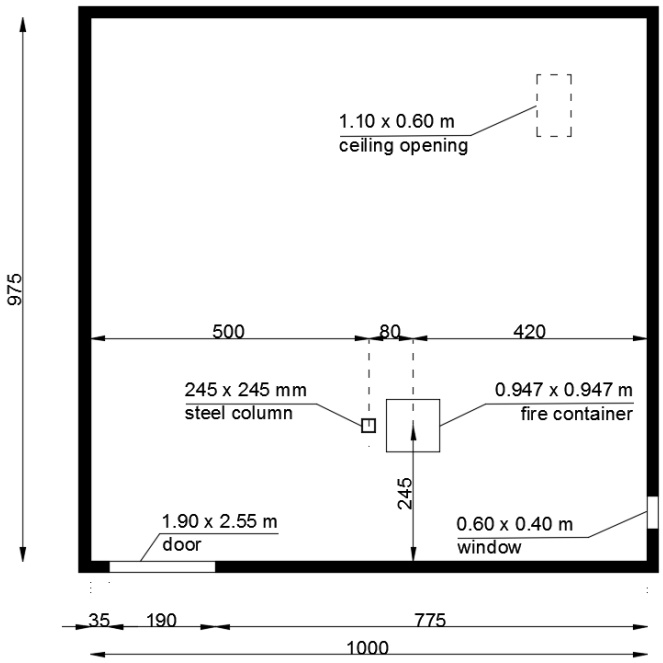

Figure 26: Compartment geometry (h=3.0m)

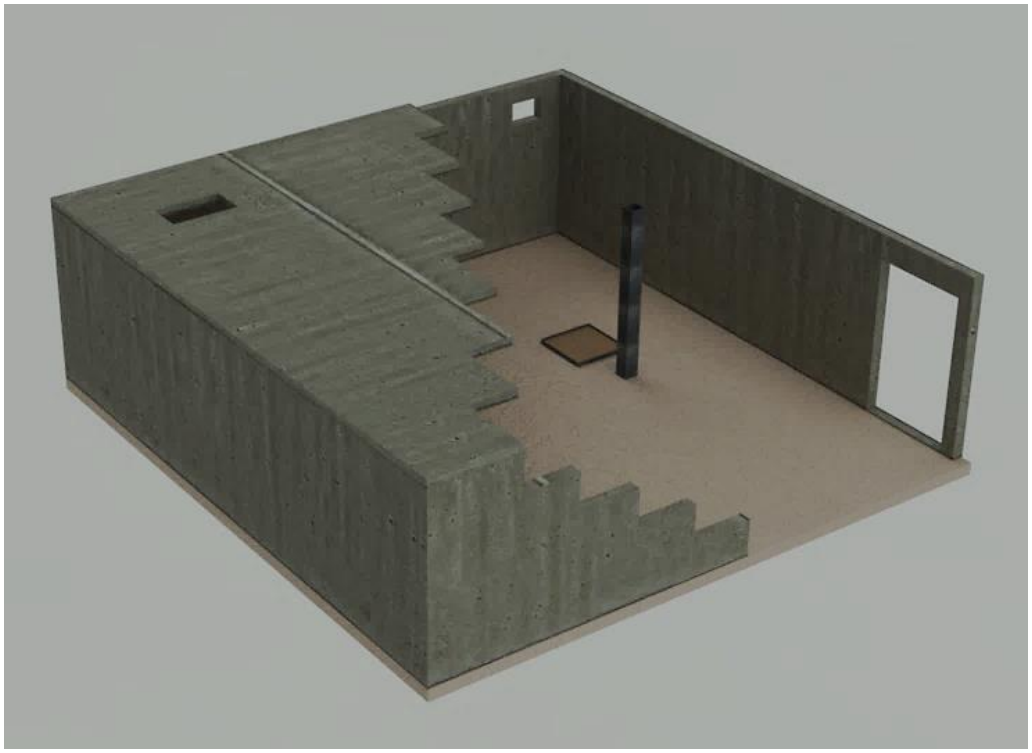

Figure 27: 3D visualization of the compartment

3.1.2.2 Fire pool and column geometry

In the experiments circular fire pool and column were used. Due to FDS limitation of using rectilinear geometry pool and column had to be approximated by rectangular pool and column.

Diameter of the pool was 1.10 m and 5 cm depth, while column was hollow cold rolled, 2.90 m height, with diameter of 245mm, 10mm thickness .

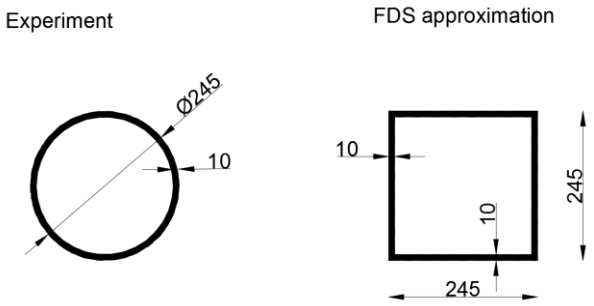

Figure 28: Steel column approximation (mm)

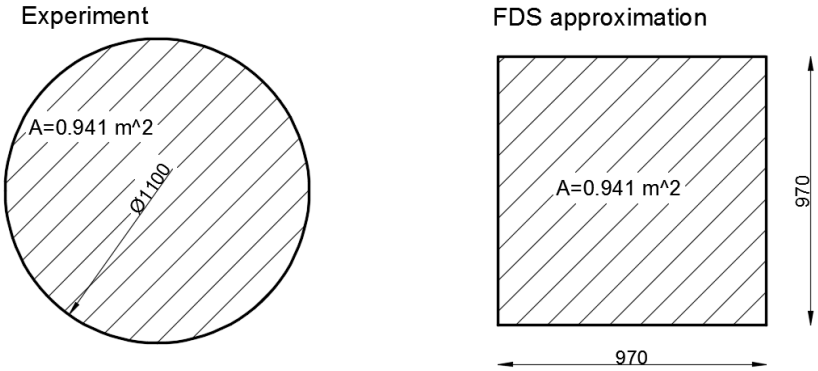

Figure 29: Pool geometry approximation (mm)

Figure 30: 3D visualization of the pools and columns

3.1.3 Computational domain

The grid sizes used is one of the most important numerical parameter in CFD dictating its numerical accuracy. The necessary spatial resolution for a proper LES simulation is customary defined in terms of the characteristic diameter of a plume.

Computational domain of the fire compartment consists of two rectangular computational meshes (Multiple meshes), finer one covers region around the observed pool fire and steel column and coarser one which covers rest of the compartment. Maximum ratio of 2:1 between to different meshes grid sizes has to be satisfied [8].

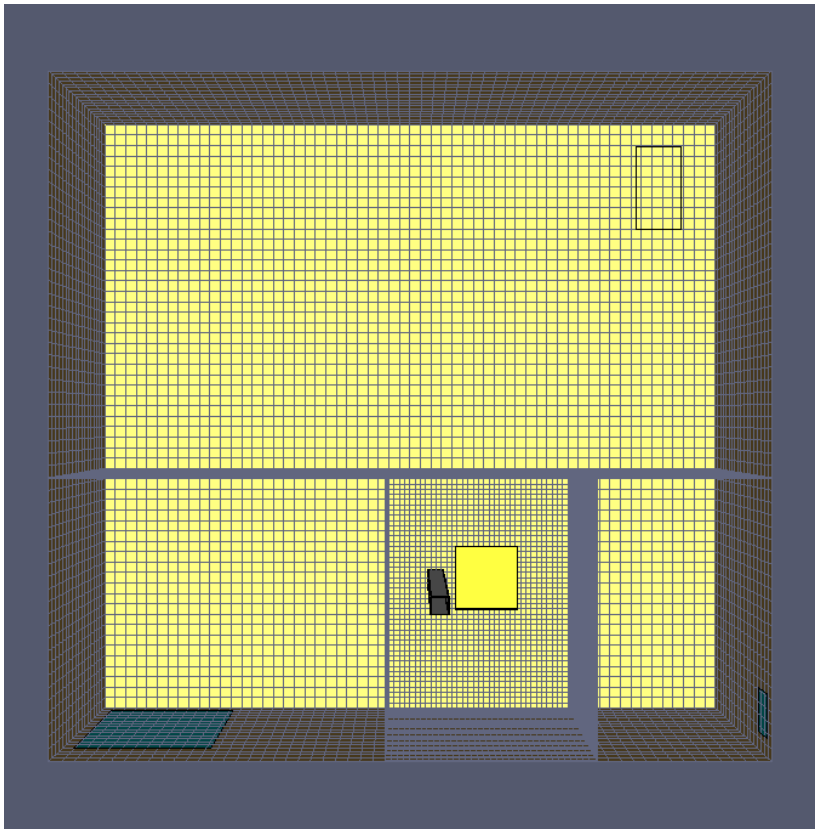

Figure 31: Computational domain

Two different grid sizes were used in order to investigate the sensitivity of the results due to this parameter. For simulations involving buoyant plumes, a measure of how well the flow field is resolved is given by the non-dimensional expression $R^*=D^*/\delta x$, where D^* is a characteristic fire diameter and δx is the nominal size of a mesh cell. The quantity $D^*/\delta x$ can be thought of as the number of computational cells spanning the characteristic diameter of the fire.

$$D^* = \left(\frac{\dot{Q}}{\rho_\infty c_p T_\infty \sqrt{g}} \right)^{2/5} \quad \text{(Eq. 44)}$$

Where:

$\dot{Q}$ - heat release rate (kW)

ρ_∞ - density of ambient gas (kg/m^3)

c_p - specific heat capacity of ambient gas (kJ/kg-K)

T_∞ - ambient temperature (K)

g - gravity (m/s^2)

The more cells spanning the fire, the better resolution of the calculation [8]. The necessary resolution suggested in most studies is between 1/5 and 1/20 (8). Lin et. Al. [39] suggested R*=1/13 is enough for CFD simulations to resolve the fire characteristics (flame height and thermal radiation), however this suggestion is not good enough to resolve fire behaviour distant from the fire source.

Compartment openings were defined as a surface named *Open vent*, which provide constant oxygen inflow. Disadvantage is that this kind of opening doesn't provide exact air flow conditions as in the experiment. However, since geometry outside of observed compartment was unknown, *open vents* were accepted as the appropriate, and geometry outside of the compartment was neglected.

3.1.4 Thermal load

3.1.4.1 Fuel properties

As mentioned before pool fire was defined as a S235 steel container with diameter 1.10m. In the experiments 30±2 l of diesel was used. Since diesel is not a well-defined substance the exact compostion of the fuel was not known. Only known parameter was the density of diesel, which was measured as 0.838 kg/l. Lack of the diesel properties was the most significant limitation during the calibration of the fire plume. Some of the most important diesel properties are listed below.

Table 5. Fuel properties

Properties	**Unit**	**Value**	**Reference**
Volume	(l)	30	(2)
Density	(kg/m^3)	838	(2)
Chemical formula	-	$C_{12}H_{23}$	(29)
Specific heat	(kJ/kgK)	1.80	(31)
Vaporization temperature	(°C)	165	(32)
Heat of combustion	(kJ/kg)	$4.50E^4$	(34)
Heat of vaporization	(kJ/kg)	232	(31)
Conductivity	-	0.13	(41)

3.1.5 Steel properties

This section is based mainly on the EN 1993-1-2 (2005) [36]. Steel properties used in the numerical model will be described.

The unit mass of steel (kg/m^3) may be considered to be independent of the steel temperature and it is ρ=7850 (kg/m^3).

Specific heat (J/kgK) can be described in the dependence of the temperature and material. It expresses heat quantity which is necessary to heat up 1 kg of a material by 1 K. Numerical model consists of the linear approximation of the curve given in the following figure.

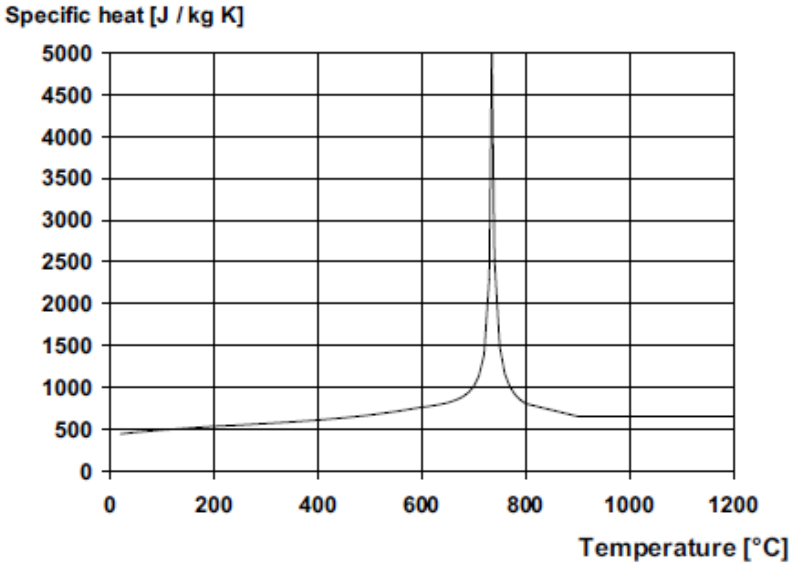

Figure 32: Specific heat of carbon steel as a function of the temperature [36]

Thermal conductivity (W/mK) is the property of a material to conduct heat. It is evaluated primarily in terms of Fourier's Law for heat conduction [37]. It can be also determined as a function of the temperature. The variation of the thermal conductivity with temperature is illustrated in the following figure.

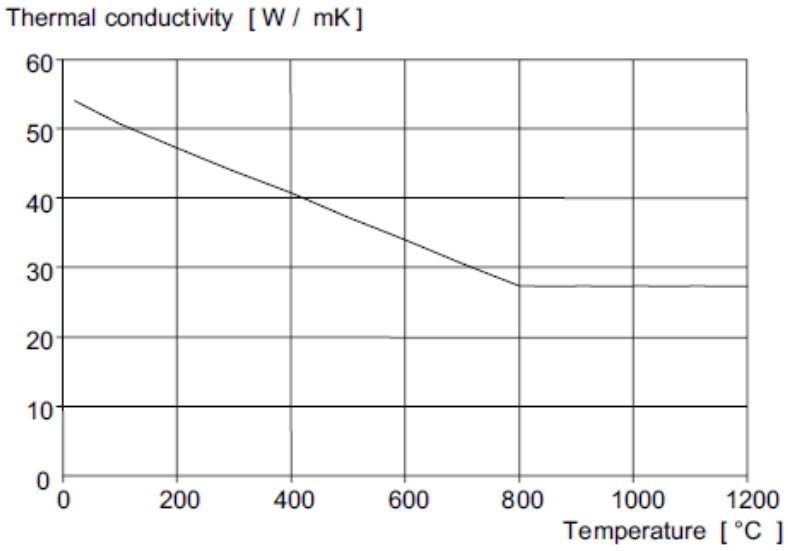

Figure 33: Thermal conductivity of carbon steel as a function of the temperature (36)

Emissivity coefficient indicates the radiation of heat from a 'grey body' according to the Stefan – Boltzmann Law, compared with the radiation of heat from an ideal 'black body' with the emissivity coefficient $\varepsilon = 1$. Value for the oxidized steel is given by [46] and it is $\varepsilon=0.75$.

3.1.6 Grid size estimation

In order to test model sensitivity on grid size, few grid sizes were tested. Estimated value of Heat Release Rate was used to calculate characteristic pool diameter (Eq. 47). Afterwards, calculated characteristic pool diameter is used to determine appropriate grid sizes.

As mentioned above the equation given by Babrauskas [43] was used to estimate Heat Release Rate (Q):

$$Q = \dot{m}''_{\infty} \cdot \chi \cdot \Delta H_c \cdot A_f \cdot (1 - e^{-k\beta D}) \qquad \text{(Eq. 45)}$$

Where:

$\dot{m}''_{\infty}$ - maximum burning rate per unit area and time

χ - efficiency of combustion

ΔH_c - heat of combustion

A_f - horizontal burning area of the fire source

$k\beta$ - empirical constant

D - diameter of the pool

Table 6. HRR estimation equation properties

Property	Unit	Value	Reference
$\dot{m}''_{\infty}$	$(kg/m^2 - \sec)$	0.045	[43]
χ	-	0.80	[25]
ΔH_c	(kJ/kg)	44.4	[43]
A_f	(m^2)	0.941	Section 3.2.2
$k\beta$	(m^{-1})	2.1	[43]
D	(m)	1.10	[2]

Finally, estimated HRR is:

$$Q = 0.045 \cdot 0.80 \cdot 0.941 \cdot (1 - e^{-2.1 \cdot 1.1 \cdot 1.1}) = 4.979 MW \quad \text{(Eq. 46)}$$

Using HRR from equation above, characteristic pool diameter is calculated:

$$D^* = \left(\frac{\dot{Q}}{\rho_\infty c_p T_\infty \sqrt{g}} \right)^{2/5} = \left(\frac{4979}{1.204 \cdot 1.005 \cdot 293 \sqrt{9.81}} \right)^{2/5} = 1.826\ m \quad \text{(Eq. 47)}$$

Different quantities of $D^*/\delta x$ were used according to [15]. $D^*/\delta x$ is the number of grid cells of length δx that span the characteristic diameter of the fire. The greater its value, the more "resolved" are the fire dynamics.Table below shows cell sizes in the region around fire pool and steel column (see *Computational domain* section). Cell sizes in the rest of the compartment are twice bigger.

Table 7. Tested cell sizes

Model	**Cell size (cm)**	***D*/δx***	**Total number of cells**	**Required computational time (hours)**
FDS_Coarse Mesh	12.0 x 12.0 x 12.5	15	33 360	≈ 4.0
FDS_Fine Mesh	6.4 x 6.4 x 6.3	30	216 192	≈50.0

3.1.7 Results and discussion

This section contains presentation of the temperature evolution on different positions compared with the experimental results. In this group of tests steel column was exposed to the thermal action described in previous sections. Column was 0.80 m distant from 30±2 l diesel pool.

Generally temperature measuring devices were labelled following next principle:

TCF*ij* – ThermoCouple above Fire source

TCC*ij* – ThermoCouple on the Column surface (steel temperature)

AST*ij* – Adiabatic Surface Temperature

i – height of obtained section

j – position on the cross section

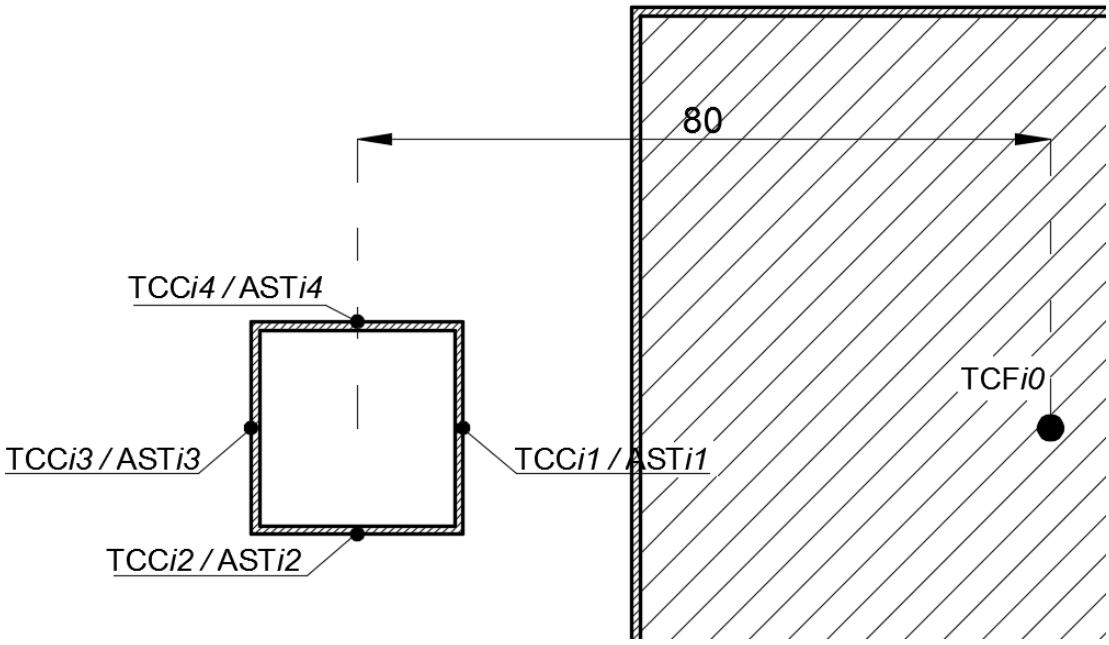

Figure 34: Temperature measuring devices positioning

Table 8. Temperature measuring devices positioning

Index		Position	Index		Position (m):
i	0	See Figure above	***j***	1	0.47
	1			2	0.94
	2			3	1.41
	3			4	1.88
	4			5	2.35
				6	2.88

3.1.7.1 Heat Release Rate (HRR)

Since there was no experimental data on HRR, prediction of HRR calculated in Section 3.1.6 showed good matching compared to calculated average HRR using the FDS model.

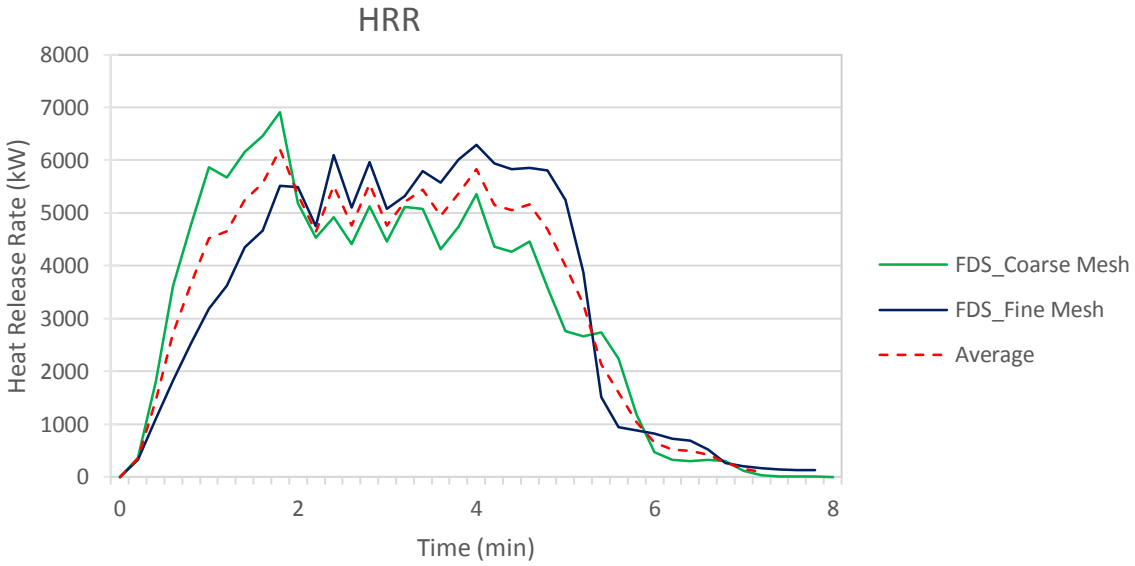

Figure 35: Heat Release Rate

3.1.7.2 Gas temperatures above pool

Temperatures above pool were measured in the vertical axis of the fire pool. In total 6 thermocouple devices were positioned above pool.

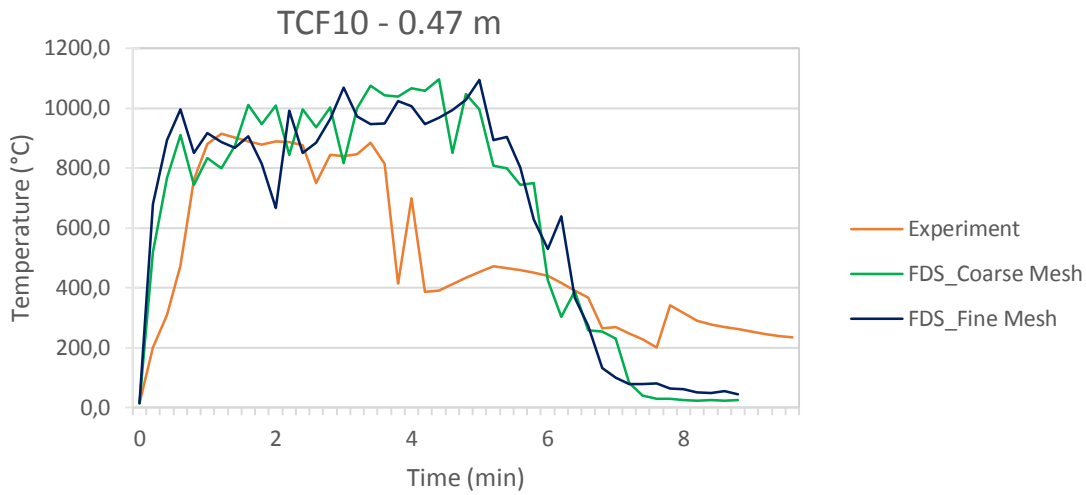

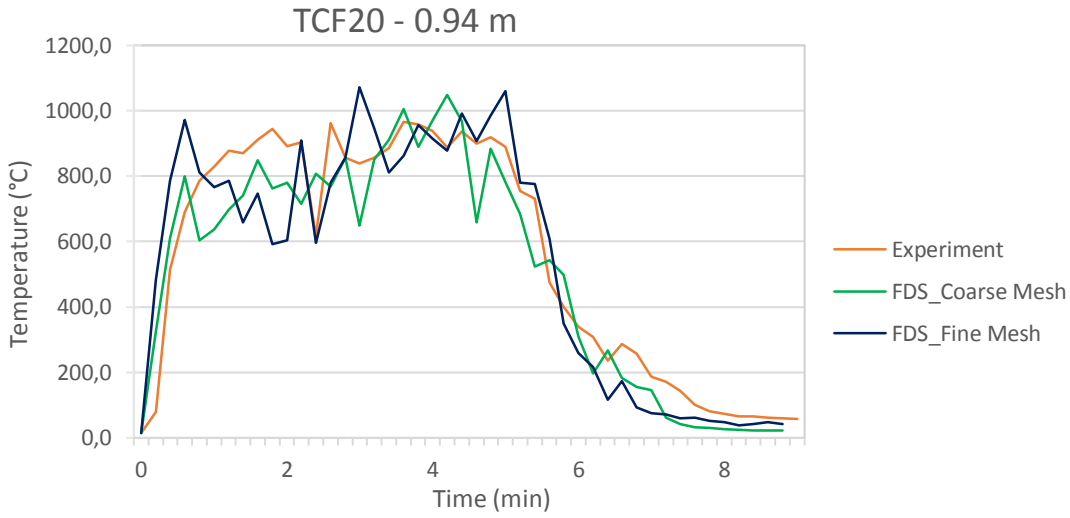

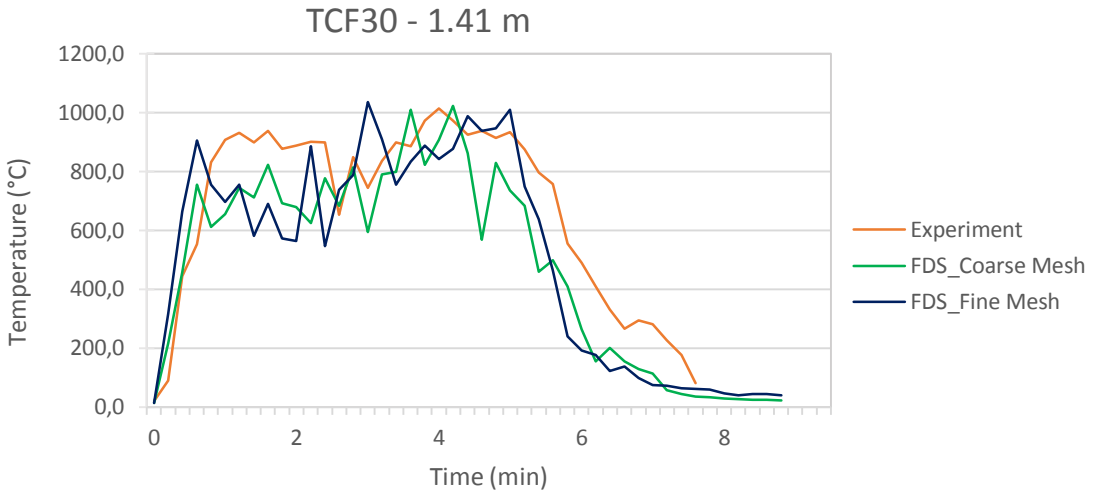
TCF30 - 1.41 m
Temperature (°C)
1200,0
1000,0
800,0
600,0
400,0
200,0
0,0
0
2
4
6
8
Time (min)
Experiment
FDS_Coarse Mesh
FDS_Fine Mesh

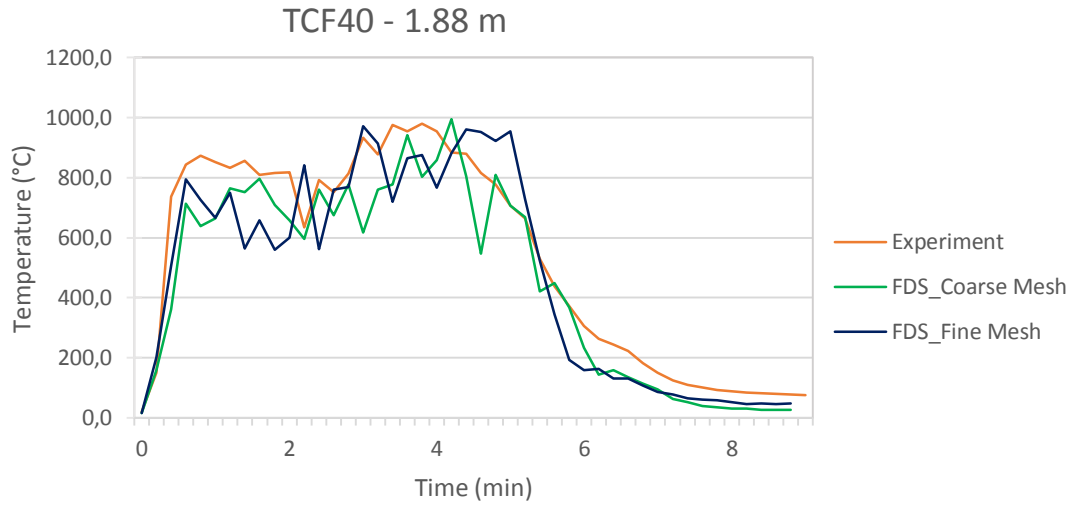
TCF40 - 1.88 m
Temperature (°C)
1200,0
1000,0
800,0
600,0
400,0
200,0
0,0
0
2
4
6
8
Time (min)
Experiment
FDS_Coarse Mesh
FDS_Fine Mesh

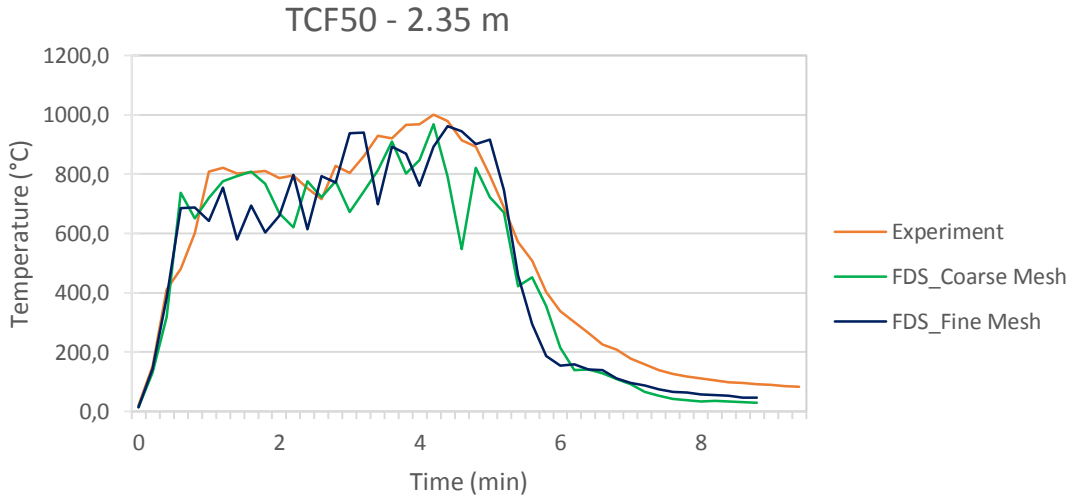
TCF50 - 2.35 m
Temperature (°C)
1200,0
1000,0
800,0
600,0
400,0
200,0
0,0
0
2
4
6
8
Time (min)
Experiment
FDS_Coarse Mesh
FDS_Fine Mesh

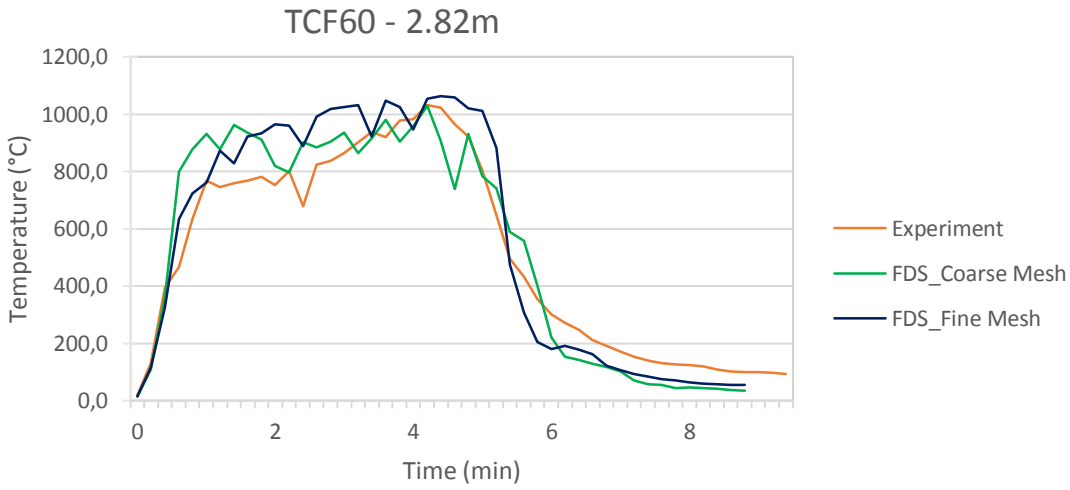

Figure 36: Temperatures measured in the vertical axis of the fire

According to the figures presented above it is obvious that FDS prediction on fire duration and temperatures is quite good. Note that sudden drop (t≈4 min) of temperature curve, measured by TCF10, from the experiment occurred due to the thermocouple failure [2]. Furthermore, it is visible that these grid sizes doesn't affect too much on the fire behaviour. Reason for peak appearances in the numerical models, so as in the experiments, is fire plume deflection caused by the wind.

Temperature slices

Temperature slices were positioned in the YZ plane, in the axis of fire pool and column. Values of temperature are expressed in *°C*. Several stages of fire development are shown to present fire behaviour, such as *fire growth, flashover, full fire development* and *extinguishment*.

Figures below shows comparison of predicted temperatures in the YZ plane trough different phases of fire between two numerical models. Numerical model *FDS_Fine Mesh* has shown more detailed prediction of fire plume fluctuations, due to bigger number of cells spanning fire pool region, as expected.

Model: *FDS_Coarse Mesh*; t=14.4 s;

Phase: *growth*

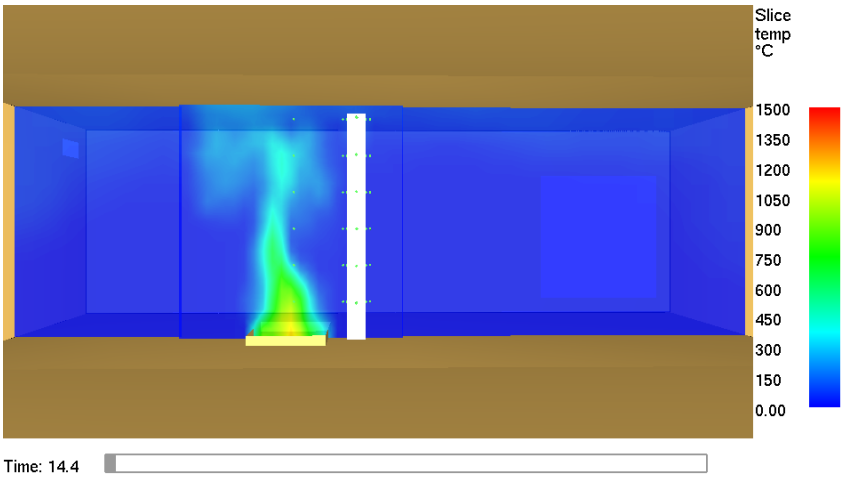

Model: *FDS_Fine Mesh*; t=14.4 s;

Phase: *growth*

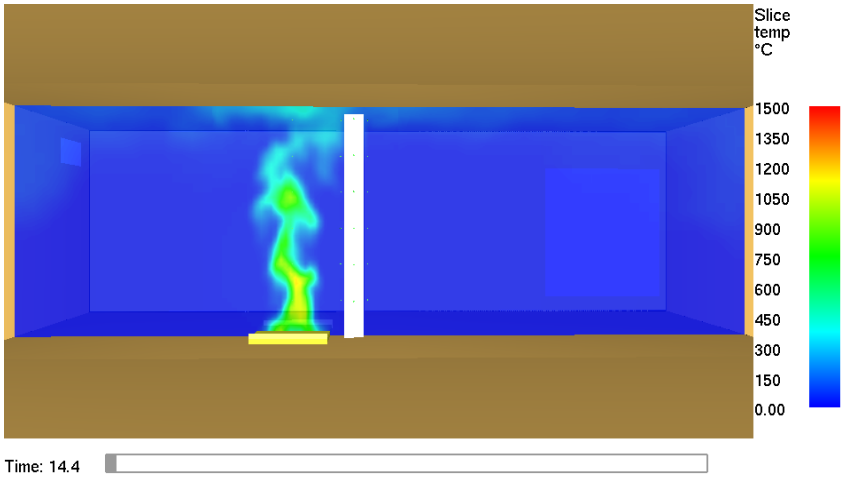

Model: *FDS_Coarse Mesh*; t=24.0 s;

Phase: *flashover*

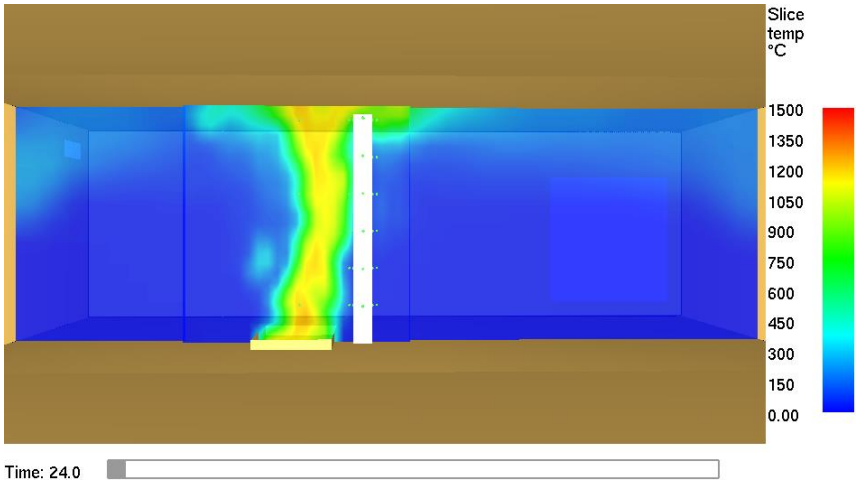

Model: *FDS_Fine Mesh*; t=24.0 s;

Phase: *flashover*

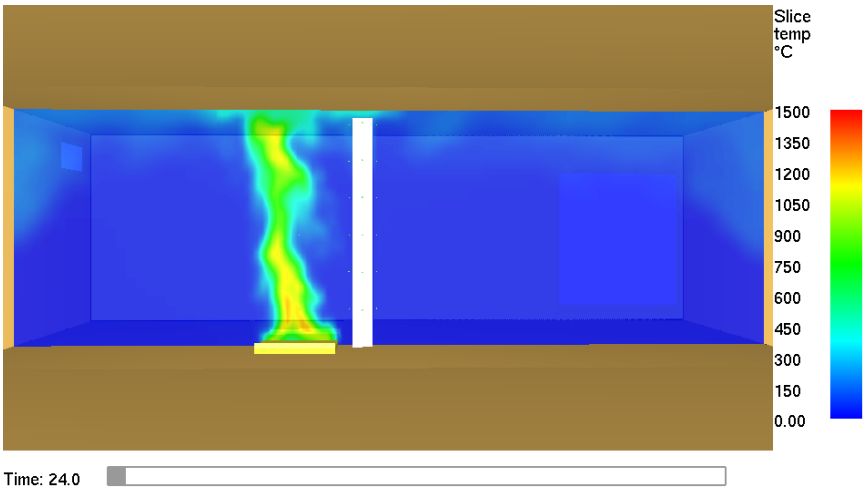

Model: *FDS_Coarse Mesh*; t=165.6 s;

Phase: *full fire development*

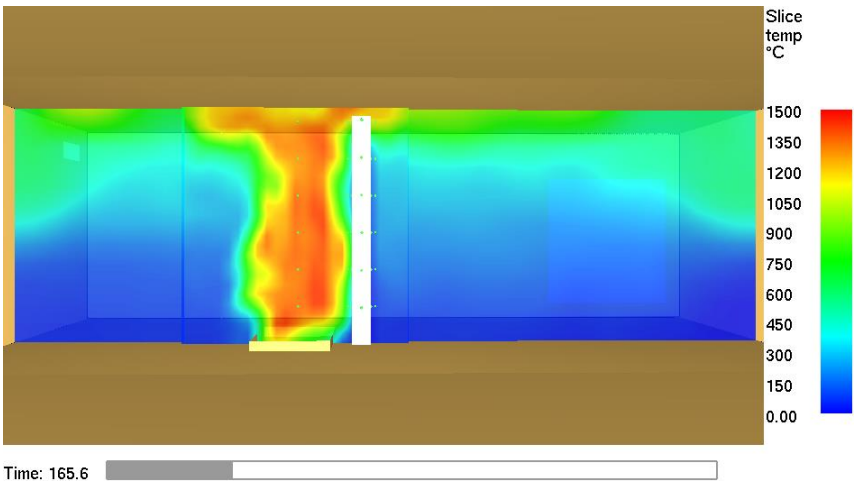

Model: *FDS_Fine Mesh*; t=165.6 s;

Phase: *full fire development*

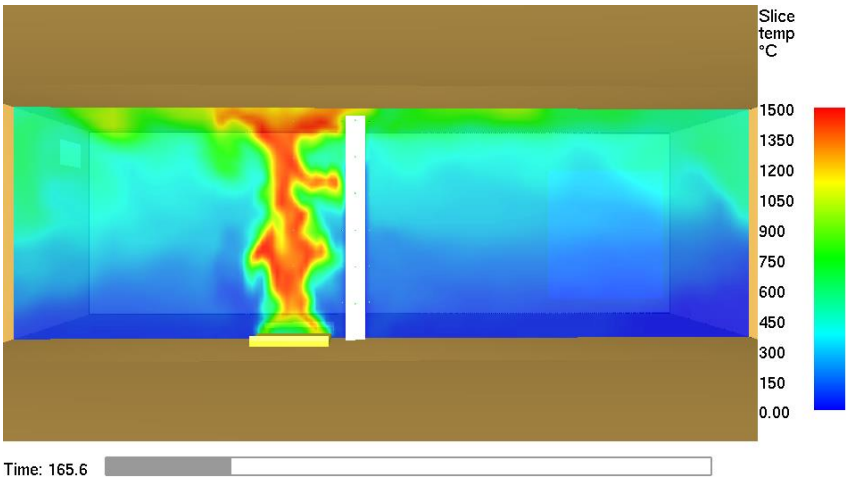

Model: *FDS_Coarse Mesh*; t=340.8 s;

Phase: *extinguishment*

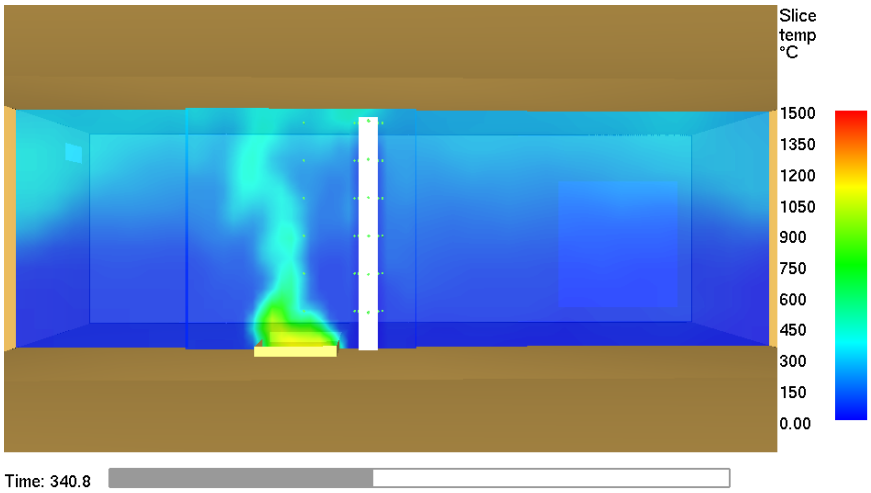

Model: *FDS_Fine Mesh*; t=340.8 s;

Phase: *extinguishment*

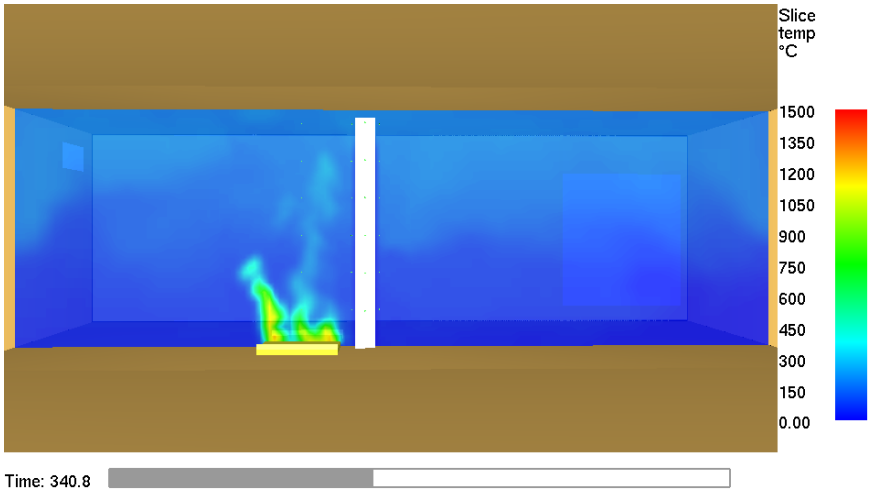

Figure 37: Temperature slices by phases

3.1.7.3 Column surface temperatures

Temperatures of the steel on the column surface were measured with the welded thermocouples type K in the experiment. Equivalent for calculating solid object temperature in the FDS is the *Wall temperature device* (DEVC namelist group) [8]. In this work they are labelled as TCC*ij*. To compute the temperature of the solids, FDS solves the one-dimensional heat transfer equation, what can lead, in some cases, to a deviation of results compared to the real situation. Steel surface temperatures in the numerical models were measured on the

front face of the steel column, because of the FDS geometry limitation. As it was mentioned before circular cross section of the column was approximated by the rectangular cross section. Consequently, shadow effect occurred, which prevented impact of a heat flux on the sides and the back column surface. As a result of that measured temperatures on these positions were underrated.

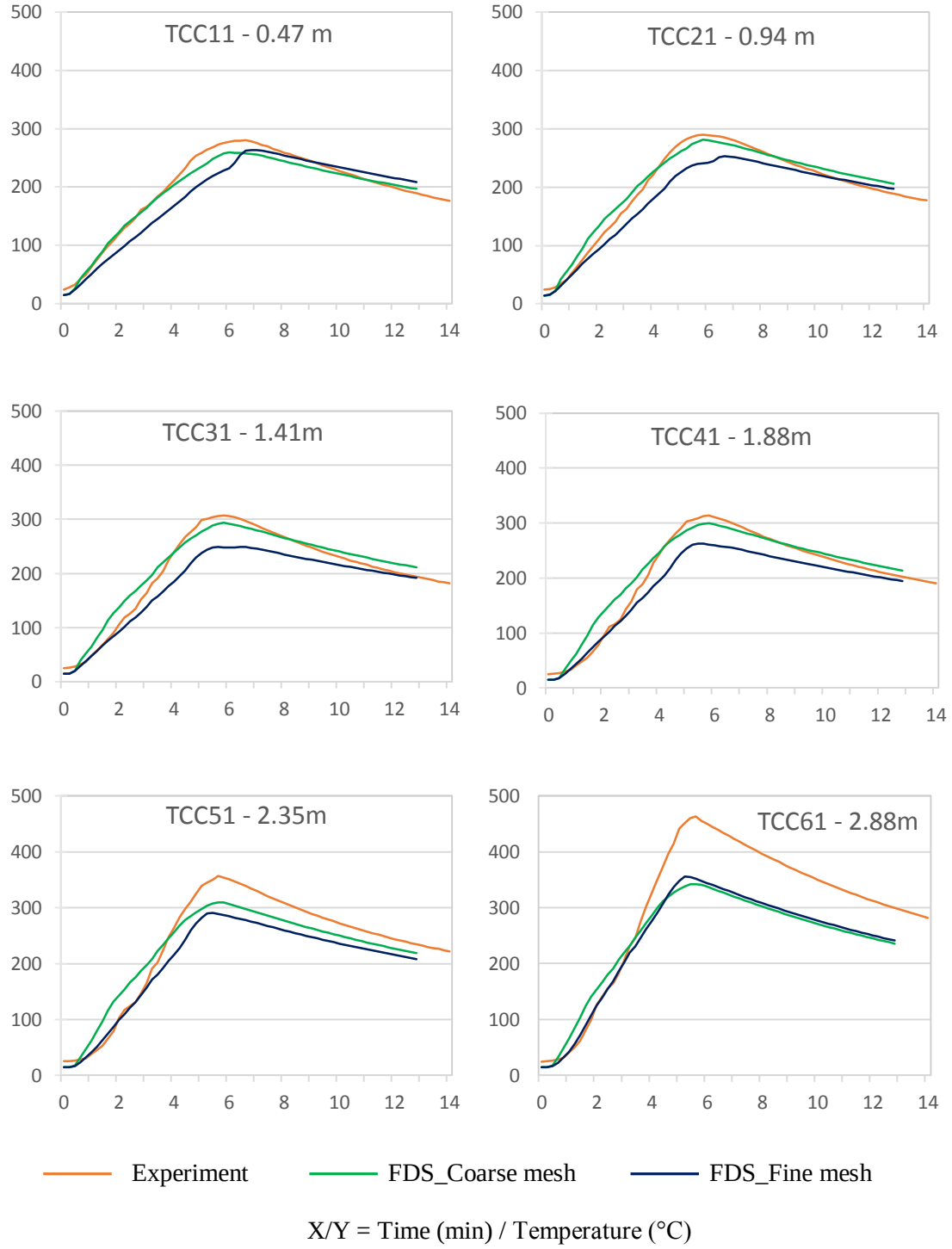

3.1.7.4 Adiabatic Surface Temperatures (AST)

The concept of adiabatic surface temperatures can also be used to express fire exposure on a structure. It's been shown that Plate Thermometer as specified in the international fire resistance test standards ISO 834 and EN 1363-1 for harmonizing fire resistance approximately measures AST [42]. Since it has been shown that FDS prediction on steel temperatures on the side and back sides of the columns wasn't good enough, AST were used to calculate three-dimensional heat transfer using FEM software.

Numerical model *FDS_Fine Mesh* was used to get AST, since it was considered as a more reliable model compared to *FDS_Coarse Mesh.*

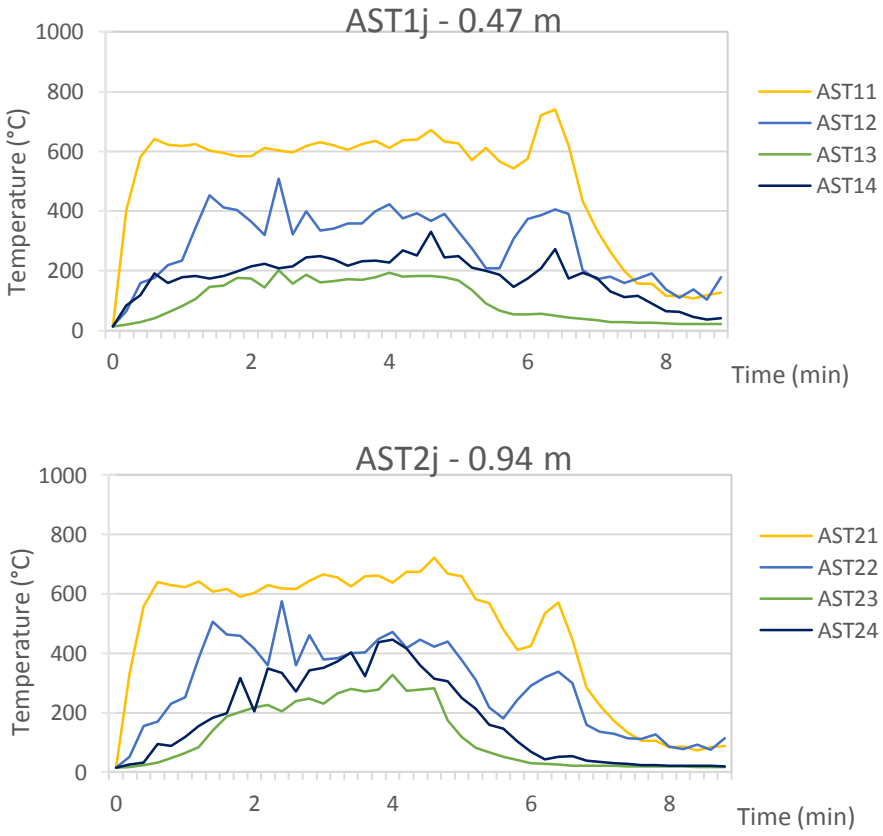

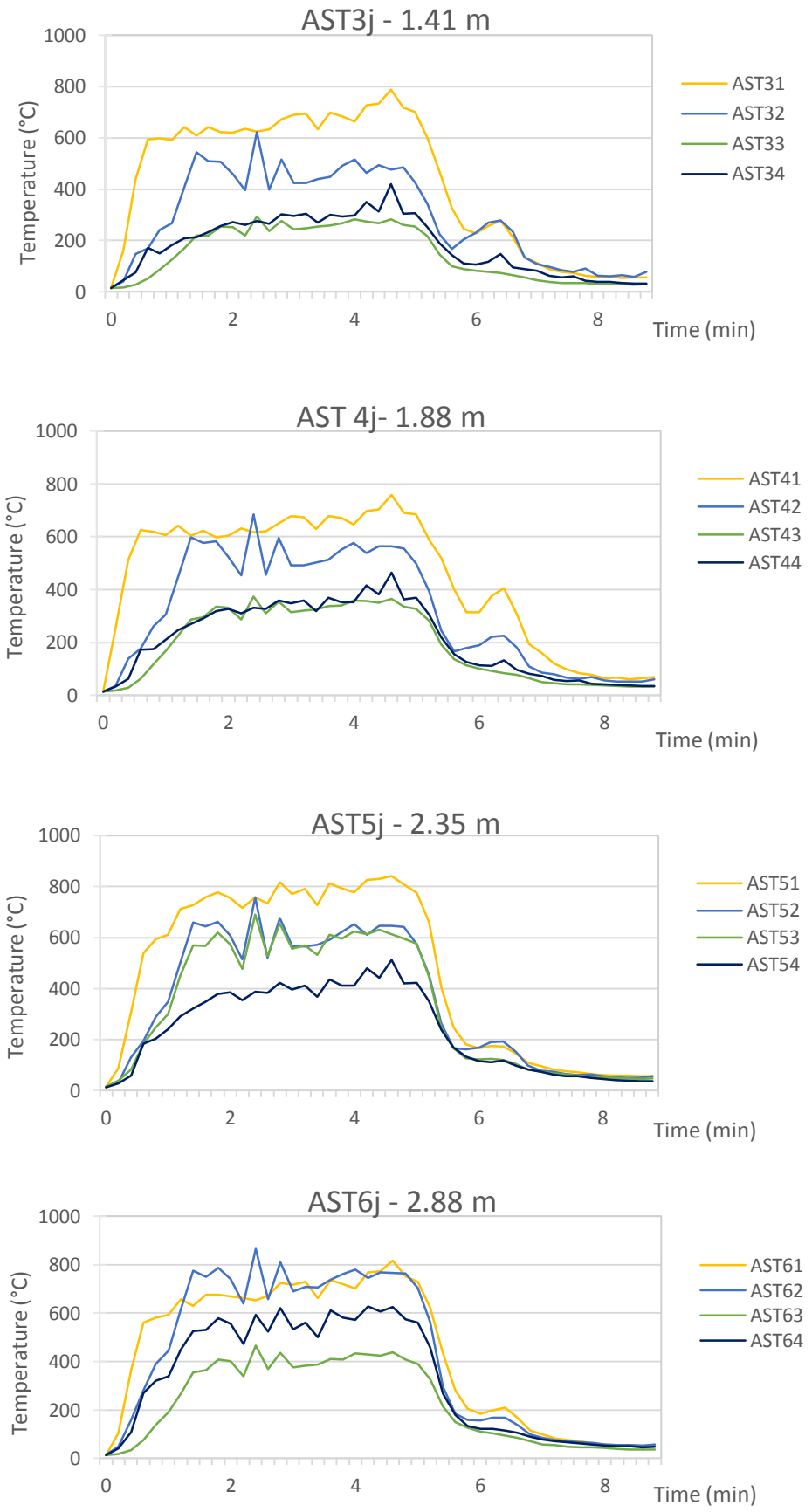

Figure 38: Adiabatic surface temperatures

3.1.7.5 Smokeview comparison

Smokeview is a software tool developed by National Institute of Standard and Technology and designed to visualize numerical calculations generated by fire models such as FDS.

In this work Smokeview is used to calibrate soot mass fraction with those from the experiment. Photos taken after the experiment [2] were the only indicator on how much soot was produced during the experiment. Figure below presents visualization of soot mass fraction. Best matching value of the fraction of fuel mass converted into smoke particulate (Soot yield) was found out to be γs=0.01.

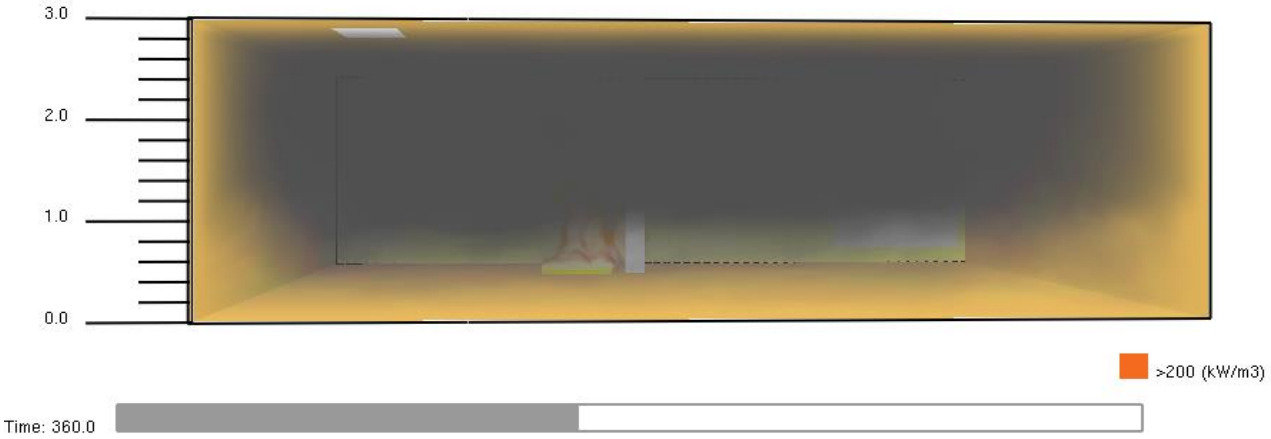

Figure 39: Visualization of soot mass fractions

Figure 40: Experimental setup after test [2]

3.2 FEM Thermal analysis

3.2.1 Numerical modelling

Numerical modelling of Heat Transfer phenomena was conducted using Finite Element Method (FEM) software Abaqus/CAE 6.13. Heat transfer was calculated as a transient state over time period of 25 min. As mentioned before the adiabatic surface temperatures were used to calculate steel temperatures.

Following the experimental measurements, the outside column surface was divided into 24 regions, 6 by the height and 4 by the cross sectional area according to the device positions (Table 8). Boundary conditions were adiabatic surface temperatures obtained in fire model. Each AST calculated in fire model was assigned to the corresponding column region. In this work air flow impact inside of the column was neglected due to complexity of modelling structure-fluid interaction.

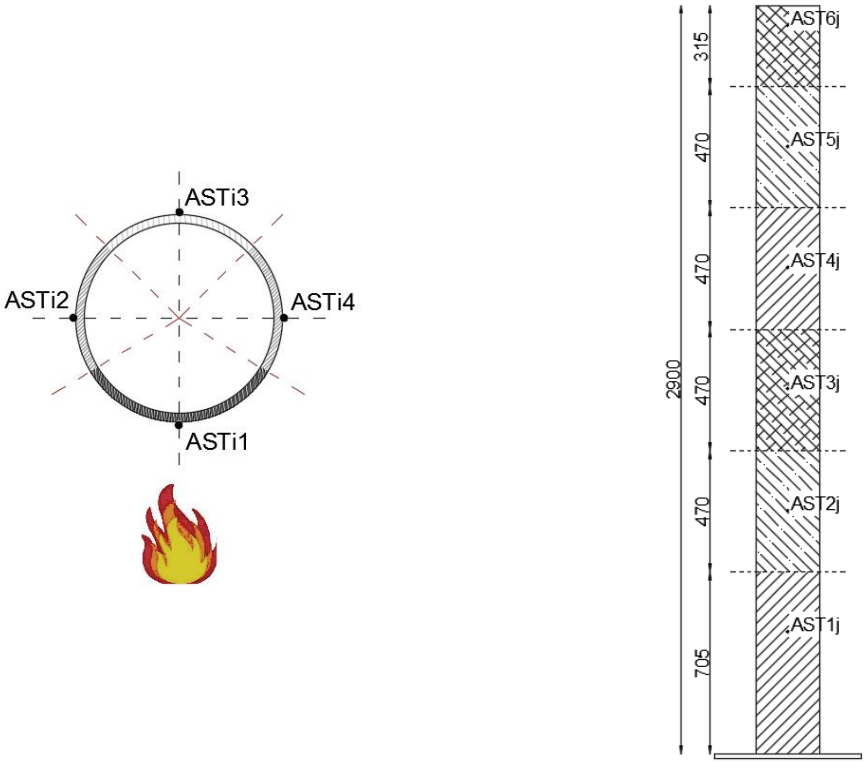

Figure 41: Scheme of temperature exposure regions

The convective heat transfer coefficient (α_c) was set to 20 W/m^{2}K [36], and the emissivity of the cold rolled steel (ε_s) to 0.75 [46]. Conductivity and the specific heat was taken as a temperature dependent, same as in Section 3.1.5.

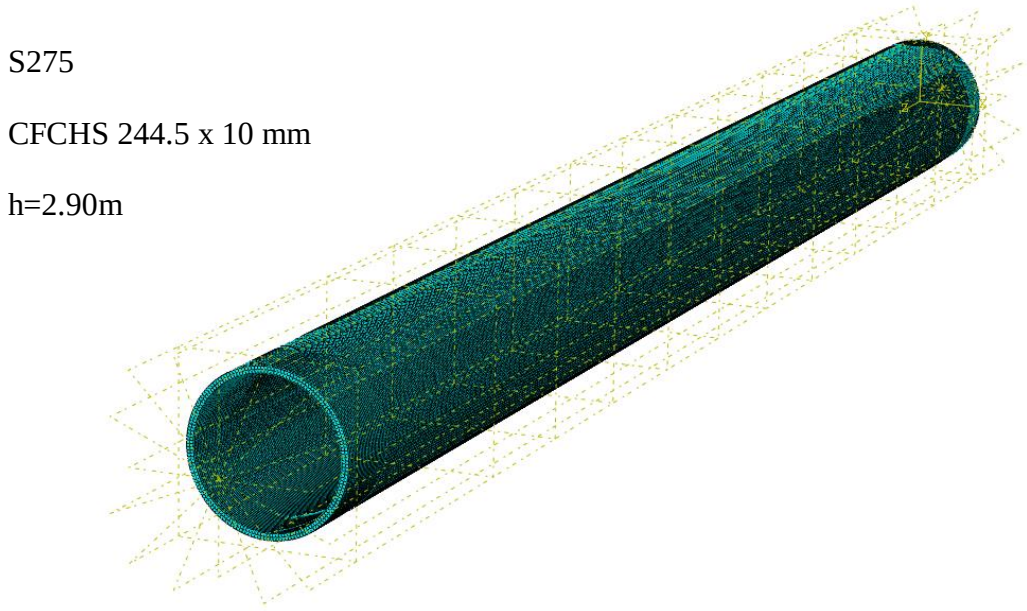

Figure 42: Meshed column geometry

Column was meshed using 5 mm DC3D8 elements, an 8-node linear heat transfer bricks.

Comparison between FEM calculations and experimental results has been shown in the following section.

3.2.2 Results and discussion

Except from *Heat Transfer* calculation using AST from the fire model, in order to investigate and compare influence of the steel temperatures on its behaviour , heat transfer using the international standard fire curve *ISO 834* prescribed in EN 1991-1-2 (2002) (Section 2.1.2.1) was calculated too. In this case temperature distribution was assumed as uniform along whole column.

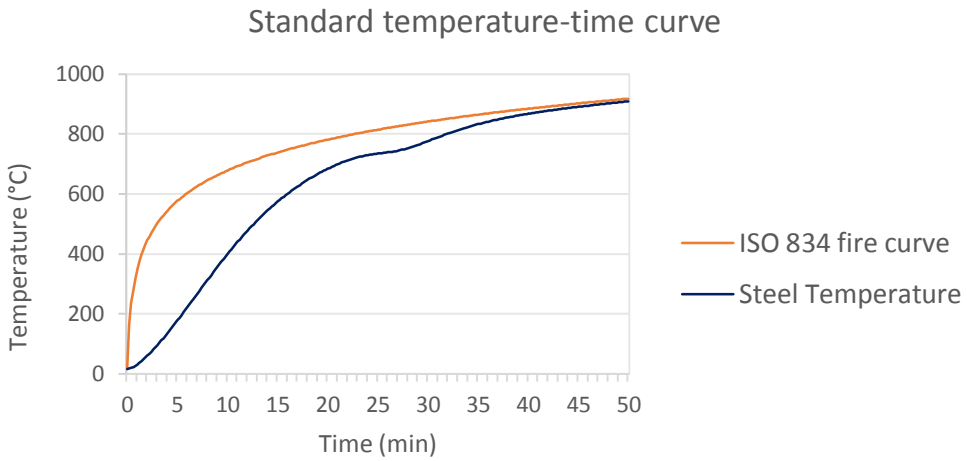

Figure 43: Steel temperatures calculated using Standard temperature-time fire curve

On the following pages results of the heat transfer analysis are presented. Temperature is measured in the column nodes positioned following same principle as in Section 3.1.7.

TS*ij* – Temperature of the Steel

i – height of obtained section

j – position on the cross section

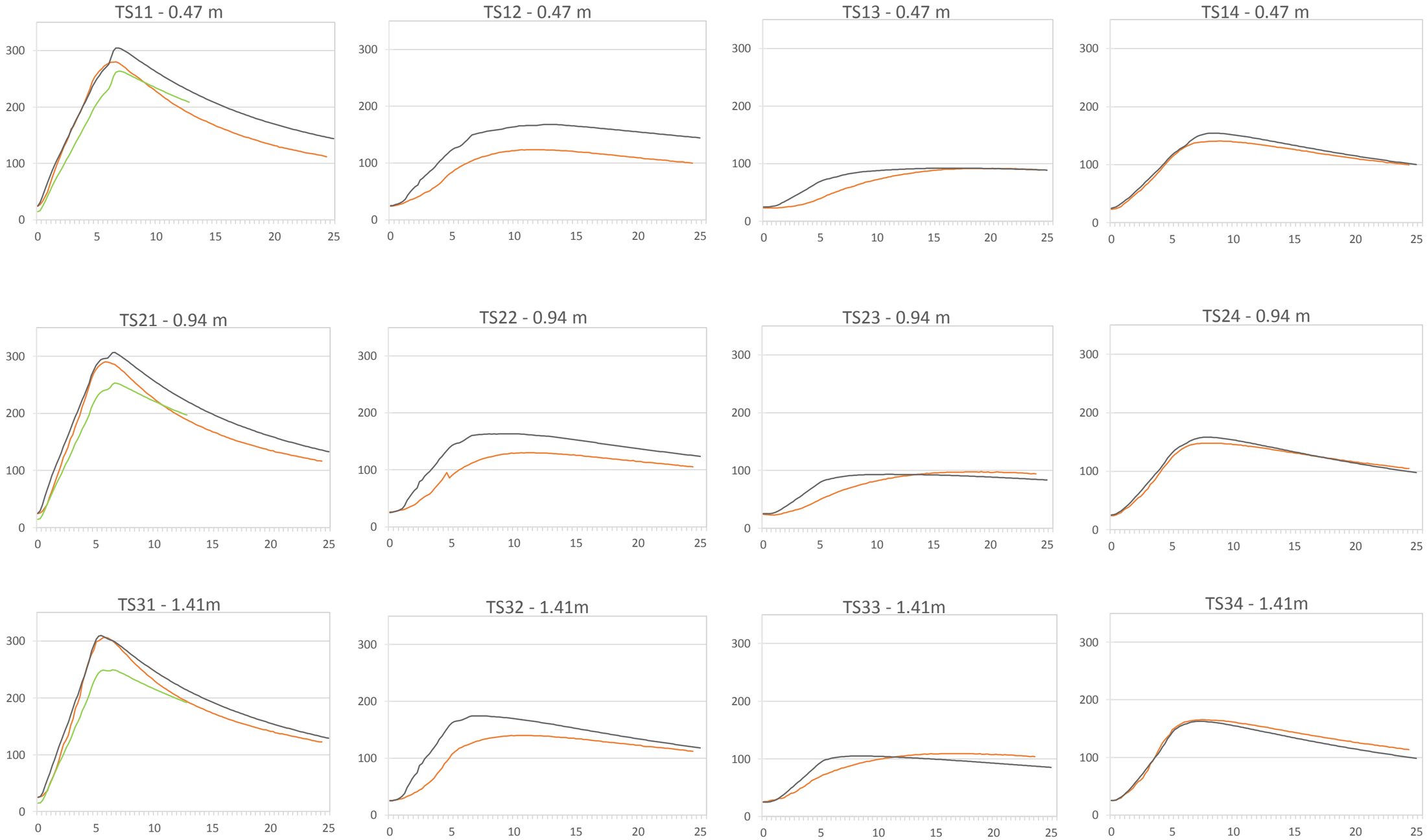
TS11 - 0.47 m
TS12 - 0.47 m
TS13 - 0.47 m
TS14 - 0.47 m
TS21 - 0.94 m
TS22 - 0.94 m
TS23 - 0.94 m
TS24 - 0.94 m
TS31 - 1.41m
TS32 - 1.41m
TS33 - 1.41m
TS34 - 1.41m
0
100
200
300
0
5
10
15
20
25
Experiment measurement
FEM calculation
FDS calculation
X / Y = Time (min) / Temperature (°C)

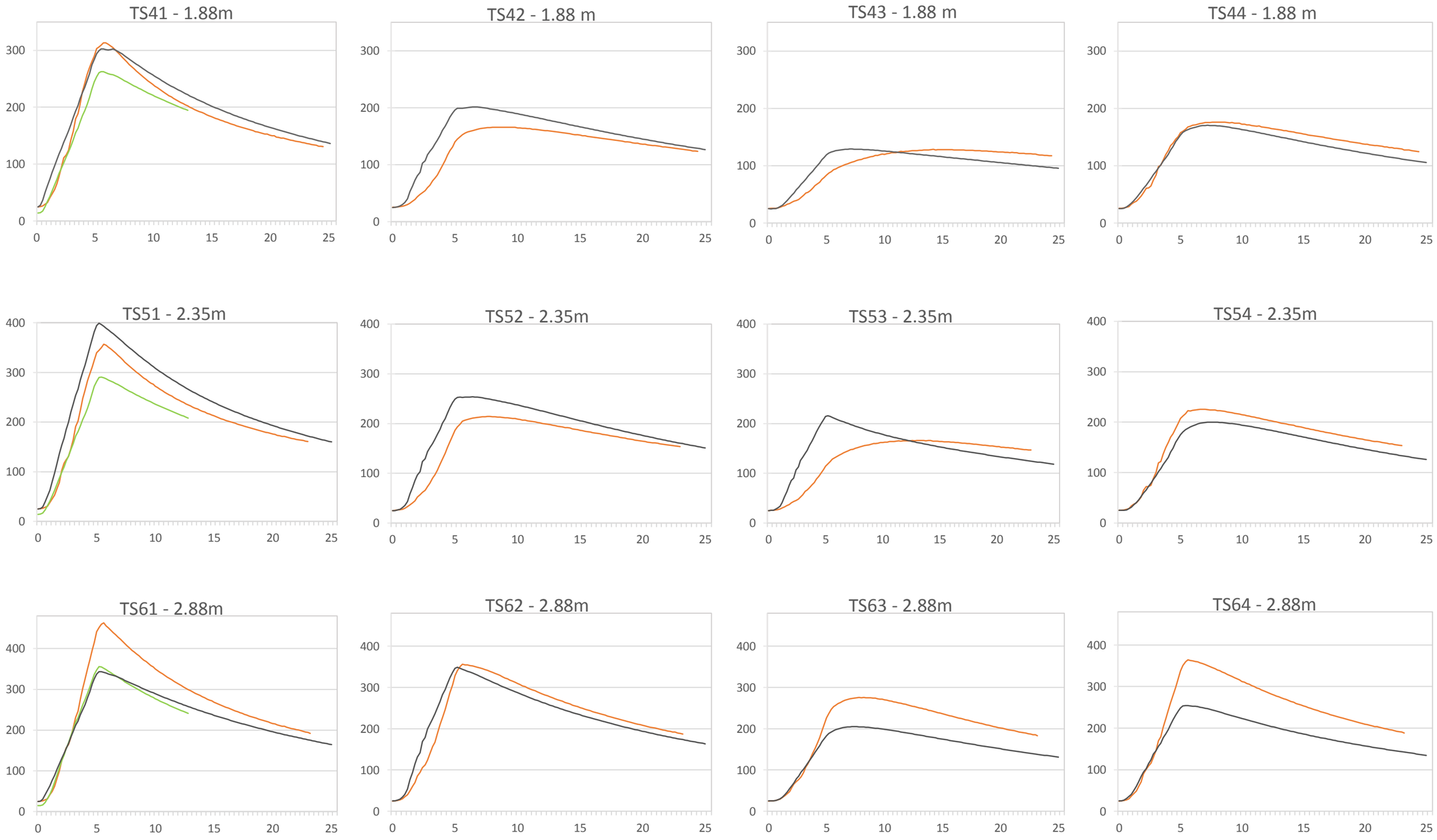
TS41 - 1.88m
TS42 - 1.88 m
TS43 - 1.88 m
TS44 - 1.88 m
TS51 - 2.35m
TS52 - 2.35m
TS53 - 2.35m
TS54 - 2.35m
TS61 - 2.88m
TS62 - 2.88m
TS63 - 2.88m
TS64 - 2.88m
Experiment measurement
FEM calculation
FDS calculation
X / Y = Time (min) / Temperature (°C)

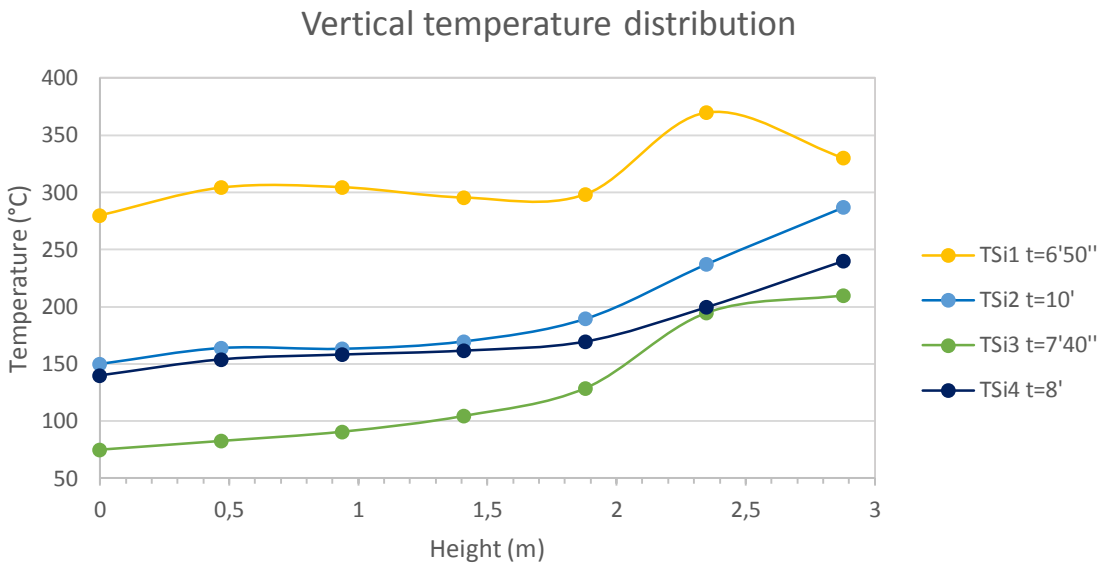

Figure 44: Vertical temperature distribution (FEA)

Looking at the results, it is possible to see the difference between heat transfer calculated in the fire model - FDS (1D heat transfer calculation) and the one calculated using FEM model (3D heat transfer calculation). Therefore, advantage of using FEM models in order resolve observed phenomena is obvious. Advantage of using three-dimensional heat transfer calculation is also noticeable in regions less exposed to the direct flame influence, where one-dimensional heat transfer calculation showed significantly underrated calculated temperatures. Despite disadvantage of FDS model to calculate accurately heat transfer in some regions, heat transfer calculated using adiabatic surface temperatures from FDS model showed good approximation compared to experiment measurements.

In the region *TSi1* calculated temperatures showed pretty good approximation compared to experimental results, except in the highest region (below ceiling) where FDS model generally underrated temperature distribution. Region *TSi2* showed slightly overrated steel temperatures along whole height of the column, due to flame deviation in FDS model. Experiment showed steadier fire plume behaviour what resulted in smaller difference of steel temperatures along the regions *TSi2* and *TSi4*. Not exposed side of the column, *TSi3*, showed well resolved steel temperature calculation in terms of maximum temperatures, but still there are differences in time development of the temperature.

3.3 FEM Structural analysis

3.3.1 Numerical modelling

Structural analysis of the column was carried out in same software, Abaqus/CAE 6.13. Geometry of the column and the column division in the regions was equal as in Section 3.2.1. Calculated steel temperatures from the thermal analysis were assigned as a predefined fields to the corresponding column regions as mentioned before. Boundary conditions were assumed as a pinned on the both column ends. GMNIA calculation was performed and compared to the GMNA calculation.

Column was meshed with the 10 mm Hex shaped C3D8R elements, an 8-node linear brick elements.

S275

CFCHS 244.5 x 10 mm

h=2.90m

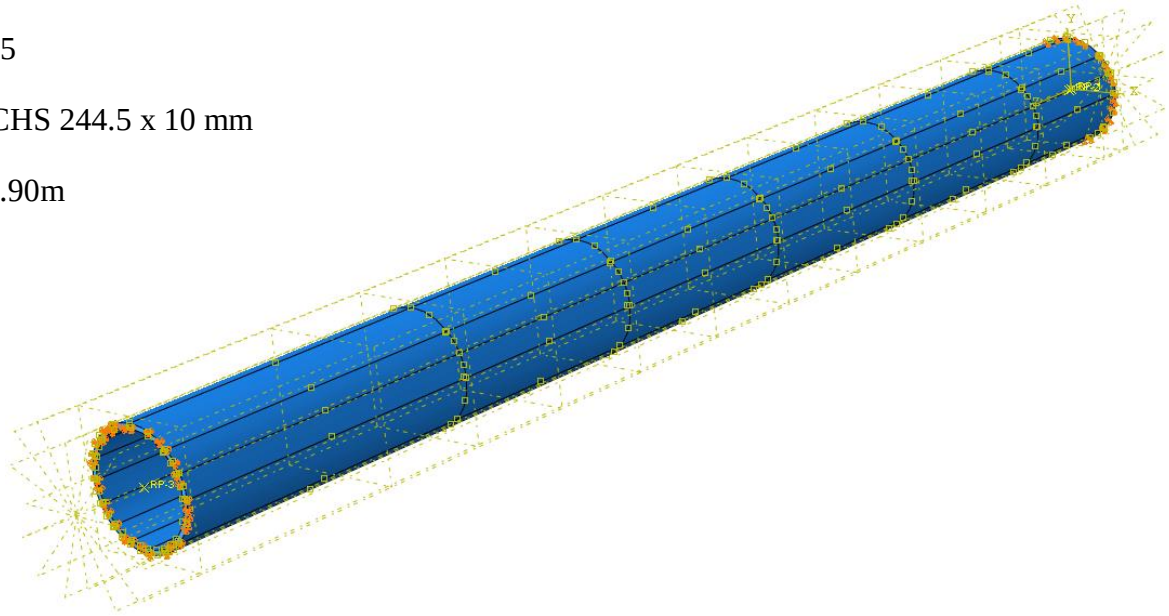

Figure 45: Column geometry

NLGEOM analysis, which includes *geometrical nonlinearity*, was included in structural model due to expected large deflections.

Geometrical imperfections are usually introduced by perturbations in the geometry. In this work geometrical imperfections are observed like *initial curvature* and *eccentrity of loading*.

Initial curvature was defined to initiate local buckling in the steel column models. The shape of imperfection was developed by conducting linear eigenvalue buckling analysis at the ambient temperature, and the amplitude of the imperfection was set equal to 10% of the column thickness. Superposition of selected eigenmodes was performed with the appropriate scale factor.

First two buckling modes were used in this work, according to the following figure, thus scale factors were set up to:

10% times section thickness for the first buckling mode;

5% times section thickness for the second buckling mode.

Eccentricity of loading was taken as 1/5 of column diameter which corresponds to 50mm, and it was applied as concentrated moment on both column ends.

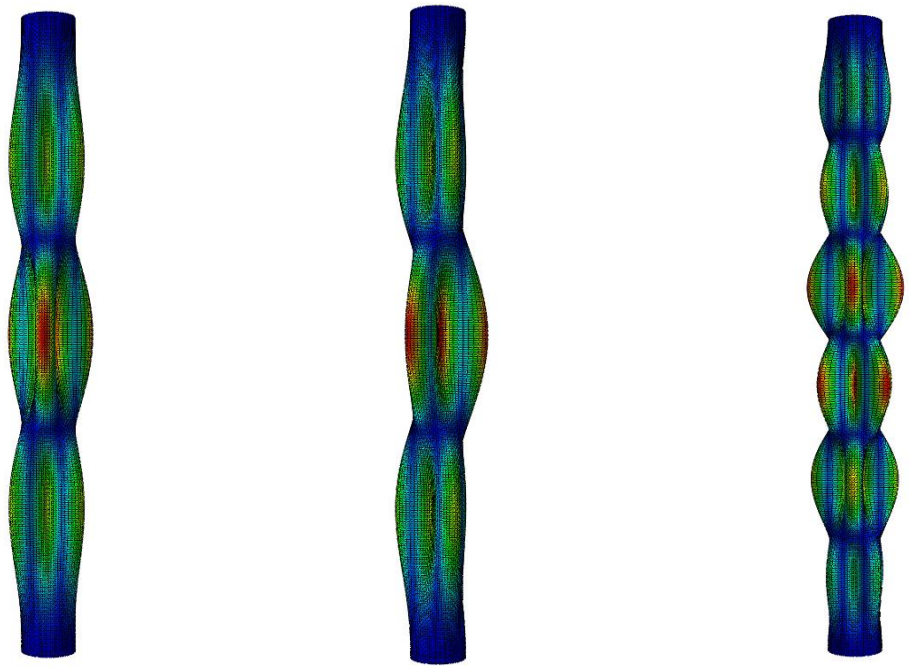

Buckling mode 1 *Buckling mode 2* *Buckling mode 3*

Figure 46: Linear buckling modes

3.3.1.1 Material properties

In this analysis steel S275 is used. Steel was modelled as an ideal elastic-plastic material, which neglects strain-hardening under high strains (see Section 2.6.2). Since steel column was subjected to a high temperatures, its mechanical properties were taken as a temperature dependent according to EN1993-1-2 (2005).

Unit mass of steel is considered as independent of the steel temperature, and it's taken as 7850 kg/m^3.

Poisson coefficient was taken as the temperature independent ν=0.30

Modulus of elasticity and *yield stress* were taken as temperature dependent following the reduction factors for elevated temperatures from Table 3.1 from [36].

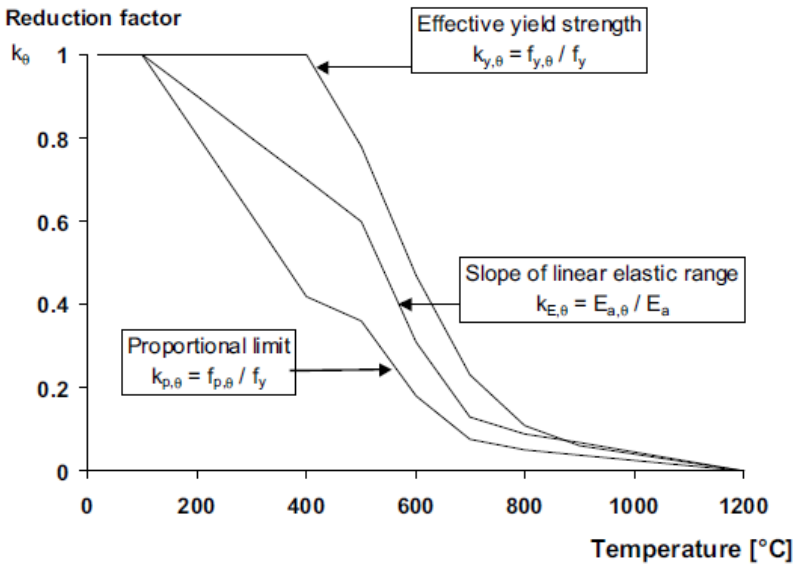

Figure 47: Reduction factors for the stress-strain relationship of carbon steel at elevated temperatures

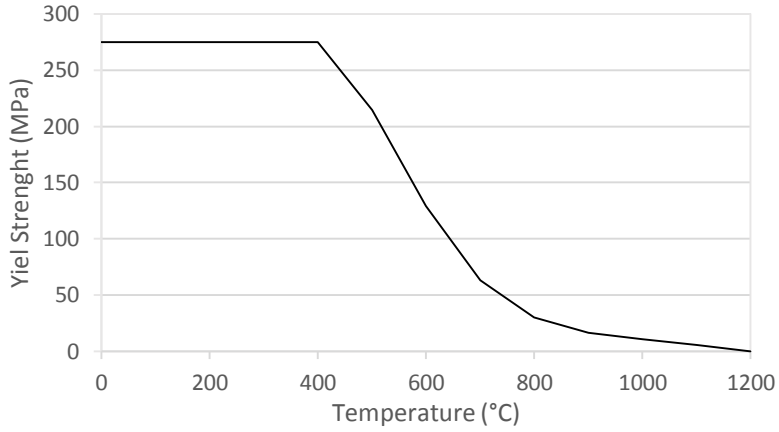

Figure 48: Yield strength – temperature dependence

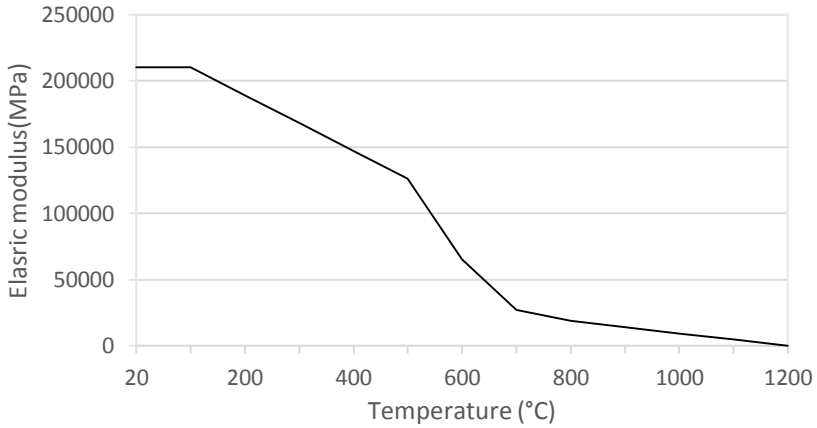

Figure 49: Elastic modulus - temperature dependence

Thermal elongation of steel is taken as the temperature dependent according to EN1993-1-2 (2005) [36].

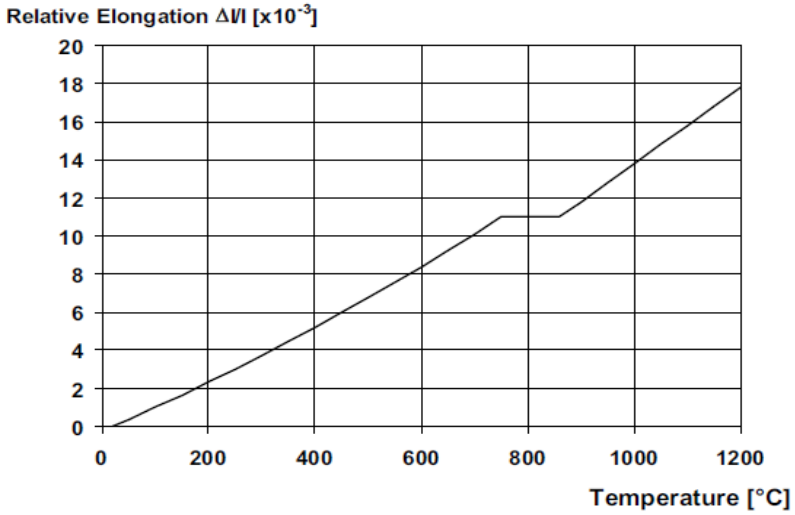

Figure 50: Relative thermal elongation of carbon steel as a function of the temperature

3.3.2 Case studies

In order to investigate and compare load capacity and failure of unprotected CFCHS 245x10mm column at high temperatures, impact of non-uniform thermal load obtained from *fire model* is compared with the *standard temperature-time* fire curve as a uniform thermal load (Section 3.2.13.2.2), and observed under several different axial compression load cases. All of cases were studied with geometrical and material non-linearity included, furthermore, comparison is made for same cases containing imperfections (initial deflection and eccentrity of loading) (GMNA and GMNIA analysis). It is worth to mention that in previously conducted experiments (on which fire model was based) top of the column was unrestrained in order to avoid deflections, so there was no experimental data on column structural response.

As mentioned before thermal load obtained in this work is assigned to the corresponding column regions, while thermal load determined by standard temperature-time curve is assigned as uniform along whole height of the column. Thermal load is then combined with the constant axial compression force.

Value of the axial compression force is determined relative to the flexural buckling resistance of observed steel column ($N_{b,Rd}$=1815 kN) at the ambient temperature, calculated in software package Scia Engineer 14, as presented on following pages.

Member height: 2,900 m CFCHS244.5X10 S 275

Note: EN 1993-1-3 article 1.1(3) specifies that this part does not apply to cold formed CHS and RHS sections.

The default EN 1993-1-1 code check is executed instead of the EN 1993-1-3 code check.

Partial safety factors

Gamma M0 for resistance of cross-sections	1,00
Gamma M1 for resistance to instability	1,00
Gamma M2 for resistance of net sections	1,25

Material S275

Yield strength fy	275,0	MPa
Ultimate strength fu	430,0	MPa
Fabrication	Cold formed	

Classification for cross-section design

According to EN 1993-1-1 article 5.5.2

Classification for Tubular Sections

According to EN 1993-1-1 Table 5.2 Sheet 3

Maximum width-to-thickness ratio	24,45
Class 1 Limit	42,73
Class 2 Limit	59,82
Class 3 Limit	76,91

=> Section classified as Class 1 for cross-section design

...::STABILITY CHECK::...

Classification for member buckling design

Decisive position for stability classification: 0,000 m

Classification for Tubular Sections

According to EN 1993-1-1 Table 5.2 Sheet 3

Maximum width-to-thickness ratio	24,45
Class 1 Limit	42,73
Class 2 Limit	59,82
Class 3 Limit	76,91

=> Section classified as Class 1 for member buckling design

Flexural Buckling Check

According to article EN 1993-1-1 : 6.3.1.1. and formula (6.46)

Buckling parameters	yy	zz	
Sway type	sway	non-sway	
System Length L	2.900	2.900	m
Buckling factor k	1.00	1.00	
Buckling length Lcr	2.900	2.900	m
Critical Euler load Ncr	12502.61	12503.24	kN
Slenderness	34.95	34.95	
Relative slenderness Lambda	0.40	0.40	
Limit slenderness Lambda,0	0.20	0.20	
Buckling curve	c	c	
Imperfection Alpha	0.49	0.49	
Reduction factor Chi	0.90	0.90	
Buckling resistance Nb,Rd	**1815.18**	**1815.19**	**kN**

Analysis was organized according to the following table:

Table 9. Structural analysis concept

	Thermal load			
	Fire Model		Standard temperature-time curve	
Group	Analysis	Load eccentrity (mm)	Analysis	Load eccentrity (mm)
#1	GMNA (a)	/	GMNA (d)	/
$N=0.8N_{b,Rd}$	GMNIA (b)	0	GMNIA (e)	0
N=1452 kN	GMNIA (c)	50	GMNIA (f)	50
#2	GMNA (a)	/	GMNA (d)	/
$N=0.6N_{b,Rd}$	GMNIA (b)	0	GMNIA (e)	0
N=1089 kN	GMNIA (c)	50	GMNIA (f)	50
#3	GMNA (a)	/	GMNA (d)	/
$N=0.4N_{b,Rd}$	GMNIA (b)	0	GMNIA (e)	0
N=726 kN	GMNIA (c)	50	GMNIA (f)	50

3.3.3 Results and discussion

3.3.3.1 Group #1

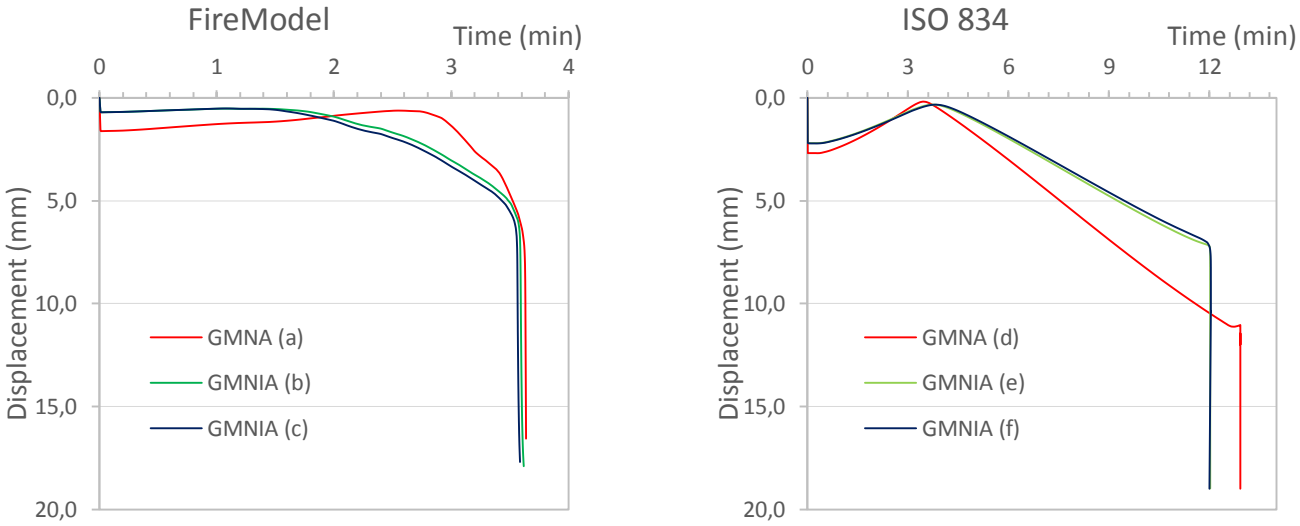

Plastic strain and stress distribution – deformation scale factor=10

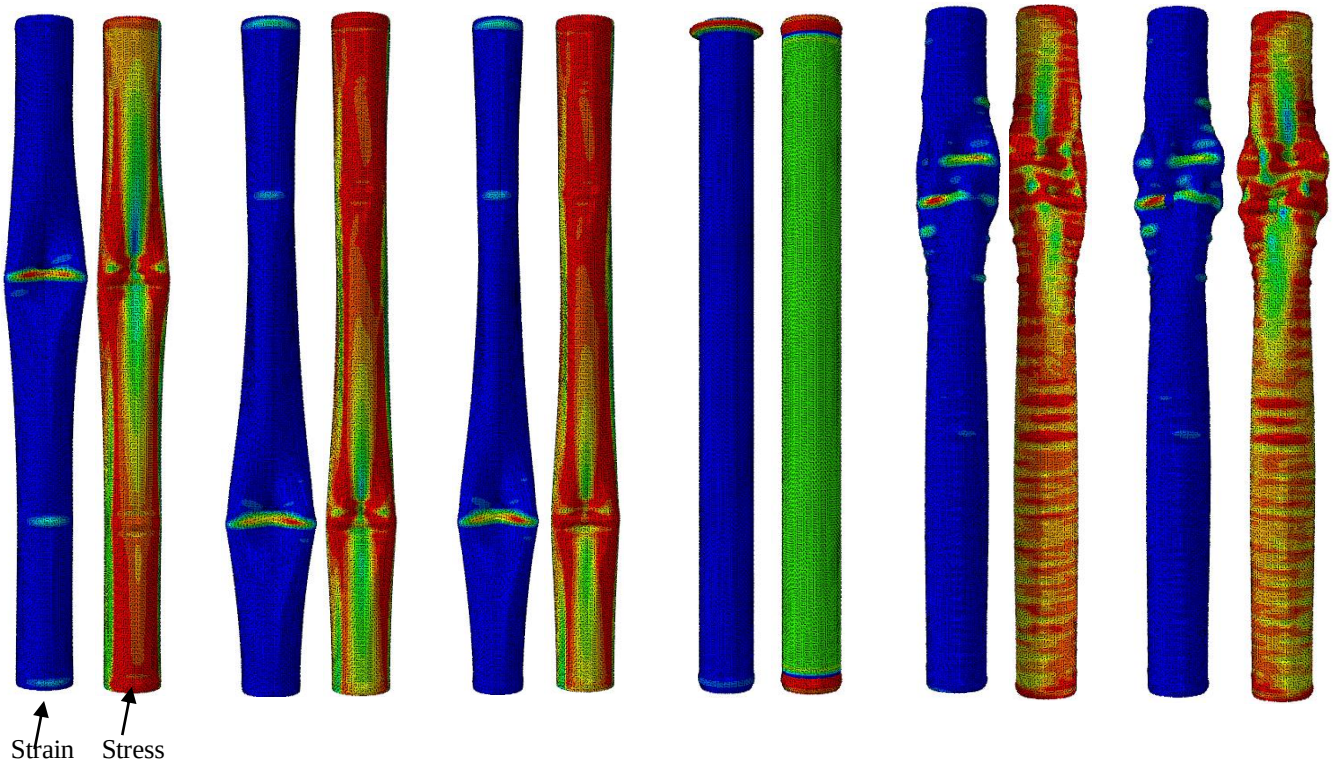

T*=260°C	T*=240°C	T*=240°C	T*=510°C	T*=480°C	T*=480°C
GMNA (a)	GMNIA (b)	GMNIA (c)	GMNA (d)	GMNIA (e)	GMNIA (f)

3.3.3.2 Group #2

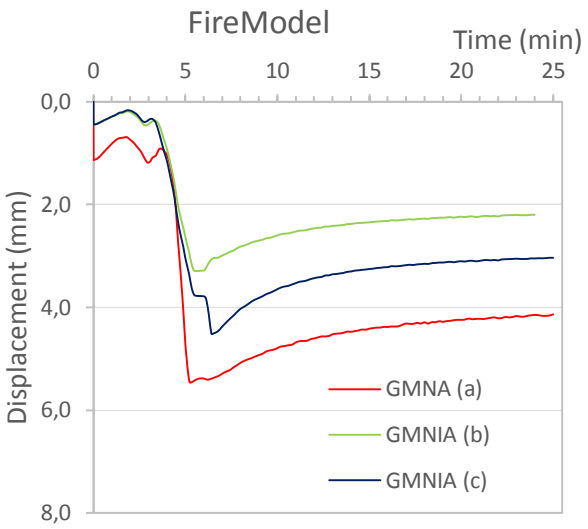

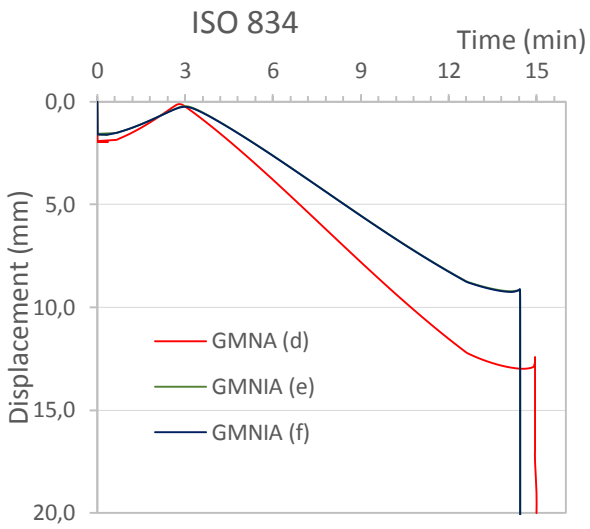

Plastic strain and stress distribution – deformation scale factor=10

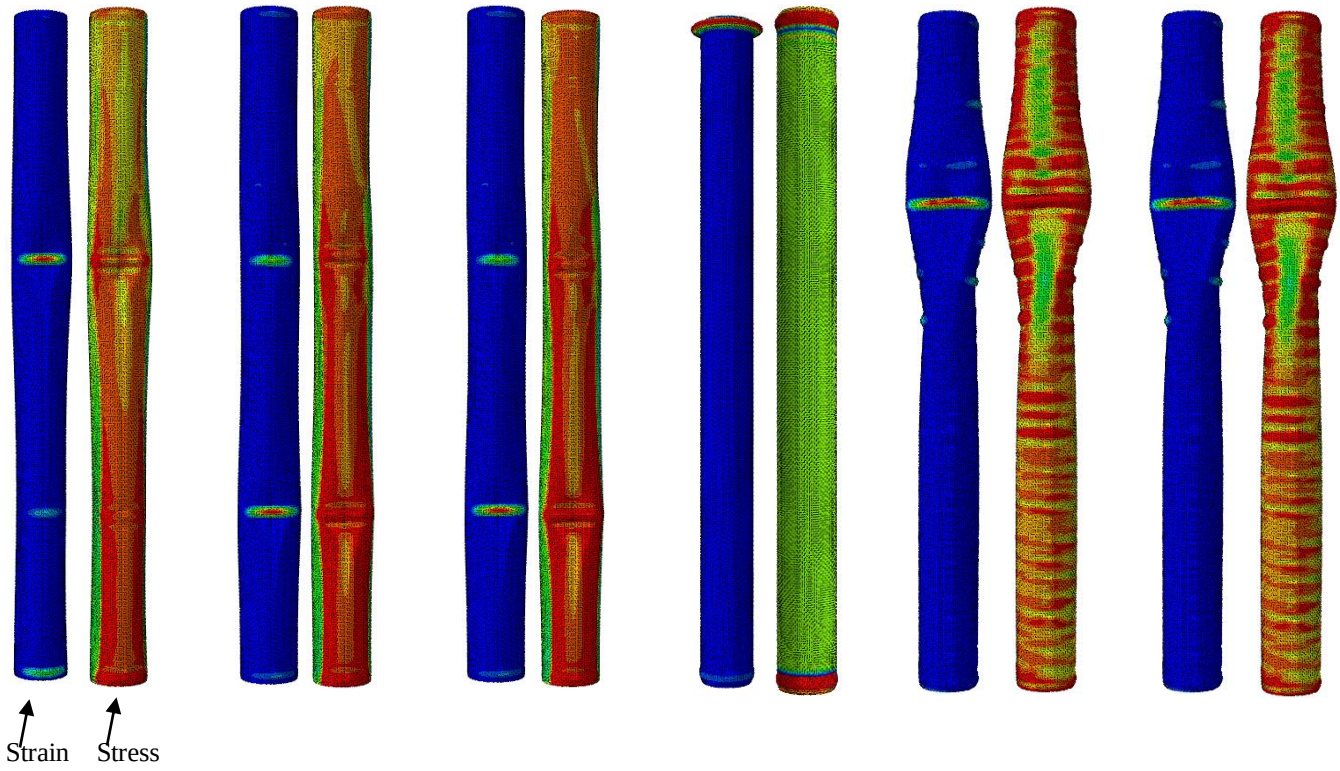

/	/	/	T*=575°C	T*=560°C	T*=560°C
GMNA (a)	GMNIA (b)	GMNIA (c)	GMNA (d)	GMNIA (e)	GMNIA (f)

3.3.3.3 Group #3

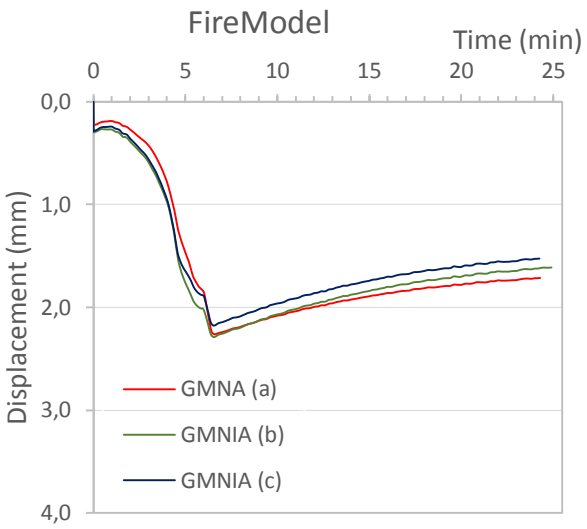

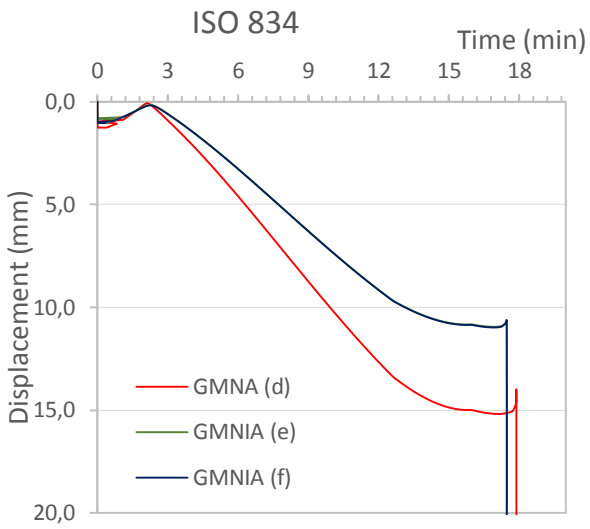

Plastic strain and stress distribution – deformation scale factor=10

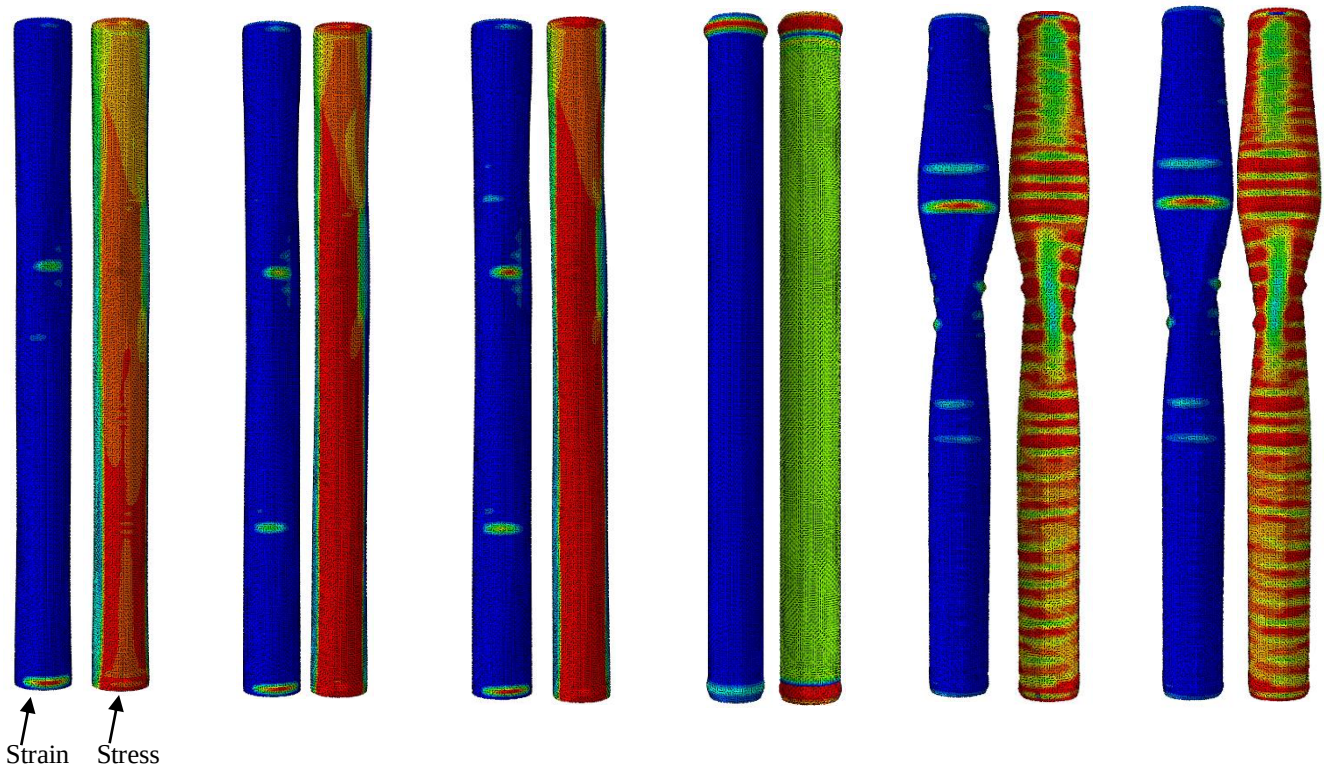

/	/	/	T*=640°C	T*=640°C	T*=640°C
GMNA (a)	GMNIA (b)	GMNIA (c)	GMNA (d)	GMNIA (e)	GMNIA (f)

(*) Note that T* represents the temperature of area where column undergo collapse in moment when collapse occurs. T* is shown only for cases where collapse occurred, but it is not necessary reason for the collapse.

Generally, failure was indicated using displacement-time graphs. Due to column low slenderness ($\lambda < \lambda_1$; 34.95<84.7; see Section 2.6.2.2) collapse occurs by local plastic squashing in all cases where the failure occurred.

Looking at the results within Group #1 where column is subjected to the highest axial load, it is clearly visible influence of uniform and non-uniform thermal load on a column load capacity. Although there is no decreasement of yield strength on temperatures where non-uniformly loaded column undergoes failure, there is decreasement of elastic modulus, what results in bigger strain appereance. Since thermal load is asymmetric, strain is asymmetric as well. Consequently, it led to column deflection and caused applied compression force to become eccentric, what caused additional internal moments to the column. With the increasment of a deflections, internal moments increased as well, what eventually brought column collapse earlier. This phenomena is called second-order effect.

Furthermore, test Group #2, so as Group #3, showed that in cases when the lower level of load is expected approach using standard time-temperature fire curve, might be too conservative. In this cases non-uniform thermal load predicts no failure for cases with or without geometrical imperfections, but still permanent deformations of the column exists. In cases where standard temperature-time fire curve is used failure occurred at approximately same temperature for all types of analysis.

Inclusion of the geometrical imperfections showed significant influence in prediction of column behaviour subjected to the uniform thermal load, and non-neglectible influence on non-uniformly loaded column, no matter of axial load level. Although behaviour of columns prior to collapse is different, columns subjected to the uniform thermal load collapsed at approximately same temperature for each load level separately. Loading eccentrity (1/5 x diameter) showed non-significant influence on load capacity. More slender column would probably be more sensitive to the geometrical imperfections.

4 CONCLUSIONS

Throughout this thesis procedure of performance based approach is show on example of steel column exposed to a localised fire, in terms of fire modelling, thermal and structural analysis. EN1991-1-2(2002) provides a simple calculation approach for determining localised fires within compartments, however, there's no simplified method to calculate heat transfer to a vertical elements. Therefore, there was a need to investigate effect of a localised fires to a vertical structural elements, such as columns.

Experiments conducted as a part of SUSCOS thesis, which was basis of this thesis, aimed to simulate a real fire scenario as a car fire within compartment. [2]

First part of performance based approach was CFD modelling of localised pool fire based on previously conducted experiments. Although modelling of fuel combustion using complex pyrolysis is complex, especially due to significant range of values of diesel properties it showed good prediction of heat release rate, temperature development above fire source, so as calculated temperatures of the steel on part the column which was most exposed to the fire. Furthermore, temperatures directly beneath the ceiling and on the less exposed parts of the column were slightly underrated compared to experimental ones, therefore further analysis have to be carried out.

Nevertheless, despite the FDS limitations, CFD model can be used to obtain adiabatic surface temperatures along the column, which can be used afterwards to calculate heat transfer using FEM software. In this work 3D heat transfer was calculated using Abaqus/CAE, furthermore, use of recommended values for convection, conduction and radiation has showed good approximation of steel temperature development compared to the experimental data. As a result of non-uniform heating scenario, asymmetric distribution of temperatures along the column height is verified. Heat transfer using standard temperature-time curve was calculated as well, as a uniformly distributed heating scenario.

Furthermore, structural analysis was carried out, based on temperatures obtained from thermal analysis. Structural response was observed using static geometrically and materially non-linear analysis with and without geometric imperfections. Except thermal load, column

was loaded with constant axial compression force. Since observed column has low slenderness, initial curvature and loading eccentrity turned out to be not decisive factor of column failure, but still it has non-neglectible effect especially for uniform thermal load. Material hardening and creep phenomena in this work were neglected, so further analysis should be done.

As a result of these analysis it has been shown how non-uniform thermal load caused by a localised fire can cause collapse of the structure, although maximum temperatures reached are significantly lower than those calculated using standard temperature time curve at the moment when failure occurs, for the same level of axial load. For the high levels of axial load column exposed to a localised fire undergo failure much before same column exposed to a uniform load. Non-uniform thermal load caused asymmetric deflections and eventually brought column collapse due to second order effects.

Therefore, it has been shown that localised fire can have unwanted consequences. For observed fire scenarios column exposed to a localised fire undergo collapse about three times faster than same column under uniform thermal load calculated using standard temperature time curve. Earlier time of column collapse means less time to get people and property evacuated.

Finally, although these analysis are complex and time consuming, benefits of it could be noticed in terms of increasing safety and reliability. Consequently, further research on localised fires should be done, in order to develop simplified methods to calculate heat transfer to a vertical structural elements.

REFERENCES

[1] Guan Heng Yeoh, Kwok Kit Yuen (2009); Computational Fluid Dynamics in Fire Engineering,Theory Modelling and Practice
[2] Gonçalo Ferraz (2014); Thermal Analysis of Steel Columns Exposed to Localised Fires
[3] Blinov, V.I., Khudyakov, G.N.(1961.); Diffusion Burning of Liquids
[4] Jorgen Carlsson (1999.); Fire modelling using CFD
[5] Alex Webb (2006.); FDS Modelling of Hot Smoke Testing, Cinema and Airport Concourse
[6] Floyd, J.D. ; Baum, H.R.; Mc Grattan, K.B. (2001); A mixture fraction combustion model for fire simulation usinf CFD Proceedings of the International Conference on Engineered Fire Protecion Design San Francisco
[7] Cox, Geoff; Kumar, Suresh (2002.); Modelling enclosure fires using CFD
[8] McGrattan, K.B.; Forney, G.P. (2004); Fire Dynamics Simulator (V4) – User's Guide, NIST
[9] Rehm RG, Baum HR (1978); The Equations of Motion for Thermally Driven, Bouyant Flows
[10] ''Basic Considerations'' Combustion Fundamentals of Flow (1995.)
[11] McGrattan, K.B. (2004); FDS Tehnical Reference Guide; NIST
[12] Smagorinsky J. (1963) Genereal Circulation Experiments with the Primitive Equations
[13] McGrattan i.a. (2017); FDS Tehnical Reference Guide Vol2: Verification
[14] Xin, Y. (2005); Baroclinic Effects on Fire Flow Field, Proceedings of the Fourth Joint Meeting of the U.S. Sections of the Combustion Institute
[15] McGrattan i.a. (2017); FDS Tehnical Reference Guide Vol3: Validation
[16] Bubbico, Dusserre, Mazzarotta (2016); Calculation of the Flame Size from Burning Liquid Pools
[17] Skarsbø Lars Roar (2011); An Experimental Study of Pool Fires and Validation of Different CFD Fire Models
[18] Quincy, Mass, Bethesda, NFPA (2002), SFPE handbook of fire protection engineering
[19] Drysdale D. (1999); An introduction to fire dynamics
[20] McCaffrey B.J. and M. Harkleroad (1989); Combustion efficiency, radiation, co and soot yield from a variety of gaseous, liquid and solid fueled bouyan diffusion flames
[21] Simo Hostika (2001); Experimental study of the localised room fires
[22] Koseki H- and G.W. Mulholland (1991); The effect of diameter on the burning of crude oil pool fires
[23] Hagen B.C. (2004); Grunnleggende brannteknikk
[24] Scanpower D. (2001); Human resistance against thermal effects, explosion effects, toxic effects and obscuration of vision

[25] Karlson B. & Quintiere J. (2000); Enclosure Fire Dynamics-Energy Release Rate, USA
[26] Hesketad G. (1998); Dynamics of fire plume
[27] EN 1991-1-2 (2002)
[28] Hasemi Y. (1986); Thermal Modeling Of Upward Wall Flame Spread
[29] https://en.wikipedia.org/wiki/Diesel_fuel#Chemical_analysis (May 2017)
[30] http://www.engineeringtoolbox.com/specific-heat-capacity-d_339.html (May 2017)
[31] http://walshcarlines.com/pdf/fueltable.pdf (May 2017)
[32] Britannica: Vaporization (https://www.britannica.com/science/vaporization) (May 2017)
[33] https://en.wikipedia.org/wiki/Heat_of_combustion (May 2017)
[34] Nist Chemistry WebBook
[35] https://en.wikipedia.org/wiki/Enthalpy_of_vaporization (May 2017)
[36] EN 1993-1-2 (2005)
[37] https://en.wikipedia.org/wiki/Thermal_conductivity (May 2017)
[38] http://www.engineeringtoolbox.com/emissivity-coefficients-d_447.html (May 2017)
[39] Lin, C.H., Ferng, Y.M. and Hsu, W.S. (2009); Investigating the Effect of Computational Grid Sizes in the Predicred Characteristic of Thermal Radiation for a Fire
[40] Hietaniemi J., Hostika S., Vaari J (2004); FDS simulation of fire spread-comparison of model results with experimental data
[41] http://www.engineeringtoolbox.com/thermal-conductivity-liquids-d_1260.html (May 2017)
[42] Wickstorm Ulf (2008); Adiabatic surface temperature and the plate thermometer for calculatin heat transfer and controlling fire resistance furnaces
[43] Babrauskas V. (2002); Heat Release Rate (SFPE Handbook of Fire Protection Engineering
[44] Sjostrom J., Bytrom A., Lange D., Wickstrom (2013); Thermal Exposure to a Steel Colum from Localised Fires
[45] Wickstrom Ulf (2007); Adiabatic Surface Temperature for Calculating Heat Trasfer to Fire Exposed Structures
[46] https://www.omega.com/literature/transactions/volume1/emissivitya.html (May 2017)
[47] EN1993-1-6, 2007
[48] Josef Machacek (2009); Modelin and analysis (lecture 6, V001)
[49] W. Schneider (2005); Stimulating Equivalent Geometric Imperfections for the Numerical Buckling Strength Verification of Axially Compressed Cylindrical Steel Shells
[50] http://fgg-web.fgg.uni-lj.si/~/pmoze/esdep/master/wg06/l0610.htm (August 2017)
[51] http://www.sandia.gov/vqsec/SON-BS.html (May 2017)